# NASA CONTRACTOR REPORT

NASA CR-2297

# DEVELOPMENT OF AN EXPERIMENT FOR VISIBLE RADIATION POLARIZATION MEASUREMENTS FROM A SATELLITE

*by Zdenek Sekera and Richard E. Bradbury*

*Prepared by*
INSTITUTE OF GEOPHYSICS AND PLANETARY PHYSICS
UNIVERSITY OF CALIFORNIA
Los Angeles, Calif. 90024
*for Langley Research Center*

NATIONAL AERONAUTICS AND SPACE ADMINISTRATION • WASHINGTON, D. C. • NOVEMBER 1973

| 1. Report No. NASA CR-2297 | 2. Government Accession No. | 3. Recipient's Catalog No. |
|---|---|---|
| 4. Title and Subtitle DEVELOPMENT OF AN EXPERIMENT FOR VISIBLE RADIATION POLARIZATION MEASUREMENTS FROM A SATELLITE | | 5. Report Date November 1973 |
| | | 6. Performing Organization Code |
| 7. Author(s) Zdenik Sekera and Richard E. Bradbury | | 8. Performing Organization Report No. NONE |
| | | 10. Work Unit No. |
| 9. Performing Organization Name and Address U.C.L.A., INSTITUTE OF GEOPHYSICS AND PLANETARY PHYSICS LOS ANGELES, CA. 90024 | | 11. Contract or Grant No. NAS 1-10107 |
| | | 13. Type of Report and Period Covered Contractor Report |
| 12. Sponsoring Agency Name and Address National Aeronautics and Space Administration Washington, D.C. 20546 | | 14. Sponsoring Agency Code |

15. Supplementary Notes

This is a final report.

16. Abstract

A GENERAL DISCUSSION OF THE INVERSION PROBLEM, I.E., DETERMINING THE ATMOSPHERIC TURBIDITY FROM POLARIMETRY OF RADIATION EMERGING FROM THE EARTH'S ATMOSPHERE, IS PRESENTED. A MAJOR THEORETICAL ADVANCE HAS BEEN MADE BY FINDING A SUCCESSFUL APPROXIMATION FOR THE FORWARD PEAK SCATTERING OF AEROSOLS TOGETHER WITH A SIMPLIFIED CHARACTERIZATION OF PARTICLE SIZE DISTRIBUTIONS.

AN ENGINEERING MODEL OF A MULTIBARRELLED PHOTOPOLARIMETER SUITABLE FOR OPERATION FROM A SATELLITE HAS BEEN EVALUATED IN LABORATORY AND HIGH ALTITUDE JET AIRCRAFT FLIGHT TESTS. COMPARISON OF THE DATA FROM FLIGHTS OVER THE MEXICAN DESERT WITH THEORETICAL CURVES FOR A RAYLEIGH ATMOSPHERE WITH NEGLIGIBLE TURBIDITY (AS MEASURED BY DIRECT SAMPLING OF PARTICULATES) IS IN REMARKABLE AGREEMENT.

| 17. Key Words (Suggested by Author(s)) POLARIMETRY (ATMOSPHERIC) AEROSOL SCATTERING AUREOLE SCATTERING APPROXIMATION POLARIZATION MEASUREMENTS IN THE ATMOSPHERE | | 18. Distribution Statement UNCLASSIFIED - UNLIMITED | | |
|---|---|---|---|---|
| 19. Security Classif. (of this report) UNCLASSIFIED | 20. Security Classif. (of this page) UNCLASSIFIED | | 21. No. of Pages 163 | 22. Price* $3.00 |

# PREFACE

This report covers work performed by the Atmospheric Radiation Group of the Institute of Geophysics and Planetary Physics, UCLA from July 1970 through June 1972 under contract NAS 1-10107, sponsored by NASA's AAFE program. The work was carried out under the direction of the principal investigator, Professor Z. Sekera.

In this preface, the editor would like to review the goals and progress of the program, and problems encountered in carrying out these goals. Some of these problems are discussed in detail in the report proper, but others do not conveniently fit into the organization of the report.

The major objectives of the program have been to study the feasibility of measuring the polarization parameters of the scattered sunlight emerging from the earth's atmosphere from a satellite platform and to study how such measurements may be used in the study of atmospheric turbidity ("Atmospheric turbidity," aerosol," and "suspended particulates" are essentially synonymous terms and are used interchangeably throughout this report.) leading naturally to a division into an experimental and a theoretical program.

It is the determination of atmospheric turbidity parameters from the polarization measurements which constitutes the inversion problem, the major concern of the theoretical program. Professor Sekera has prepared a highly detailed discursive introduction (Chapter 1) to this complex problem in which he summarizes the theoretical developments leading to the initiation of the current project.

Essential points are reiterated, risking redundancy to dispel obscurity. Step-by-step analytical derivations are omitted but complete references to material already published in the professional literature are given. A number of papers resulting from work done under this contract will also be published, and the results and significance of these papers are also discussed in this report in Chapters 1 and 2. No justification for the interest in particulates in the atmosphere is given since abundant articles on the topic have appeared in popular, professional and trade publications in recent years.

The majority of funds were devoted to the experimental program which involved the construction, testing, and use in flight experiments of an engineering model of a photopolarimeter (PPM) suitable in principle for satellite application. The instrument was constructed under sub-contract by the General Electric Space Center, Valley Forge, Pennsylvania in accordance with the breadboard design developed under an earlier sub-contract. Description of the PPM and detailed test reports are presented in the Appendix. Airborne experiments performed on board the Convair 990 (CV-990) stationed at NASA/Ames Research Center, Moffett Field, Ca. are reviewed in Chapter 3, together with additional discussion of the instrumentation.

Even though baloon experiments would have more adequately simulated satellite measurements, due to the altitude attainable, it was desirable to have adequate control over the target area selection which balloons can seldom assure. Since the aircraft measurements were not at the top of the atmosphere, it was necessary to make calculations applicable to intermediate levels of the atmosphere. Specific calculation relevant to the CV-990 experiments are presented with the data in Chapter 3.

Two major problems in the experimental program were a three-month delay in delivery of the PPM and delays in obtaining suitable flight dates on the CV-990. The three months would have been invaluable in assessing the behavior of the instrument and correcting the defects. The delays in flight time necessitated by commitment of the CV-990 to the Barium ion cloud (BIC) experiment postponed the UCLA experiment into a period which was undesirable in terms of obtaining both suitable weather and high aerosol concentrations. An additional month was lost due to an aircraft engine failure (and to frequent front passages in winter season). It was a matter of luck that the clouds cleared over the Mexican desert on the last days available for flight.

Theoretical progress was also delayed by the difficulty of finding someone at a post-doctoral level qualified to work on the theoretical problems. It was six months before Professor Sekera obtained the services of Dr. Jacob Kuriyan, who, within a short time, was making important contributions to the fundamental theory. (These contributions are discussed in Chapters 1 and 2.) At the same time, Dr. R. E. Bradbury took over management of the experimental program from Dr. N. B. Manson who left to accept an academic post in Great Britain.

Other personnel and their major functions were: Mr. R. D. Kopa, design review and inspection of the PPM engineering aspects and design and installation of the airborne scan platform; Mr. D. Friedman, interface electronics design and construction; Mr. J. Sherman, computer programming. The program is also indebted to Dr. L. L. Stowe who often acted in lieu of and as liason with Dr. Sekera though he was not directly supported under the contract. The contract provided partial support of Dr. T. Takashima's thesis work and the resulting computation of the internal field.

Though not directly supported by contract funds, the continuing work of Dr. N. C. R. Rao of the Meteorology Department (with the computational assistance of Dr. Takashima) is essential to the program since it demonstrates the usefulness of polarization measurements from the top of the atmosphere, and therefore is discussed in this report.

The contract called for the following five items to be discussed in the report:

1) A description of the analytical and experimental procedures for incorporating the effect of terrestrial surface reflection on the polarization of reflected sunlight.

2) A description of the analytical procedures for incorporating the effect of radiative transfer in a turbid atmosphere on the polarization of scattered sunlight emerging from the top of the earth's atmosphere.

3) An analysis of the performance of the engineering model together with a description of system operation.

4) A comparison of the analytical prediction of atmospheric aerosol profiles based on engineering model measurements to direct "in situ" measurements of aerosol size and vertical distribution.

5) A determination of the feasibility of conducting this experiment from an unmanned orbiting spacecraft platform.

At the initiation of the contract, the principal investigator pointed out that it would be impossible to complete the theoretical work within the time and money allocations of the contract, even if the problems mentioned above had not arisen. Indeed, if the five items above are not discussed in the depth or degree desired by NASA, sufficient support should be provided to continue the research during the period preceeding preparation and development for actual satellite flights.

Item 4 provides an excellent example. This item is totally satisfied by the discussion in Chapter 3, where comparison of the data with the theoretical curves for a Rayleigh atmosphere confirm the insignificant aerosol concentrations as measured "in situ." UCLA had predicted that it would be difficult to find significant turbidity and suitable cloud conditions during the winter, but despite NASA's promise that there would be no difficulty in obtaining flying time, a variety of conditions forced the flights to be postponed until December, 1971.

Items 1 and 2 are discussed in Chapter 1 and 2 to the degree permitted by the theoretical progress.

Item 3 is covered in detail in the appendix and in portions of Chapter 3. The result of the analysis of the performance of the photopolarimeter leaves no doubt that it is possible to construct satellite instrumentation capable of making high quality polarization measurements. It is also pointed out in Chapters 1 and 2 that several methods may be employed to determine the total atmospheric turbidity from such measurements. Particular attention is called

to Section 2.4.

This confirms the feasibility of conducting such experiments from an unmanned space platform, (though they may as well be conducted from a manned platform such as the space shuttle) thereby answering Item 5. Additional comments on Item 5 are made in Chapter 4. Any further detailed engineering analysis with respect to orbits, tracking, etc. should be contracted to a potential industrial satellite fabricator in preparation for carrying the experiment in space.

Simultaneously support for theoretical work at UCLA on a continuing basis should be initiated to construct a library of suitable models, investigate how much more information may be obtained from the measurements and devise more tractable computer programming methods to make extracting information from the measurements speedier and less costly.

## TABLE OF CONTENTS

# LIST OF TABLES

# APPENDIX

## LIST OF FIGURES

# DEVELOPMENT OF AN EXPERIMENT FOR VISIBLE RADIATION

## POLARIZATION MEASUREMENTS FROM A SATELLITE

By Zdenek Sekera and Richard E. Bradbury
Institute of Geophysics and Planetary Physics
University of California, Los Angeles

## INTRODUCTION

The Inversion Problem in Turbid Atmospheres. - Chandrasekhar
(ref. 1) has shown that, in a plane parallel atmosphere composed
of Rayleigh-type scatterers, the radiative transfer problem includ-
ing multiple scattering is soluble. The intensity and polarization
parameters of the scattered sunlight have been numerically evaluated
(ref. 2, 3, 4) and measured values of skylight polarization under
very clear atmospheric conditions agree with the theoretical values.
(ref. 5, 6, 7, 8).

Turbid atmospheres contain suspended particles which, because
of their size and form, do not obey the Rayleigh law of scattering.
This results in skylight polarizations which differ from those for
pure Rayleigh atmospheres, thereby opening a new way to study at-
mospheric turbidity. If the computation of the effect of the par-
ticulate matter were as easy as for a pure molecular atmosphere,
the determination of atmospheric purity and other related quanti-
ties would be a straightforward procedure. Unfortunately, this is
not the case; the law of scattering of light in a polydisperse
medium is much more complicated, and the determination of particulate
characteristics from optical measurements requires highly complex
and sophisticated procedures.

The main reason for this difficulty is that the characteristics
of scattering by particulates depends on many more parameters (e.g.,
particle number-size distribution, spatial distribution, etc.) than
can be measured. Consequently, it is impossible to use a direct
inversion method, i.e., direct computation with the observed quan-
tities alone as input data, such as is used in temperature deter-
minations from satellite measurements. Since direct measurements
of all the different parameters involved requires sophisticated and
tedious techniques yielding results which may be applicable only in
a limited region, it is necessary to resort to calculations based
on a pre-selected set of data, a so-called "model."

The selection of which parameters are of interest is obviously
determined by the purpose for studying the atmospheric turbidity,
and the larger the scale of interest, the more restricted is the
number of parameters. Fortunately, the physical processes in the
atmosphere considerably restrict the size ranges of the particles
and disperse products of local origin over a relatively small,
isolated area. The general characteristics of particles normally
responsible for turbidity over larger areas and throughout all

levels of the atmosphere are more or less known to the atmospheric physicist and he has at his disposal a rather restricted number of models. If the scattering behavior and therefore the polarization of light emerging from the atmosphere for his set or "library" of models has been calculated, he can determine the atmospheric turbidity by comparing the polarization measurements with his library and selecting from this the model that matches the data. This process will by no means be unique. The confidence in the uniqueness may be increased by utilizing measurements at a number of different wavelengths and requiring that the model calculation agree with the measurements at all wavelengths.

Since there are usually more parameters of atmospheric turbidity than equations from which they are to be determined using the polarization measurements, it is obvious that there is no other method available than that of the "library technique." No direct inversion method exists for the general case and most likely will never exist, the theory of radiative transfer in a general turbid atmosphere being untractable and too difficult for even the best existing computers.

The reasons for these difficulties are well understood and are due to the interaction of the incident radiation with the scatterer. If the interacting matter is an electromagnetic dipole, the resulting field of scattered radiation is quite simple (Rayleigh scattering). Complications appear and are augmented when adjacent dipoles are grouped into multipoles of various orientations to form particles of different sizes and shapes. The differing positions of these individual centers produce complex interference patterns becoming more bizarre with increasing particle size.

It is well known that the analytical theory of scattering by large particles is almost untractable and attempts have been made to solve only a few special cases (ref. 9). Fortunately, the effect of the shape of the particle decreases with its size and the cases typically encountered in atmospheric studies can be approximated well by treating the particles as small dielectric spheres and hence almost all mathematical analyses have treated aerosol scattering as Mie scattering.

The construction of libraries for entirely general cases is almost impossible; not only the computation of entries but the selection of entries corresponding to measured values, represents enormous effort even for the most modern facilities. (The problem might be likened to thumbing through a library card catalog arranged by author to find a call number matching one we have.) It is imperative to introduce further approximations, inevitably restricting the number of parameters or character of information which may be deduced from the polarization measurements of the radiation emerging from the earth's atmosphere.

2

In the following we will list some such approximations and the type of information which may be derived from them. We can begin with the case of a pure molecular (Rayleigh) atmosphere, for which (spectral) optical thicknesses are known or can be calculated. The corresponding polarization quantities can be found in existing tables or calculated by relatively simple and straightforward means. With a library consisting of such tables for specific wavelengths, (nadir) angle of observation and angle of solar illumination, we can compare the measured value of the degree of polarization with the computed value for the molecular atmosphere. Any difference indicates the presence of some kind of turbidity. By simple interpolation, we can determine the number of additional molecules (or the equivalent optical thickness) needed to produce the same polarization. The ratio of the two optical thicknesses, $\tau$observed/$\tau$theoretical may serve as a rather primitive measure of the atmospheric turbidity. This is, however, only a qualitative measure answering the question "Is the atmosphere turbid or not?" By more sophisticated manipulations with satellite polarization data, one can instead of a library technique, use a direct inversion method which yields either four independent values of the optical thickness if the earth's surface is fully absorbing (zero albedo) or two independent values of the optical thickness together with two independent estimates of the albedo for the case of Lambertian (isotropic, unpolarized) reflection (ref. 10). (The problem of the effect of ground reflection will be discussed in greater detail in a later section.)

If the direction or angle of observation is preselected, then the inversion is simplified. The optical thickness can be read from a simple diagram for any zenith angle of the sun. In Fig. (1-1) such a diagram is shown for the case when the polarimeter is directed toward the nadir. The methods discussed above are based on the simplifying assumption that the particulates in the atmosphere can be treated as molecules (or submicron particles) and their effect can be noticed only in the increase of the optical thickness of a pure molecular atmosphere. In this way, one may arrive at an "effective" optical thickness of a turbid atmosphere and although this measure is almost purely qualitative, it is surprising in how many problems it may be usefully applied.

For any more quantitative assessment of atmospheric turbidity one has to consider the characteristics and behavior of scattering by particulates that differs from molecular scattering.

The Forward Peak in Aerosol Scattering. - While in Rayleigh Scattering the polarization parameters (such as those introduced by Stokes, discussed in a later section) depend only on the scattering angle (between incident and scattered ray), they depend critically on the size in large particle scattering. Therefore, in the models of turbid atmosphere, size distribution of particulates in a unit volume, i.e., variation of the number-density of particles of a

3

given size, enters as a very important factor.

Size distribution of particulates in the atmosphere obviously depends on the origin of these particulates, and there is practically no limit on the number of different types that could be included in models of our library. Fortunately, for the natural aerosol, i.e., particulates originating in the atmosphere, the physical processes in the atmosphere are leading to a very reasonable guess of the form of the particle distribution, especially in haze or dust. The coalescence of the minute water or ice coated condensation nuclei is responsible for the increase of the number of submicron particles, while the sedimentation of micron and larger particles produces a sharp decline of the number-density of large particles. The resulting curve will then be bell-shaped with the maximum around $1\mu$. Such a curve can be approximated by a three-parameter one of the form $N(a) = N_0 a^\alpha e^{-ba^\gamma}$ where $N(a)$ is the number of spherical particles of radius a in a unit volume. The size distribution can then be characterized by only three parameters $\alpha$, b and $\gamma$.

The scattering characteristics of polydispersions with such distribution for a few selected sets of these parameters have been thoroughly discussed by Deirmendjian (ref. 11) who considered Mie particles with the above size distribution and by integrating over the size derived the polarization parameters of a unit volume of such polydispersions. In the dependence on the scattering angle (all these parameters are illustrated in several instructive pictures in his outstanding book of tables), one can notice a pronounced maximum in the forward direction, usually denoted as the "forward peak." The origin of this peak is the addition of the diffraction peak of each single particle in the considered volume. From this fact, all the characteristics of a forward peak follow, such as the larger the particles in the volume, the more pronounced the peak. Consequently, for a rain model the intensity of scattering is $10^3$ larger in the forward maximum than in a sideward direction. The forward peak is without any doubt the most important feature of the scattering by such polydispersions. This becomes even more obvious if the intensity or other parameters are plotted in a linear scale, as was done in Fig. (1-2) by Takashima (ref. 12) for two of Deirmendjian's models, and not in a logarithmic scale as is usually done. This forward peak is also the origin of the difficulties occurring in the evaluation of multiple scattering in a turbid atmosphere. If the elements of the phase matrix, defining the relation between polarization elements of the incident and scattered radiation, are developed in a Legendre series of the scattering angle, it is necessary to include a considerable number of the terms in this series in order to accurately reproduce the forward peak. The solution of radiative transfer equations reduced then to the same number of separate integral equations as the number of the terms in the Legendre series for the elements of the phase matrix. In this complicated procedure, truncating errors can easily shoot up to a magnitude rivaling that of the resulting value. Analogous

4

difficulties occur in the so-called "Monte Carlo" method. Here the intensities change their meaning into probabilities of photons, and in the case of a strong forward peak (of the order $10^3$ or higher) it is necessary to perform the computation with an abnormally large number of photons, if the statistics outside the peak are to give reliable results.

To surmont the difficulties of radiative transfer in a turbid atmosphere, it is quite appropriate to look for some simplification or suitable approximation. The fact that the forward peak is so pronounced and differs clearly from the scattering at other angles, leads naturally to the "method of separation of the forward peak." This method was applied first in the atmospheric problems by Romanova (ref. 13) who replaced the forward peak by a delta function. That, however, differs quite substantially from the actual intensity distribution in the forward region and since this peak contains the largest intensity, the approximation should be the best possible. Weinman (ref. 14) used a Gaussian distribution for a scattering function in a rain cloud, and gained surprisingly good agreement. Had he used another normalization constant, however, he undoubtedly would have gotten even better agreement. The forward peak of the dispersion or of a single particle can be approximated by innumerable ways more or less successfully. It is quite clear, however, that the best approximation will be obtained from approximations that are based on physical law. This has been fully demonstrated by a few unsuccessful attempts by students at UCLA. The physical background for successful approximations has been given by Saxon (ref. 15) who from Maxwell's equation derived an expression for scattered field as a combination of volume and surface integrals. These integrals were then evaluated by the K.W.B. method and Deirmendjian (ref. 16) has shown that the values of the intensity in the forward direction agree very well with the Mie values computed by Penndorf (ref. 17) (1955). With a slight numerical correction (including $X = 2\pi a/\lambda$) a complete agreement with Mie theory could be found in the entire range $3 \leq X \leq 100$.

This extraordinary agreement of the theory with Mie-calculation motivated us to continue the previous research and start the study of analytical approximation of forward peak with scattering of single particle approximated by the diffraction law well known to physicists before or derived recently by Saxon.
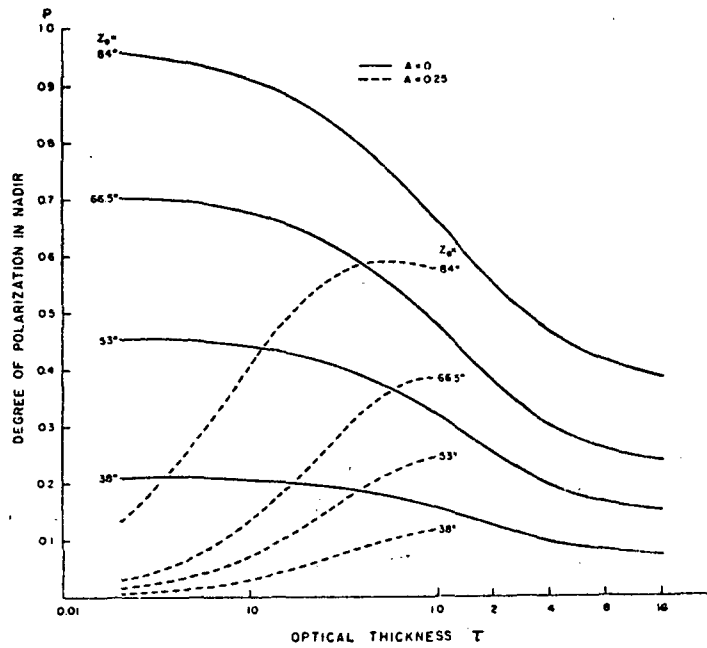
Fig.(1-1) -- Degree of Polarization of the Radiation Emerging from the Top of A Rayleigh Atmosphere.
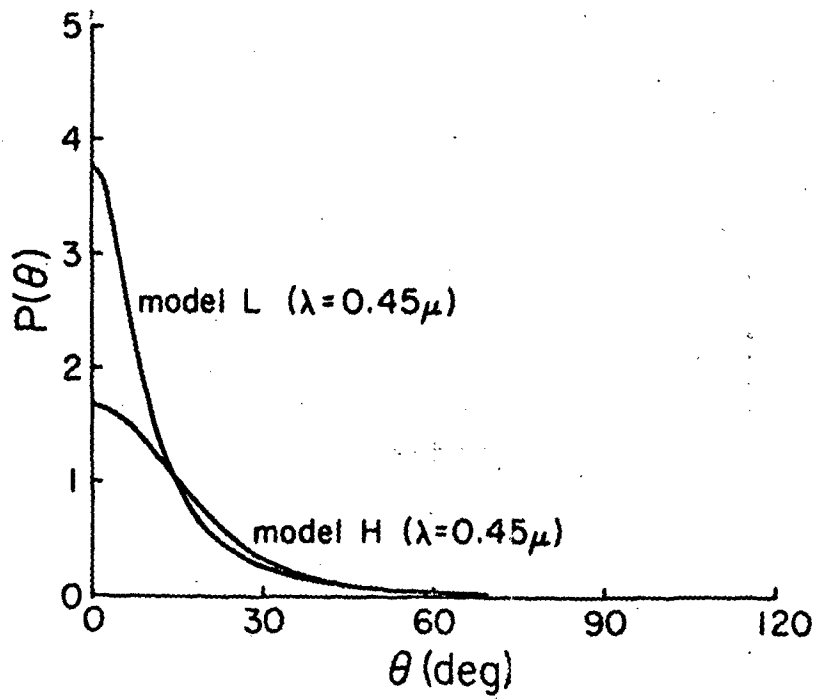
Fig.(1-2) -- Normalized Scattering Intensities of the
Two Aerosol Models (after Deirmendjian).

# 2.0 THEORETICAL PROGRAM

2.1 The Forward Peak Approximation and the Effective Size Distribution for Aerosol Scattering. - It was decided that obtaining an analytical approximation of the forward peak was the fundamental task of the theoretical part of this project and the first, therefore, to pursue. Following Deirmendjian's (ref. 11) notation, the elements of the phase matrix $P_i$ (i = 1, 2, 3) all indicate the forward peak, i.e., maximum at $\theta = 0$, with decrease toward the larger value of scattering angle $\theta$. As mentioned before, this feature is due to the addition of the diffraction peak of each single particle in the volume in question. Hence the analytical expression for $P_i$ for small $\theta$ ( < 10°) is the integral

$$P_i(\theta) = \int_0^\infty D_i(\theta, a)N(a)da \qquad (i = 1, 2, 3) \qquad (1)$$

where $D_i$ is the diffraction peak of single sphere of radius a, and N(a) - the weight function - the previously mentioned number-density, (number of particles of radius a in the volume) given by the so-called polygamma function, indicated before, with three independent parameters $\alpha$, b, $\gamma$. Among these parameters, $\alpha$ and $\gamma$ determine the size of the distribution, and b is related to the position of the maximum $(1/b = (\alpha/\gamma)a_{max})$.

The project director has shown that by simple change of variable the integral $P_i(\theta)$ can be transformed into a Laplace integral. In this way the existing tables of Laplace transformations, as well as the calculus associated with these transformations may be used for evaluation of the forward peak integral for large class of functions $D_i$ and of the parameters $\alpha$, b, $\gamma$.

A meaningful approximation in Eq. (2-1) will be obtained if the approximation used for $D_i(\theta)$ is valid in the region where the given size distribution N(a) is a maximum. This principle, stated for the first time by Kuriyan, contributed greatly to the success of our approximation of the forward peak. He considered first the Born approximation for $D_i(\theta, a)$ and found that this represented a good approximation if the weight function N(a) was vanishingly small for all $a > \lambda/2\pi(m^2-1)$, and $(m^2-1) < 1$. Almost all models that Deirmendjian labels as "haze" satisfy these conditions. On the other hand, the Fraunhofer approximation for $D_i(\theta, a)$ is valid in the range $2\pi a(m^2-1) > \lambda(m^2-1) \leq 1$. This would then apply more for the region of raindrops. The idea of different validity regions for the approximation of diffraction by a single particle has not been realized and applied before, and the success of the approximation discussed here as well as the explanation of a few failures by previous authors, should be attributed to Kuriyan's ability.

There are several ways to evaluate the integral in (2-1). They will be given elsewhere. If the expression for $D_i$ in the Born approximation is substituted in (2-1) in the integrand,

8

the square of the Bessel function $J_{3/2}^2$ is developed into a series and integrated term by term, one gets easily

$$\overline{P}_1(\theta) \equiv P_1(\theta)/P_1(\theta = 0) = \sum_{n=0}^{\infty} \frac{(-)^n (2,n)}{n! \, (4,n) \, (5/2,n)}$$

$$\frac{\cdot \tau(\epsilon + 2n/\gamma)}{\tau(\epsilon)} \qquad 2k \, (b/2)^- \, \sin\theta/2 \,^{2n} \qquad (2)$$

where $\epsilon$ $(\alpha + 7)/$ and, as usual, $k = 2\pi/\lambda$ ($k$ = wavenumber of the monochromatic radiation) $(a,n) \equiv \tau(a+n)/\tau(a)$, $\tau( \; )$, the Gamma function.

For an integer $\gamma$, $\overline{P}_1(\theta)$ reduces to the general hypergeometrical function $_uF_v*$, that then for $\gamma = 1$ assumes the form $_3F_2$

$$\overline{P}_1(\theta) = {_3F_2}(2, \; \epsilon/2, \; (\epsilon+1)/2; \; 4, \; 5/2; \; -z) \qquad (3)$$

with

$$\sqrt{z} = 4kb^{-1} \sin\theta/2. \qquad (4)$$

For integer $\alpha$, $\overline{P}_1(\theta)$ in (2-3) reduces even further either to finite series or a closed expression. Hence, for $\alpha = 2$,

$$\overline{P}_1(\theta) = \frac{3z^3 + 16z^2 + 35z + 70}{70(1 + z)^5} \qquad (5)$$

For the other matrix elements we get for the Born approximation

$$\overline{P}_2(\theta) = \cos^2\theta \; \overline{P}_1(\theta); \; \overline{P}_3(\theta) = \cos(\theta)\overline{P}_1(\theta), \; \overline{P}_4(\theta) = 0. \qquad (6)$$

---

$$* \; _uF_v(p_1, \; p_2, \ldots, p_u; \; q_1, q_2, \ldots, q_v; z) = \sum_{n-0}^{\infty} \frac{(p_1,n)\ldots(p_u,n)}{} \; \frac{z^n}{n!}$$

In the expression for $\overline{P}_1(\theta)$ there is only one variable appearing, namely $z - 16k^2b^{-2}\sin^2\theta/2$. Hence all distributions for a given pair of parameters $\alpha$ and $\gamma$ have <u>the same form</u> of the forward peak or belong to the same curve. In Fig. (2-1) the curve $\overline{P}_1(\theta)$ as a function of $z$ is compared with the values of $z$ computed for various scattering angles from Deirmendjian's tables (22-23). The agreement is very good, even in a region where the intensity has dropped to 30% of the forward intensity ($\overline{P}_1(\theta) = 0.4$). The tables of Deirmendjian where $x - ka$ violates the Born criterion have been deliberately omitted.

The evaluation of the integral (2-1) for $\gamma \neq 1$ is very elaborate, although it can be done for any $\alpha$ and $\gamma$. It is interesting to mention that for $\gamma = 2$ the expressions in the Fraunhofer approximation contain as a factor $\exp[-\frac{1}{2}(ka_0\sin\theta)^2$, $(a_0 = b^{-2})$, Weinman's (ref. 14) empirical solution. That would then explain such a good agreement with Deirmendjian's data.

In the parametrization used by Deirmendjian for his polydispersions, namely $\gamma = \frac{1}{2}$, $1$, $2$, the theoretical expressions for the forward peak intensity $\overline{P}_1(\theta)$ are simple for $\gamma = 1$, but rather complicated for $\gamma = \frac{1}{2}$, leading to infinite series, the convergence of which still should be studied and established. The closed analytic expression can be applied to the haze H ($\gamma = 1$, $\alpha = 2$) but not for the haze of the type L and M, for which $\gamma = \frac{1}{2}$. Kuriyan has correctly pointed out that, since $\gamma$ enters in the exponent of the weight function, $\exp[-ba^\gamma]$, it may be possible by retaining $\gamma = 1$ to reproduce the basic features of the size distribution (within the limits of experimental error) that Deirmendjian obtains with $\gamma = \frac{1}{2}$ by simply changing $b$. This is quite justifiable because the experimental data are such that the curves for $\gamma = \frac{1}{2}$ and $\gamma = 1$ are barely distinguishable (especially in the critical region, i.e., near maximum particle concentration). Within this educated guess, Kuriyan has retained the values of the parameters $\alpha = 2$ and $\gamma = 1$ for all types of haze particle distributions and then has varied the parameter $b$ to reproduce Deirmendjian's results for haze types H, L, and M.

To illustrate such procedure for haze M, Kuriyan first computed from tables 12-16 (ref. 11) one value of $\overline{P}_1(\theta)$, say $p_1$, for fixed $\lambda$ and $\theta$ ($0 < \theta < 10^\circ$). From the analytic formula (2-3) he found a value $z$, say $z_1$, that corresponds to $p_1$. Since $\lambda$ and $\theta$ are fixed and known, he determined the new value of $b$, say $b_M$. This process had been repeated for a few points and the average value of $b_M$ obtained. With this value $b_M$ for all those $z$ values from $0 < \theta < 20^\circ$ from tables 12-16 $\overline{P}_1(\theta)$ was computed and compared with original Deirmendjian's values. Fig. (2-2) demonstrates such comparison and shows again that all these calculated points (from Mie theory) fall on the curve, showing that the analytical formula (2-3) for a H distribution (with a new $b_M$) reproduces in the forward direction Deirmendjian's exact phase matrix element for haze model M (with a

10

different b).  A similar analysis has been performed on the haze type L.  The new value $b_L$ that leads to the same point on the curve for haze L when computed from (2-3) with $\alpha = 2$, $\gamma = 1$, has been computed as before, and the resulting values of $\overline{P}_1(\theta)$ plotted in Fig. (2-3) in a curve that again represents a good approximation of Deirmendjian's computations (ref. 11), (Tables 19-26).

Summarizing previous discussions, we see that significant scattering properties of these different types of hazes can be described with good accuracy by using only one type, leading to a very simple analytical expression: $\overline{P}_1(\theta)$ in (2-3) for $\alpha = 2$ and $\gamma = 1$.  It is quite conceivable that an assembly of different objects could give rise to the same scattered field.  The unique size or shape of the constituent haze particles, however, cannot be concluded from these results.  It has only been established that, in the forward direction, the scattering can be related to one fundamental model characterized by the weight function (number density) $N(a) \sim a^2 e^{-ba}$.  In conclusion, it should be mentioned that the formulae presented imply that in the forward direction the normalized phase matrix elements are only functions of one variable, $2k \sin\theta/2$.  This is, therefore, a necessary condition for the validity of an approximation.

This observation will help decide if the data points for $\overline{P}_1(\theta)$ can be approximated by our formulae.  For instance, if $\overline{P}_1(\theta)$ is plotted against $2k \sin\theta/2$, and if the points for various k and $\theta$ cluster around one curve, then the formula may be applicable.  If, on the other hand, the points are distributed randomly, then our formula is not applicable.  To illustrate this method we used Deirmendjian's haze M tables 1-15 where the wavelength varies between $0.45\mu$ and $16.6\mu$ and the real part of the refractive index varies in the vicinity of 1.3.  The scattering angle $\theta$ is restricted to be in the range $0 < \theta \le 30^0$ and the plot is made (see Fig. (2-4) of $\overline{P}_1(\theta)$ against $2k \sin\theta/2$.  The points, evidently, cluster around one curve and this reassures us that our approximation is a consistent one.
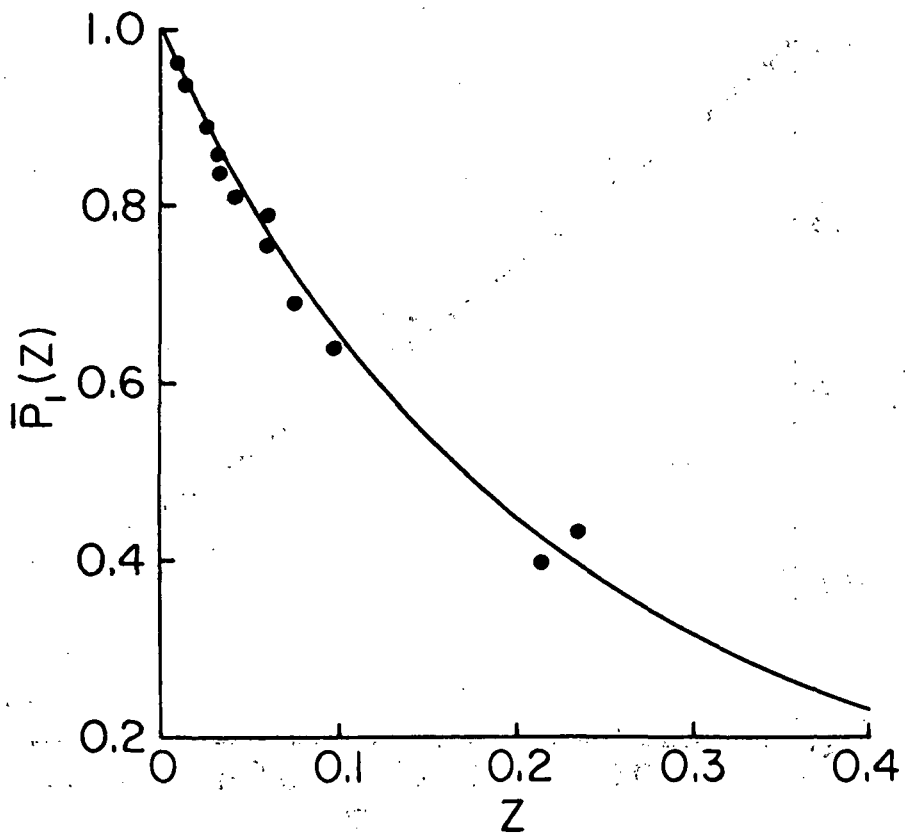
Fig.(2-1) -- Normalized Forward Scattering for Haze H as a Function of Z. Points are obtained from Deirmendjian's Tables 27-32. The curve is that of the analytic formula

$$\bar{P}_1(z) = \frac{3z^3 + 16z^2 + 35z + 70}{70(1+z)^5} .$$
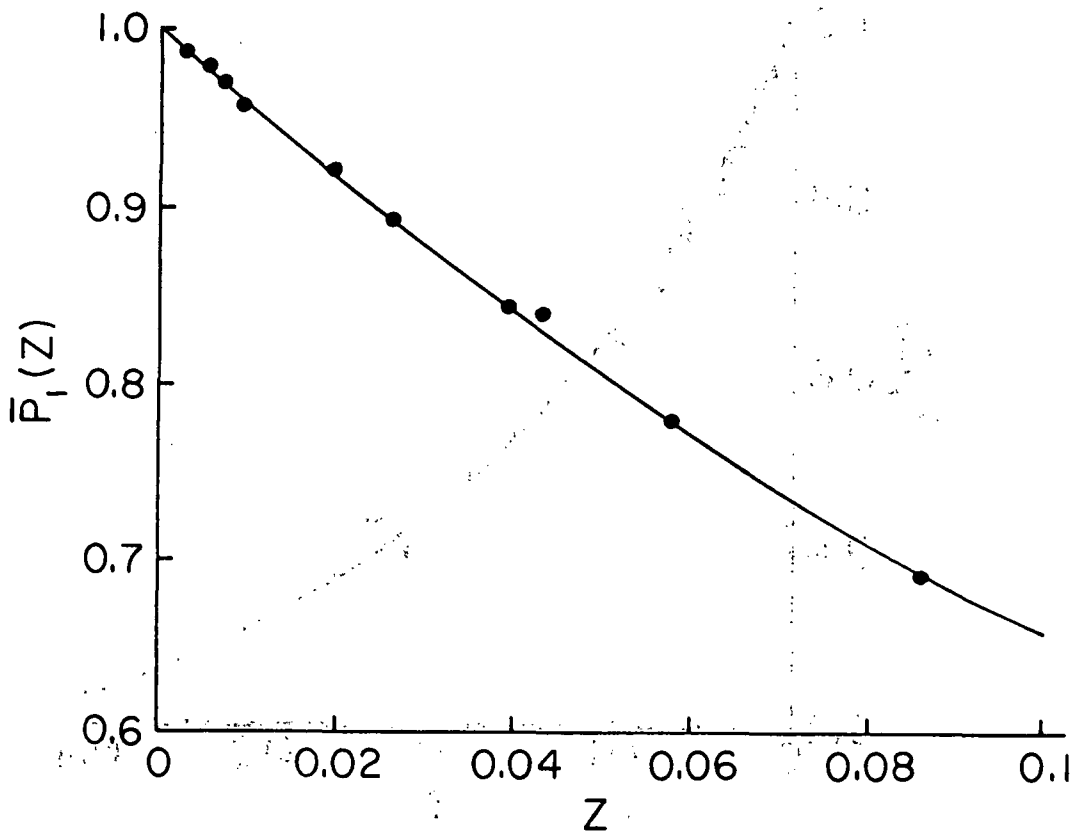
Fig.(2-2) -- Normalized Forward Scattering for Haze M as a
Function of Z.   Points are obtained from Deirmendjian's Tables
12-16, $b^2 = 8 \times 10^5$, $\gamma_8 = \frac{1}{2}$, $\alpha = 1$.   The curve is that of $\overline{P}_1(z)$
with new $b^2 = 7.4 \times 10^8$, $\gamma = 1$, $\alpha = 2$.

13
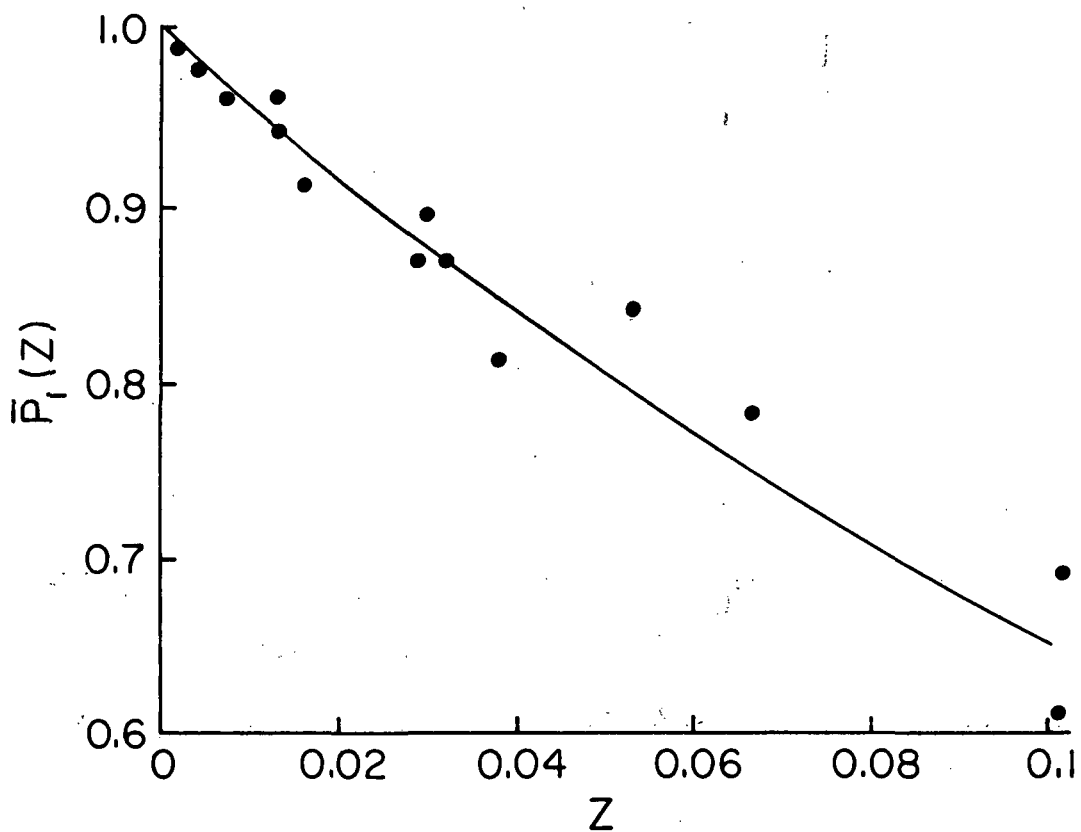
Fig.(2-3) -- Normalized Forward Scattering for Haze L as a Function of Z. Points are obtained from Deirmendjian's Tables 19-26, $b^2 = 2.3 \times 10^6$, $\gamma = \frac{1}{2}$, $\alpha = 2$. The curve is that of $\bar{P}_1(z)$ with a new $b^2 = 40 \times 10^8$, $\gamma = 1$, $\alpha = 2$.

$$\overline{P}_1(\theta)$$

$$2k \sin\frac{\theta}{2} \times 10^4/cms$$

HAZE M (tables 1-15)    $0.45\mu \leq \lambda \leq 16.6\mu$

Fig.(2-4) -- Normalized Forward Scattering as a Function of $\theta$.

15

2.2   Separation of the Forward Peak in the Radiative Transfer
Equations. -  As discussed in the previous section, it is possible
by using the Born approximation for the diffraction by a single
particle, and then integrating over the size range, to achieve not
only a very good approximation with Mie-theory, but also a useful
parametrization of the forward peak by reducing four parameters
(characterizing the size distribution) namely $N$, $\alpha$, b, and $\gamma$ to
only two, $N_0$ and b.  $N_0$ is related to the total number of particles
and b is related to the position of the maximum in number-density
of this distribution.  Hence, in our inversion scheme only two
parameters appear, $N_0$ and b, from which only the latter is needed
for the knowledge of the forward peak, the most important part of
aerosol particle scattering.  However, for longer wavelengths,
when k is rather small, it is easy to find cases where the validity
of the Born approximation applies throughout the entire range of
$\theta$ ( $0 \leq \theta \leq 180^\circ$) and thus the formula (2-3) gives $\overline{P}_1(\theta)$ accurately
for all scattering angles beyond the forward peak.

   It is easy to see from Deirmendjian's tables that this may
not be true for shorter wavelengths.  Then the method of separation
(truncation by Potter (ref. 19 )) of the forward peak can be used.
This is based on the favorable circumstance that the phase matrix
P appears linearly in the equation of radiative transfer and that
therefore it can be split into two parts (or more, if needed).
Let $P_f$ be the part of the phase matrix containing the "forward peak"
elements, given by the analytical expressions (such as (2-3)) and $P_w$
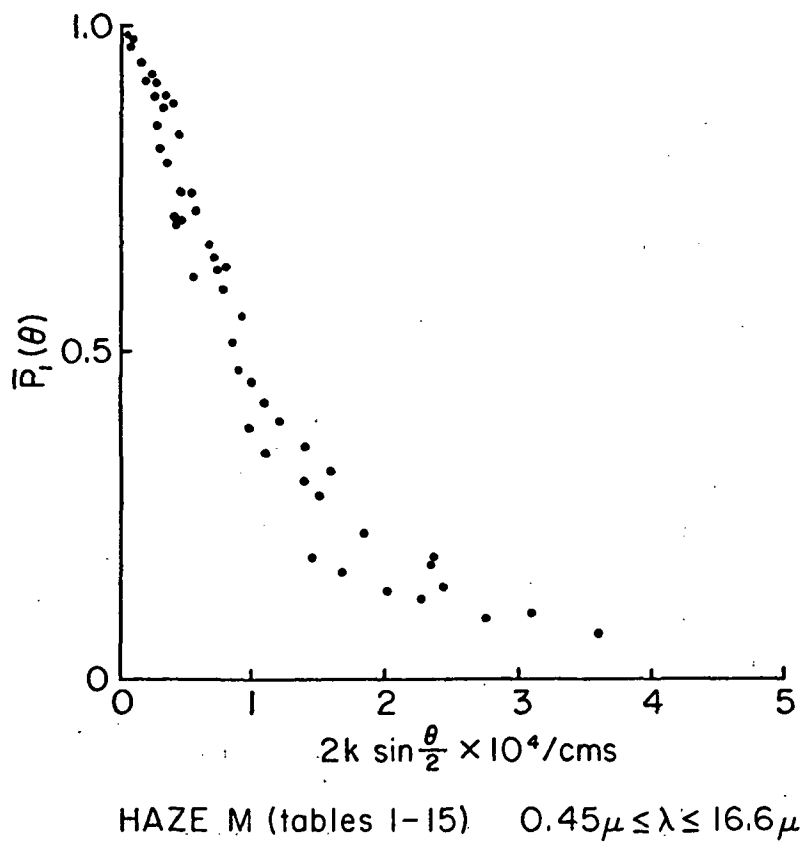the remaining part of the phase matrix such that $P = P_f + P_w$.  Since
the higher order terms in the Lengendre series for the matrix elements
needed for proper representation of the steep forward peak are in-
cluded in the first part $P_f$, the elements of $P_w$ will then be repre-
sented by a Legendre series of fewer terms, or they can even be
neglected with respect to the magnitude of the forward peak (see
Fig. (1-2).

   In addition, we can exploit another advantage based on the
linearity of equations of radiative transfer.  They can be split
into two equations, one containing terms related to the forward
peak's part of the matrix, $P_f$, and the other to the remaining terms.
Physically, the first equation defines the intensity and polariza-
tion parameters as observed after scattering in the forward peak
only.  This is the well-known aureole that an observer sees as a
bright ring around the sun.  The equation for the aureole, exten-
sively studied and described by Deirmendjian ( (ref. 11) p. 100ff),
can be easily solved with the expression (2-3).  The second equation
for the radiation field in directions off the forward direction
that remains after separating the equation for the aureole, retains
the form of the original equation, except for a new term that
represents the irradiation by the aureole.  This suggests that in
radiative transfer in a turbid atmosphere two sources appear:  The
sun ($10^6$ times brighter than the diffuse skylight) and the aurole
(in some cases up to $10^3$ times birghter than the skylight).

16

Although this equation will contain the phase matrix with elements which can be developed in much fewer terms, it is still mathematically very difficult to solve. Hence, the question arises of wheather it is necessary to solve these equations with different parameters for a "model library," or simply to replace the side-angle scattering by Rayleigh scattering with the same volume scattering coefficient. In such case only slight modification is needed of the computational scheme of molecular scattering based on the already existing tables. To compare these two methods, and to assess the accuracy of such an approximation is a considerable task. The time available in this contract has allowed us only to outline the basic principles of such an approximation.

2.3 Effect of Ground Reflection. - In order to avoid unnecessary complication, the assumption has been made in the previous text that the sky radiation transmitted by the atmosphere is completely absorbed by the earth's surface and hence is not reflected upwards. Unfortunately, this happens only under rather rare conditions and the effect of so-called ground reflections has to be taken into consideration and proper modification established.

For this purpose we need first to know the reflecting properties of the ground. These have been measured from an airborne platform, primarily the total amount of reflected energy from all directions - albedo or reflectivity. If the ground reflects according to Lambert's law, i.e., if the reflected radiation is isotropic (equal in all directions) and unpolarized, irrespective of the variation in intensity and the polarization of the incident radiation, such an albedo is all that is needed. For a more general case, it is necesary to introduce so-called bi-directional reflectivity, $R(\pi, \pi')$, that gives the reflected intensity in the direction $\pi$ in relation to the intensity of the incident radiation from $\pi'$. If we consider also the state of polarization of the incident and reflected radiation, then $R(\pi, \pi')$ has to be replaced by a 4 x 4 reflection matrix, in order to relate the polarization parameters of these two radiations. All these quantities have been measured by several investigators (ref. 20 and 21). The laboratory measurements indicated surprisingly similarity between different soil samples, and suggest that the ground reflection may be classified in several types that would considerably decrease its variability and facilitate simple parametrization. In radiative transfer theory the ground reflection can be introduced rather simply, as it was first done by Chandrasekhar ((ref. 1) p. 270 ff) as an additional source irradiating the atmosphere from below. Experimental studies of bi-directional reflectance were first started by Coulson (ref. 22 ), extended for polarization by Coulson (ref. 23 ) and Chen and Rao (ref. 21 ). Systematic studies of ground reflection in laboratories, and from airborne platforms have been conducted for several years by the UCLA radiation group under Professor Sekera's and Dr. Rao's direction with grants from the National Science Foundation, and a comprehensive article is being prepared for Advances in Optics.

17

Before closing this part, it should be mentioned that although the ground reflection adds a few new parameters to the "model library," these parameters differ in one point substantially from those related to atmospheric turbidity; except for seasonal changes, they are constant, and a few measurements under extremely clear conditions will be needed for their determination.

2.4 <u>Evidence for the Validity of the Proposed Inversion Method.</u> A cursory reader may question the possibility of determining from satellite observation the optical characteristics of the atmosphere. One must be aware that these observations are a consequence of complicated interaction of matter and radiation. In reality, satellite observations deal mainly with the reflection properties of the atmosphere. Ground based observations provide complementary information such as transmission properties of the atmosphere.

Chandrasekhar's theory of radiative transfer (ref. 1) and subsequent computations by other workers (ref. 20) established quantitative predictions of the diffusely reflected and transmitted light in a Rayleigh atmosphere. One reason for the deviations of experimental measurements from the theoretical predictions should be attributed to scattering by the particulates in a turbid atmosphere. Quite extensive skylight polarization measurements by the UCLA Radiation Group and others provided definite proofs that this was exactly so and that the observed deviations from the theoretical polarization of a molecular, Rayleight atmosphere are the most sensitive indicators of atmospheric turbidity. These classical, almost entirely qualitative determinations gave rise to the idea of changing them into quantitative ones, allowing estimates of turbidity parameters first from ground based and finally airborne or satellite observing platforms. Hence one should first look for the verification of the theoretical "inversion" method in ground observations. There are few such efforts, but one deserves mention in connection with the "forward peak" separation discussed above. Shortly after the polarization computations for a pure molecular atmosphere, and a dependable photopolarimeter became available, Dr. E. De Bary (ref. 25) performed an extensive series of skylight polarization measurements at UCLA with the intention of comparing the measurements of the polarization in the sun's vertical with the theoretical values. She found in a large number of days with moderate turbidity the curves of measured degree of polarization ran close to the theoretical curves, and substantial deviation appeared only near the sun. This fully supported the previously mentioned idea that the aerosol scattering in a turbid atmosphere can be well approximated by forward peak only, considering the off side scattering as Rayleigh scattering with properly modified scattering coefficient.

As another attempt, even more closely related to verification of the mentioned theoretical approach one should mention the work of Kevin Pang (ref. 25) who has applied the suggested method (ref. 10) of estimating the optical thickness of Rayleigh atmosphere from

satellite measurement to skylight measurements. Results of his measurements proved completely the correctness of this method and the theories on which it was based.

Finally, we should stress that careful measurements of the sun's aureole from platforms at different elevations are needed, not only to prove our forward peak analysis, but also to study the physically plausible invariance of particle size distribution in normal turbid atmosphere. Although it may seem that such analysis is irrelevant to the immediate goals of the contract, its value as a supporting study cannot be underestimated.

Under another program, sponsored by the National Science Foundation, several attempts were made to measure the polarization of underlying atmosphere and the disappearing effect of surface features from high altitude balloons. These polarization measurements made from elevation of 92,000 to 95,000 feet over the White Sand Desert resemble much more those from a satellite since the thickness and hence the effect of the atmosphere above the observation level can be neglected. Drs. C. R. N. Rao and T. Takashima undertook the difficult task of evaluating the amount of the aerosol particles and the Lambert reflectivity for several pairs of these quantities by matching the computation and observation in the sense of a "model library." This has been done under two simplifying assumptions, namely the "homogeneity" of turbidity (i.e., invariance of the ratio of the number of aerosol particles and the air molecules) and of the Lambert reflection. Both assumptions are to a great extent justified over a heated uniform desert. In Fig. (2-5) their results are presented in four wavelengths, the curves representing the computed distribution of degree of polarization in the sun's vertical, the dots are measured values. On each diagram two values are given, the so-called "turbidity factor" $T = (\tau_a + \tau_R)/\tau_R$ from which the total amount of particles can be derived, and the reflectivity A of the ground. The agreement of the computed and observed data are excellent not only in individual points, but also with respect to the identical run of the curves. A more convincing proof can hardly be found than that by a "model library" it is possible to find the fundamental parameters of a turbid atmosphere from satellite polarization measurements.

The proof of feasibility to determine turbidity parameters from polarization measurements performed at lower levels brings with it one difficulty, namely the knowledge of the Rayleigh radiation field <u>within</u> the atmosphere. The project director has studied the method of computation of the internal field of Rayleigh atmosphere and the corresponding paper, entitled "Evaluation of the Internal Field in a Plane Parallel Atmosphere from Diffuse Reflection and Transmission" submitted for publication to the Journal of Quantitative Spectroscopy and Radiative Transfer. T. Takashima worked out the computational programs and computed the degree of polarization for the elements of the Convair 990 experiment described in Chapter 3.

Computed values in Fig. (3-15) were plotted in dashed curves. Here again the reader must admit very good agreement with the measurements on a day with negligible atmospheric turbidity.

2.5 Other Applications of Polarization Measurements from a Satellite. - In addition to many applications where the same quantitative measure of atmospheric turbidity is needed (for example, transparency of the atmosphere for earth resources studies, effect of aerosol particles on temperature and humidity measurement (ref. 26), determination of ozone, etc.) there are problems when the knowledge of polarization may be successfully used. In all these applications it is not the diffuse reflection that is used for the analysis, but rather direct reflection with respect to the attenuation in the atmosphere.

As an example one can mention the reflection of sun's rays over large bodies of water (glitter) where the inclination of the reflecting wavelets can be easily determined from Fresnel's law, if the degree of polarization of the reflected ray is known. Since in this law the refractive index of the liquid enters in a significant way, the polarization studies can be extremely useful in detection of oil slicks and similar surface features. All these problems were discussed by several authors and will be summarized in the already mentioned comprehensive article being prepared for Advances in Optics.

The law of reflection on the crystalline features of ice particles is more complicated. This will produce polarization of moderate values allowing a very simple distinction between layers of ice and water clouds. Theoretical and experimental studies leading toward such distinction are in initial stages at the UCLA Radiation Laboratory as part of a grant from the National Science Foundation.

The application of polarization measurements from a satellite, mentioned above, are mere examples and do not exhaust all possible cases. Measurements of the polarization of light (of all wavelengths, from UV to IR) together with its intensity, will without any doubt be a necessity of the future, and judging from the overall and quite extensive interest in polarization problems by a series of Russian scientists dating from the last century (as may be seen from Rozenberg's (ref. 27 ) bibliography) we shouldn't be surprised if the new types of Russian meteorological or geophysical satellites were equipped with similar photopolarimeters as described in Chapter 3.
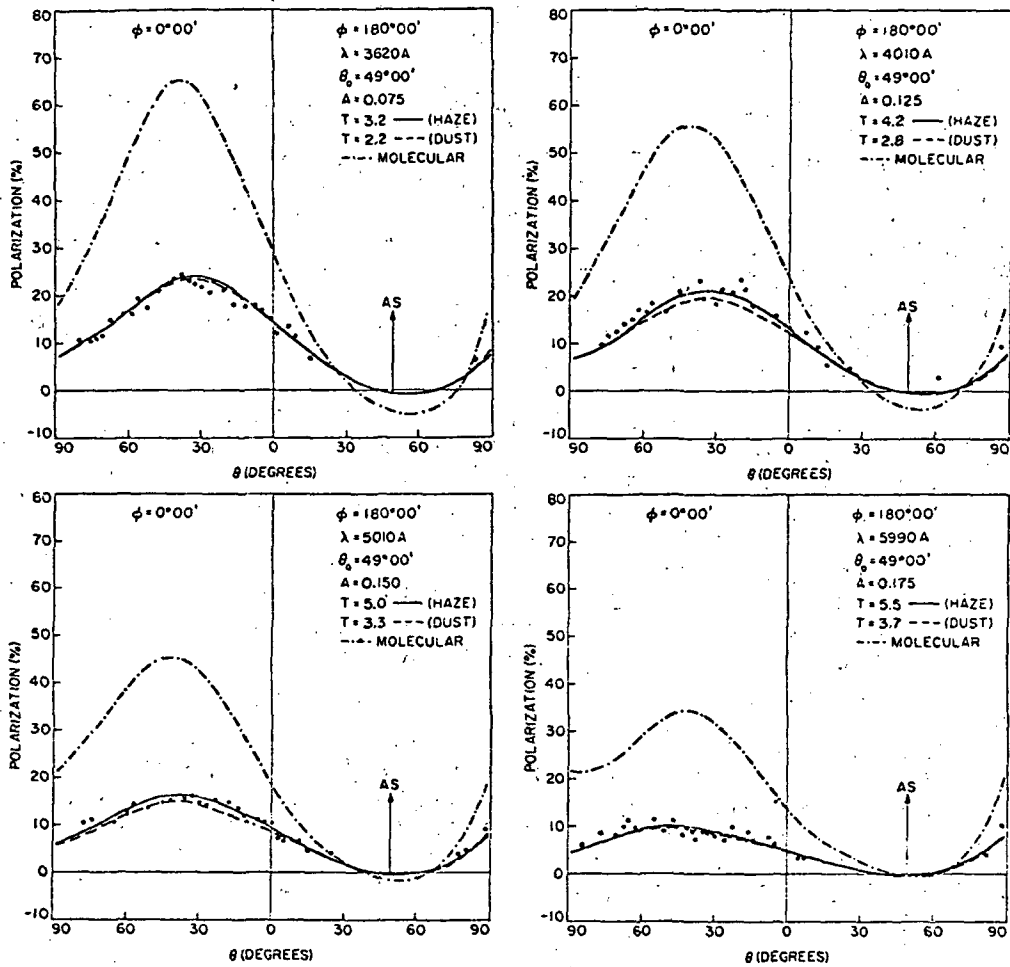
20

Fig.(2-5) -- Results of Polarimetry Studies over White Sands
from a Balloon at 80,000 feet at Four Wavelengths As Indicated.
See text for details.

21

# 3. THE EXPERIMENTAL PROGRAM

## 3.1 Description of Equipment and Experimental Flights

3.1.1 The Photopolarimeter and Associated Equipment. - To facilitate discussion of the practical aspect of gathering data and calibrating the instrument we present here a brief operational description of the system.

Operational Principles - The quantities that are to be measured are the so-called STOKES polarization parameters. These parameters are defined in the following way: If a polarized light beam passes through an analyzer with the transmission plane deviated by the angle $\omega$ from the vertical direction and then through a retardation plate, introducing a phase difference $\theta$ between the vertical and horizontal oscillations of the electric vector, then the intensity of light emerging from the retardation plate is given by the expression:

$$I(\varphi) = \tfrac{1}{2} \left[ I + Q \cos 2\varphi + (U \cos\theta - V \sin\theta) \sin 2\varphi \right] \qquad (1)$$

where I, Q, U, V are the STOKES parameters of the measured light stream. They completely define the state of polarization of the light stream, $I = I_\ell + I_r$ being the total intensity, $Q = I_\ell - I_r$, where $I_\ell$, $I_r$ are the intensity components in the vertical and horizontal direction, respectively. The inclination $\gamma$ of the plane of polarization (containing the maximum intensity component) from the vertical direction is given by Q and U, ($\tan 2\gamma = U/Q$). Finally V defines the ellipticity ($V/I = \sin 2\beta$, where $\beta = b/a$, the ratio of the minor and major semi-axis of the ellipse described by the end part of the electric vector). If the ellipticity is small and can be disregarded, as is the case in atmospheric scattering, the retardation plate can be omitted, and the state of linear polarization is given only by three parameters, I, Q, U. Then as it follows from Eq. (3-1) for $\theta = 0$, the measurements of I for three positions of the analyzer are needed for the determination of these parameters. This can be simplified even more if the measurement in one position is replaced by the direct measurement of the intensity (without analyzer). Such procedure has been applied in a new photoelectric polarimeter (PPM) proposed to be used in this experiment. The basic parts are three barrels (see Fig. (3-1)) one (barrel $\tfrac{1}{2}$ containing only a diaphragm filter of 50% transmission, the other two containing an analyzer in a horizontal direction (barrel B) and an analyzer inclined by $45°$ (barrel D). Substituting the corresponding value of $\omega$ ($90°$ for B and $-45°$ for D) in Eq. (3-1) we see that the parameters Q and U are obtained by subtracting the intensities from barrels B and D from the intensity in barrel A. The subtraction of these intensities is being done electronically. For this purpose, a barrel selector, placed behind the analyzer, has an opening arranged in such a way that, as it rotates, it lets consecutively pass through the light from

22

barrels A, B, A, D, A, respectively. By a proper adjustment, it can then be arranged that the voltages are measured directly proportional to A-B and A-D, i.e., to the STOKES parameters Q, and U. The light beams from the three barrels are collected, after the barrel selector, by fiber optics light guides that illuminate the same photodetector after a passage through narrow band filters in a filter wheel rotated by a Geneva mechanism. The speed of the rotation of the barrel selector and filter wheel is adjusted to give the measurements for all four filters in one second. In the fabricated model by Space Science Laboratory of General Electric Co., the fiber optics bundle has been bent back and the photodetector assembly mounted parallel to the barrels in order to reduce the length of the instrument.

Subsequent to delivery on July 17, 1971, it was discovered that the polarizing prisms were installed $90°$ from their prescribed positions so that $\omega$ is $0°$ for B and $-45°$ for D. This may be accounted for simply by making the inversion Q to -Q and U to -U.

SEMICONDUCTOR PHOTODETECTOR

SPECTRAL FILTER WHEEL

FIBRE OPTIC MIXER

BEAM SELECTOR WHEEL

FOCUSING LENS

3° FIELD STOP

GLAN THOMPSON PRISM

NEUTRAL DENSITY FILTER

OBJECTIVE LENS

1/2 BEAM

LIGHT INPUT

B BEAM

D BEAM

PREAMPLIFIER

PROCESSOR

A/D CONVERTER

DIGITAL RECORDER
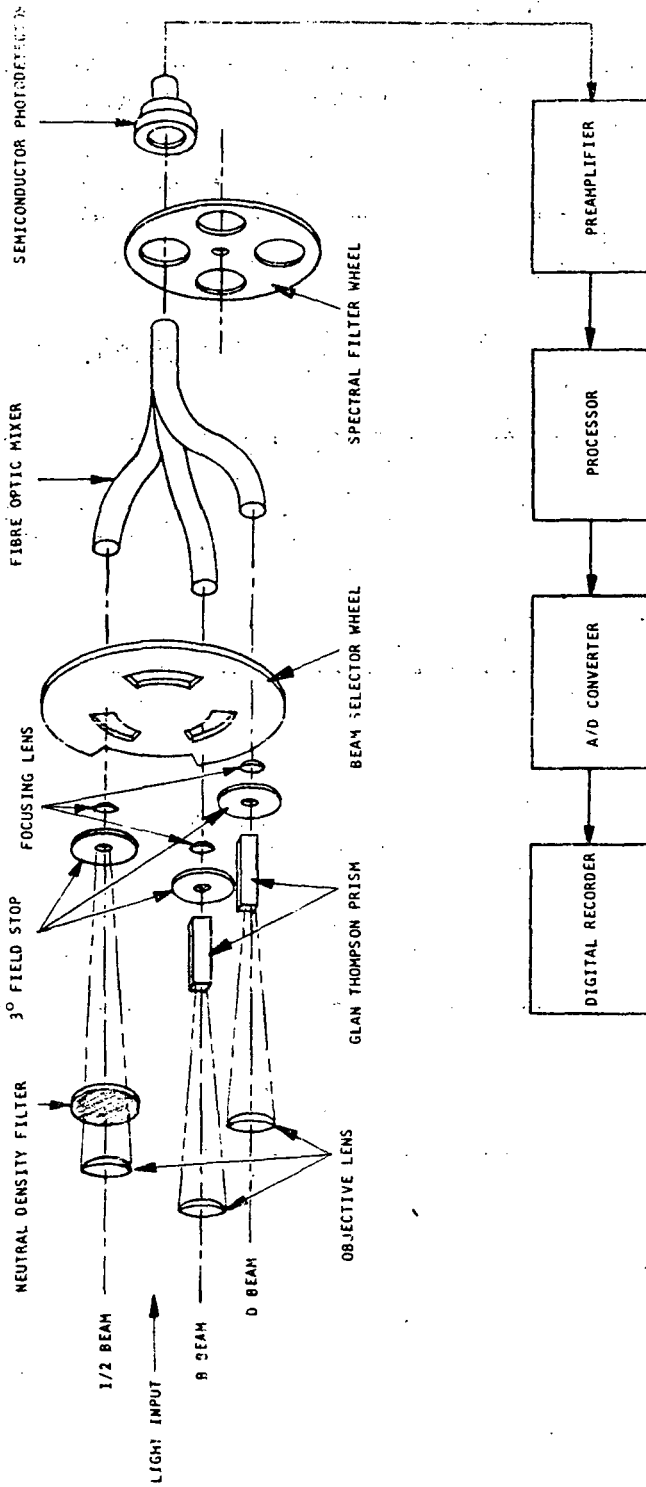
Fig.(3-1) -- Schematic of the Photopolarimeter and Data Recording System.

Table 3-1 -- Redundant Notation

Horizontal equivalents in the table below are used
interchangeably throughout this report.

| Old | New | Quantity |
|-----|-----|----------|
| I | $S_0$ | Intensity |
| Q | $S_1$ | Stokes Parameters |
| U | $S_2$ | |
| q | $b_0$ | Output voltages from photopolarimeter |
| u | $b_1$ | |
| I | $b_2$ | |
| Q/I | $\eta_1$ | Coordinates in $\eta$-plane |
| U/I | $\eta_2$ | |
| q/I | $\eta_1'$ | |
| u/I | $\eta_2'$ | |
| f | $f_1$ | Calibration (trim) factors |
| g | $f_2$ | |

Data Acquisition and Recording System. - The information from the photopolarimeter goes to the multiplexing system, which arranges it serially together with a voltage indicating the scan angle and a voltage indicating the temperature of the optical module. The signals are then converted to digital form and recorded on tape.

The beginning of a data cycle is indicated by a pair of pulses (referred to as the color pulses), one of which is generated by the position of the filter wheel and its "echo" generated from the first electronically. After the color pulses, the sequence is as follows:

$$q_1, \text{ gain, scan, temp,}$$
$$u_1, \text{ gain, scan, temp,}$$
$$i_1, \text{ gain, scan, temp,}$$
$$q_2, \text{ gain, scan, temp,}$$
$$u_2, \text{ gain, etc.}$$

The color channels are numbered from one to four in order of increasing wavelength. q, u, and i denote the values obtained directly from the instrument. The actual Stokes parameters (Q, U, i) are calculated by taking into account the measured "zero" levels and the instrumental trim factors (these latter quantities are determined by independent calibration).

Thus each complete cycle (1 second) contains 48 pieces of information. After 15 cycles, the time is recorded and a new block begins (The total block period is thus 16 seconds.) The basic computer program averages the scan angle and temperature for each Q, U, I sequence and calculates the corresponding degree of polarization and plane of polarization.

Calibration Factors - Formalisms. - In order to discuss the quantities that characterized the actual behavior of the photopolarimeter, it is necessary to introduce an extended notation. Results of attempts to measure the quantities discussed will be given in Sect. 3.1.2. The color channel will be supressed in this section, the results being applicable to all colors.

The Stokes parameters for the incident radiation are designated by $s_0$, $s_1$, $s_2$, and $s_3$, corresponding to I, Q, U, and V in the previous notation. The output voltages from the three barrels will be designated $b_0$, $b_1$, and $b_2$, corresponding to I, 2B, and 2D (see Table 3-1).

In this program it will always be assumed that $s_3$ = V = 0, so we will deal with the three component vectors

$$\bar{s} = \begin{pmatrix} s_0 \\ s_1 \\ s_2 \end{pmatrix} \quad ; \quad \bar{b} = \begin{pmatrix} b_0 \\ b_1 \\ b_2 \end{pmatrix} \quad , \text{ etc.,} \tag{2}$$

which are related by

$$\bar{b} = U\,\bar{s}$$

where U is a 3 x 3 matrix defined as the instrumental matrix. Ideally, U would have the form

$$U = \begin{pmatrix} 1 & 0 & 0 \\ 1 & 1 & 0 \\ 1 & 0 & 1 \end{pmatrix} \tag{3}$$

according to the instrument design principles. (We have taken into account the $90^o$ misorientation of the prisms here. (Note: In all that follows, the calibration of the I barrel is taken as unity.)

Since the three barrels do not have the same transmission characteristics, the ratio of transmission of the $b_1$ or $b_2$ barrels to the $b_0$ barrel must be taken into account. These are designated $f_1$ and $f_2$, respectively, and U then has the form

$$U = \begin{pmatrix} 1 & 0 & 0 \\ f_1 & f_1 & 0 \\ f_2 & 0 & f_2 \end{pmatrix} \tag{4}$$

The processor performs an operation represented by a matrix $\pi$ where the output $\bar{\nu}$ if given by

$$\bar{\nu} = \pi\bar{b} = \pi U\bar{s} \tag{5a}$$

where ideally,

$$\pi = \begin{pmatrix} 1 & 0 & 0 \\ -1 & 1 & 0 \\ -1 & 0 & 1 \end{pmatrix} \qquad (5b)$$

The calibration problem is to find the calibration matrix C such that

$$C = (\pi U)^{-1} = K^{-1} \qquad (6)$$

If $\pi$ and U have the ideal forms given by Eqs. (3-4) and (3-5) we have only two factors to determine for each color channel. K will have the form

$$K = \begin{pmatrix} 1 & 0 & 0 \\ f_1-1 & f_1 & 0 \\ f_2-1 & 0 & f_2 \end{pmatrix} \qquad (7)$$

and for C

$$C = \begin{pmatrix} 1 & 0 & 0 \\ -\dfrac{(f_1-1)}{f_1} & \dfrac{1}{f_1} & 0 \\ -\dfrac{(f_2-1)}{(f_2} & 0 & \dfrac{1}{f_2} \end{pmatrix} \qquad (8)$$

it is useful to define $\bar{\pi}$ by

$$\bar{\eta} = \frac{\bar{s}}{s_0} \qquad (9)$$

Since $\eta_0 = 1$ always, it is convenient to consider $\bar{\eta}$ as a two-component vector. The $\eta$- plane is the plane with $\eta_1$ and $\eta_2$ as coordinates, $\eta_1$ being taken here as the abscissa. Recalling

28

that

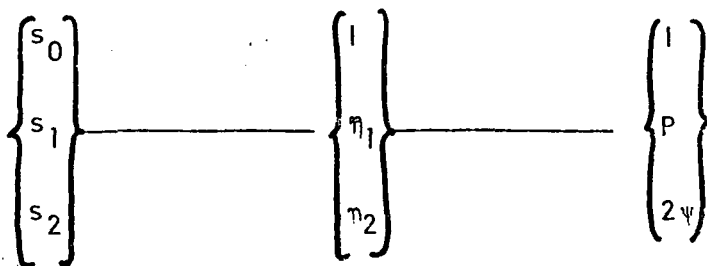$$P = \frac{\sqrt{s_1^2 + s_2^2}}{s_0} \qquad (10)$$

$$\tan 2\Psi = \frac{s_1}{s_2}$$

where P is the degree of polarization (which we will call simply "polarization") and $\Psi$ is the angle of polarization (measured clockwise looking at the light source), we then have

$$P = \sqrt{\eta_1^2 + \eta_2^2}$$

$$\tan 2\Psi = \frac{\eta_1}{\eta_2} \qquad (11)$$

Thus, in the $\eta$-plane the vector from the origin to a given point has a magnitude equal to the polarization, and the angle with respect to the abscissa is twice the angle of polarization. Thus P and $2\Psi$ are polar coordinates corresponding to the Cartesian coordinates $\eta_1$ and $\eta_2$ (Figs. (3-2) & (-3). We now have three equivalent forms for expressing the state of polarization of the light:

$$\left\{ \begin{array}{c} s_0 \\ s_1 \\ s_2 \end{array} \right\} \text{------} \left\{ \begin{array}{c} 1 \\ \eta_1 \\ \eta_2 \end{array} \right\} \text{------} \left\{ \begin{array}{c} 1 \\ P \\ 2\Psi \end{array} \right\}$$

For our purposes here, the latter two forms describing the behavior of the light in the $\eta$-plane will be most useful for discussing the calibration and behavior of the instrument. We have for example

$$\overline{\eta} = P \begin{pmatrix} \cos 2\psi \\ \sin 2\psi \end{pmatrix} \quad (= \overline{P}) \tag{12}$$

Consider the vector $\overline{\nu}$ defined analogously to $\overline{\eta}$ by

$$\nu \triangleq \frac{\overline{\nu}}{\nu_0} \tag{13}$$

and using Eqs. (3-5a)and (3-8)

$$\overline{\nu} = \overline{K} + K\overline{\eta} \tag{14a}$$

where

$$\overline{K} = \begin{pmatrix} f_1 - 1 \\ f_2 - 1 \end{pmatrix} \tag{14b}$$

$$K = \begin{pmatrix} f_1 & 0 \\ 0 & f_2 \end{pmatrix} \tag{14c}$$

It is convenient to maintain the same symbols for certain matrix operations in reducing to the $\eta$-plane description. There should be no confusion since different symbols are used for the state vector in the $\eta$-plane. The requirements for the reduction from the 3-d Stokes space to the 2-d $\eta$-plane of an arbitrary matrix

$$M = M_{i,j} \quad (i,j = 0, 1, 2)$$

is that

$$M_{0,1} = M_{0,2} \equiv 0 \tag{15a}$$

30

Then the 3 X 3 matrix operation is replaced by a 2 X 2 matrix operation.

$$M = M_{i,j} \qquad (i,j = 1,2) \qquad\qquad (15b)$$

plus a translation $\quad m = \begin{pmatrix} M_{10} \\ M_{20} \end{pmatrix}$

i.e., $s' = Ms$ $\qquad\qquad (15c)$

becomes

$$\overline{\eta}' = M\overline{\eta} + m. \qquad\qquad (16)$$

For successive operations,

$$\overline{s}' = NM\overline{s} \qquad\qquad (17)$$

on the Stokes vector we have

$$\overline{\eta}' = \overline{\eta} + N(m + M\overline{\eta})$$

$$= \overline{\eta} + N\overline{m} + NM\overline{\eta} \qquad\qquad (18)$$

on the $\eta$-vectors.  As an example, the product matrix CK from (3-7) and 3-8) becomes

$$CK \longrightarrow \overline{c} + C(\overline{k} + \overline{K}) = \overline{c} - \overline{c} + CK = \begin{pmatrix} 1 & 0 \\ 0 & 1 \end{pmatrix} \qquad (19)$$

(Note that if we had designated C as $K^{-1}$ we might be tempted to reduce

$$K^{-1}\overline{s} \Longleftarrow -\overline{k} + K^{-1}\overline{\eta} \qquad\qquad (20)$$

31

which would be incorrect.) (The validity of the assumption eq. (3-15a) will be discussed later. This implies that the reading from the 1-barrel is invariant to the polarization of the incoming light.)

Returning to Eq. (3-14), the form of K given is not general. We choose to write the general form as

$$K = \begin{pmatrix} f_1 T_{11} & f_1 T_{12} \\ f_2 T_{21} & f_2 T_{22} \end{pmatrix}$$

(21)

which is consistent with our definition of the f's. We will call

$\overline{\eta}$ = the state vector or "state" (or polarization vector);

$\overline{\nu} = \overline{k} + K\overline{\eta}$ = the output vector or "output";

$\overline{\eta}' = \overline{c}' + C'\overline{\nu}$ = the computed state vector or "computed state",

in order to distinguish the various vectors we will be dealing with. The last quantity defines a situation in which we are using an incorrect calibration matrix constructed analogous to C but using incorrect calibration factors.

Special Cases. - If the instrument is rotated about its axis while viewing a source whose polarization remains fixed during the time of rotation, the state vector $\overline{\eta}$ will move along a circle of radius P in the $\eta$-plane centered at the origin. For a $180^\circ$ rotation of the instrument, $\overline{\eta}$ will make one full transit of the circle and for a full $360^\circ$ rotation of the instrument $\overline{\eta}$ will travel twice about the circle.

If the instrumental matrix is not unity, the output vector will describe some different closed curve. (In full generalities the curve is required to close on itself only after two full rotations of $\overline{\eta}$.) We will now discuss how certain special cases affect what happens to the circle.

Case 1: $K_{12} = K_{21} = 0$. The expected case with no coordinate mixing but unequal barrel transmissions. From eqs. (3-14) and (3-12) we see that the curve generated by the output vector will have its center displaced by the vector K. There will also be an elliptical distortion of the circle.

The equation for this ellipse is

$$\left(\frac{b_1 - (f_1-1)}{f_1}\right)^2 \left(\frac{b_2 - (f_2-1)}{f_2}\right)^2 = p^2 \qquad (22)$$

Note that it is not necessary to determine the elliptical properties of the curve in order to determine $f_1$ and $f_2$, since these quantities are fully determined by locating the center. This suggests two methods of determining the f's:

a) <u>90° Intervals</u> - Taking a measurement at an arbitrary setting, rotating the instrument through 90° and taking another measurement. Then

$$\frac{\overline{b}(\psi_0) + \overline{b}(\psi_0 + 90°)}{2} = \left(\begin{array}{c} f_1 - 1 \\ \\ f_2 - 1 \end{array}\right) \qquad (23)$$

b) <u>Ring-A-Round</u> - (RAR) - Rotating the instrument through 360° continuously and graphically determining the center of gravity of the resultant data curve.

While these two methods are ostensibly the same, the first requires an accurate knowledge of the angle of rotation of the instrument. A variation of the first method was investigated in order to attempt to make use of in-flight data in determining the f's. This method which follows requires knowledge of the direction of polarization ($\psi$) but not the degree (P).

c) <u>Special angles</u> - When $\psi = \pm 90°$, $0°$ then from (3-12) and (3-14) we find

$$\left.\begin{array}{c} b_2(0°) \\ \\ b_2(90°) \end{array}\right\} = f_2 - 1$$

and if $\psi = \pm 45°$, $\qquad (24a)$

$$b_1(\pm 45°) = f_1 - 1. \qquad (24b)$$

This method requires an accurate knowledge of $\Psi$ since an error $\delta\Psi$ will contribute an error $P\delta\Psi$ to the measurement $(\sin\delta\Psi \approx \delta\Psi)$. On the other hand, since $\cos\delta\Psi \approx 1 - \frac{(\delta\Psi)^2}{2}$ , a more reliable value might be obtained from

$$\frac{b_1(0^O) + b_1(90^O)}{2} = f_1^{-1} \qquad (25a)$$

and

$$\frac{b_2(45^O) + b_2(-45^O)}{2} = f_2^{-1}. \qquad (25b)$$

If the angles are slightly off from the desired values but known, we would have to solve two simultaneous linear equations:

$$b_1(\Psi') = (f_1-1) + f_1 P \cos 2\Psi'$$
$$b_1(\Psi'') = (f_1-1) + f_1 P \cos 2\Psi'' \qquad (26a)$$

for $f_1$ and $P$, and

$$b_2(\Psi') = (f_2-1) + f_2 P \sin 2\Psi'$$

$$\qquad (26b)$$

$$b_2(\Psi'') = (f_2-1) + f_2 P \sin 2\Psi''$$

and $f_2$ and $P$.

As before, we would expect a better value for $f_1$ if $\Psi'$ and $\Psi''$ are near $0^O$ or $90^O$ and a better value for $f_2$ if $\Psi'$ and $\Psi''$ are near $\pm 45^O$, since the effects of errors in the angles would then be minimized.

Case II - Effects of prims misalignment (misorientation). We will show by a series of transformations that the general result of prism misalignment may be considered as a rotation in the $\eta$-plane plus an elliptical deformation.

The essential axes in real space are defined in Fig. (3-2). $(\eta_1)$ is primary reference plane of the instrument corresponding to $\Psi = 0$ plane of polarization. We label it $(\eta_1)$ since the corresponding vector in $\eta$-space will be along the $\eta_1$-axis. The prism of the B-barrel should have its transmission plane oriented along

34

$(\eta_1)$, but if it is misaligned we will label its error angle by $\beta$ as shown. The same statements apply for the axis $(\eta_2)$ and $\delta$ is, the error angle of the D prism.

The axis $(\zeta_1)$ is the bisector of $(\eta_1)$ and $(\eta_2)$, and $(\zeta_1')$ is the bisector of $(B)$ and $(D)$. In the $\eta$-plane, $\zeta_1$ is located at $2\psi = 45°$ and its conterpart $\zeta_2$ is at $2\psi = 135°$.

If the f's have been properly accounted for, we may assume them to be unity in what follows.

From Eq. (3-1) we see that the effect of error angles $\beta$ and $\delta$ on the output voltages is given by

$$\bar{b} = \begin{pmatrix} 1 & 0 & 0 \\ 1 & \cos 2\beta & \sin 2\beta \\ 1 & -\sin 2\delta & \cos 2\delta \end{pmatrix} \bar{s} \qquad (27)$$

or in the $\eta$-plane by (3-14a) with

$$K = T = \begin{pmatrix} \cos 2\beta & \sin 2\beta \\ -\sin 2\delta & \cos 2\delta \end{pmatrix} \qquad (28)$$

and k = 0.

If we reduce the data without properly accounting for T, then we will be plotting

$$\overline{\eta'} = T\overline{\eta}, \qquad (29)$$

i.e., our plot axes $\eta_1'$, $\eta_2'$, will not be identical with $\eta_1$, $\eta_2$, as desired and the curve generated in a rotary-type experiment will no longer be a circle. To see what effect T has, we first define

$$\epsilon = \frac{\delta + \beta}{2} \; ; \quad \gamma = \frac{\delta - \beta}{2} \qquad (30a)$$

and the inverse transformation,

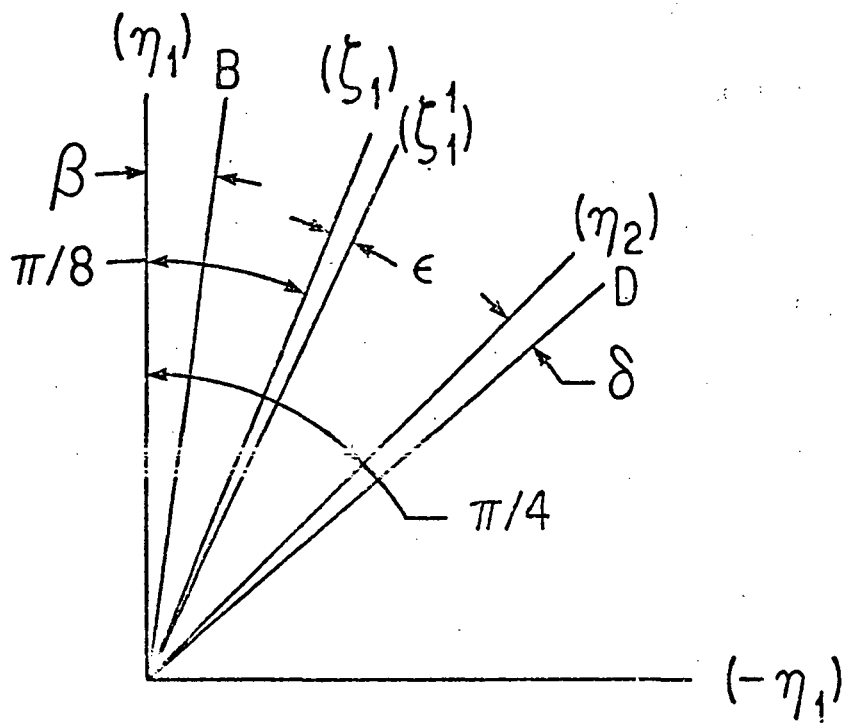$$\delta = \epsilon + \gamma; \quad \beta = \epsilon - \gamma \qquad (30b)$$

Fig.(3-2) -- Definition of Axes in Real Space
(See text for details).

and substitute Eq. (3-30b) into Eq. (3-28). Define the rotation matrix $A(\theta)$ by

$$A(\theta) = \begin{pmatrix} \cos\theta & \sin\theta \\ -\sin\theta & \cos\theta \end{pmatrix} \qquad (31)$$

we notice that T can be factored into

$$T = G(2\gamma)A(2\epsilon) \qquad (32)$$

where

$$G(2\gamma) = \begin{pmatrix} \cos2\gamma & -\sin2\gamma \\ -\sin2\gamma & \cos2\gamma \end{pmatrix} \qquad (33)$$

which we will call the deformation matrix.

$A(2\epsilon)$ is the rotation mentioned earlier; it remains to show the character of the deformation. We note that $G(2\gamma)$ is diagonalized by the transformation

$$G'(2\gamma) = A(\tfrac{\pi}{4})G(2\gamma)A(-\tfrac{\pi}{4}) = \begin{pmatrix} \cos2\gamma + \sin2\gamma & 0 \\ 0 & \cos2\gamma - \sin2\gamma \end{pmatrix} \qquad (34ab)$$

corresponding to the transformation

$$\zeta = A(\tfrac{\pi}{4})\overline{\eta}' = A(\tfrac{\pi}{4})G(2\gamma)A(-\tfrac{\pi}{4})A(\tfrac{\pi}{4})A(2\epsilon)\overline{\eta} \qquad (35)$$

Noting the inverse

$$\qquad (36)$$

$$G(2\gamma)^{-1} = \frac{1}{\text{Det } G'} \qquad G'(-2\gamma) = \begin{pmatrix} \dfrac{1}{\cos2\gamma + \sin2\gamma} & 0 \\ 0 & \dfrac{1}{\cos2\gamma - \sin2\gamma} \end{pmatrix}$$

37

or

$$G'(2\gamma)^{-1}\overline{\zeta} = A(\tfrac{\pi}{4})A(2\epsilon)\overline{\eta}. \tag{37}$$

Taking the magnitude of the vectors on both sides we have

$$\frac{\zeta_1^2}{(\cos2\gamma + \sin2\gamma)^2} + \frac{\zeta_2^2}{(\cos2 - \sin2\gamma)^2} = P^2 \qquad \tag{38}$$

recalling that the matrix $A(\theta)$ does not alter the length of a vector. We now see clearly that the circle is distorted into an ellipse with the ratio of major to minor axis given by

$$e - \frac{a}{b} - \frac{\cos2\gamma + \sin2\gamma}{\cos2\gamma - \sin2\gamma} \approx 1 + 4\gamma \quad \text{for } (\gamma \ll 1). \tag{39}$$

Rotating to the $\overline{\zeta'}$ system,

$$A(\tfrac{\pi}{4})\overline{\eta} = A(-2G)G'(2\gamma)^{-1}\overline{\zeta} \tag{40}$$

and finally

$$\overline{\eta} = A(-\tfrac{\pi}{4})A(-2\epsilon)G'(2\gamma)^{-1}A(\tfrac{\pi}{4})\overline{\eta'} \tag{41a}$$

or

$$C = A(-\tfrac{\pi}{4})A(-2G)G'(2\gamma)^{-1}A(\tfrac{\pi}{4}) \tag{41b}$$

giving the calibration matrix in terms of matrices already explicitly stated.

38

Case III: Non-specific component mixing. The case of a completely general form for K is applicable to the instrument in the scan platform housing, where the gross effect of the quartz window including reflections, and the instrumental optics must be accounted for. In general we would expect

$$K_{12} \ll K_{11}; \quad K_{21} \ll K_{22}.$$

From the form of Eq. (3-14a) we see that even in the most general case, method (b) under Case I is applicable for determining $\bar{k}$. Accounting then for $f_1$ and $f_2$, we have to determine the matrix T. While measurements at two known angles ($\Psi$) could determine the ratios $T_{12}/T_{11}$, $T_{21}/T_{22}$, $T_{11}/T_{22}$, we would have to know the degree of polarization in order to determine the individual values. In fact, if we take measurements at three known angles, the quantities which we can determine directly are

$$(f_1^{-1}), \quad f_1 P T_{11}, \quad f_1 P T_{12}$$
$$(f_2^{-1}), \quad f_2 P T_{21}, \quad f_2 P T_{22}.$$

The statement above follows from this.

Effect of Errors in the Calibration Matrices. - If the calibration factors used for computation are incorrect we will have

$$\bar{\eta} = \bar{c}' + C' \bar{\nu} = \bar{c}' + C'\bar{K} + C' K \eta \tag{42}$$

The center of the closed curve described as the instrument rotates about its axis is displaced from the origin by the vector

$$\bar{e} = \bar{c}' + C'\bar{k} \tag{43}$$

which becomes, using (3-8);

$$\bar{e} = \begin{pmatrix} \dfrac{f_1 - f_1'}{f_1'} \\[3em] \dfrac{f_2 - f_2'}{f_2'} \end{pmatrix} \tag{44a}$$

If the difference is sufficiently small, we can write this as

$$\bar{e} = \begin{pmatrix} \dfrac{\delta f_1}{f_1} \\[3em] \dfrac{\delta f_2}{f_2} \end{pmatrix} \tag{44b}$$

This leads to an uncertainty in P of $\pm |\bar{e}|$ . Assuming that K has the form of Eq. (3-7) letting $f - f_1 = \delta f$, we have

$$C'K = \begin{pmatrix} 1 - \dfrac{\delta f_1}{f_1}\ldots & 0 \\[2em] 0 & 1 + \dfrac{\delta f_2}{f_2}\ldots \end{pmatrix} \tag{45}$$

leading to an error in P of

$$\frac{\delta P}{P} = \frac{\delta f_1}{f_1} \cos^2 2\psi + \frac{\delta f_2}{f_2} \sin^2 2\psi. \tag{46}$$

40

Note that this error is proportional to P, while the effect above was not. Since P is always less than 1, the e term will always dominate the error, and for low polarization ( < 0.2) we can ignore this distortion altogether.

It is then possible to interpret the effect of this error by geometric interpretations in the $\eta$-plane (see Fig. (3-3)). As an immediate example, if we measure a value of P to be 0.10, but do not know our f's to better than 1%, then we have an uncertainty of $\pm14\%$ in P ($\delta P = \sqrt{2(\frac{\delta f}{f})^2} = \bar{e}$) or P = 0.10 $\pm$0.014.

3.1.2 Aircraft Installation. - Purpose of the Polarimeter Scan Platform - The scan platform serves a twofold purpose: (1) By facilitating the scanning motion of the polarimeter, it makes possible the taking of quasi-simultaneous measurements of the radiation field in several directions; (2) It provides means for aiming the polarimeter continuously on selected ground targets during the flight over the designated territory. Consequently, the important contribution of the ground reflection to the radiation field in the atmosphere remains an invariant function as seen by the polarimeter during the scan over the target area.

Furthermore, the scan platform (with the other aircraft instrumentation) provides means for a check on the accuracy of the determination of the polarimeter line-of-sight nadir and azimuth angles at different local sun elevations.

Scan Platform Design and Location of the CV-990. - The polarimeter scan platform described below was designed and constructed as an interface between the UCLA skylight polarimeter with a bore-sighted television camera and the experimental aircraft Convair 990. The design requirements were postulated as follows:

1) Full $360^\circ$ scan capacity.

2) Means for aiming the polarimeter on a target and TV recording of the target environment.

3) Provision of a pressurized and thermally insulated compartment for the polarimeter and the bore-sighted TV camera.

4) Streamlined shape of the exposed section to prevent any vibration due to aerodynamic forces.

5) Ability to withstand the aerodynamic forces at extreme flight-load factors of the aircraft

6) Electronic remote control of all functions of the system.

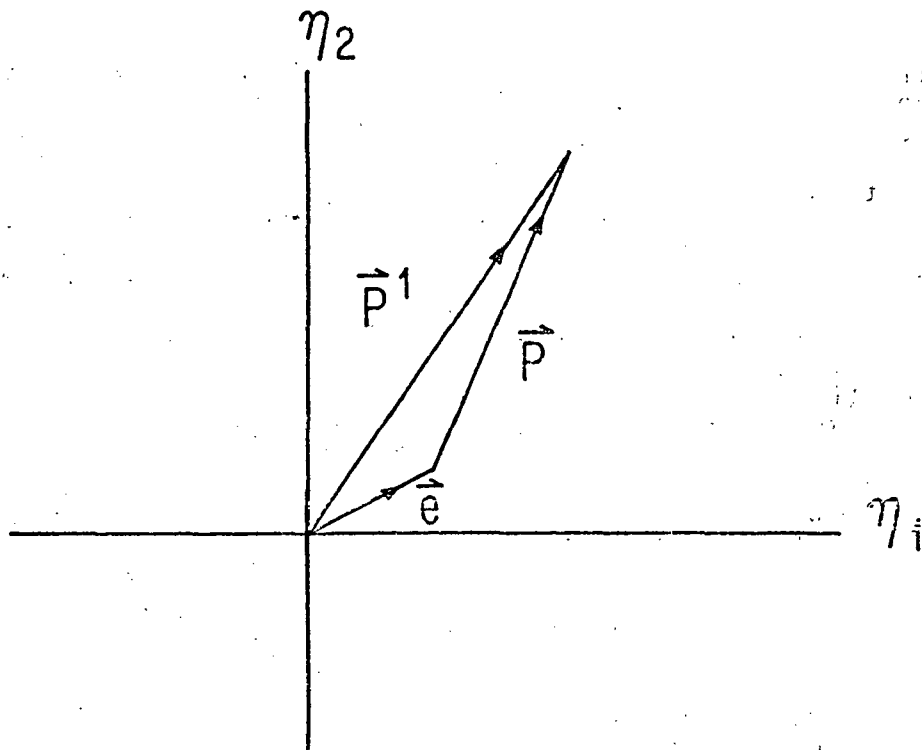7) Easy access to all parts for installation and calibration purposes.

41

Fig.(3-3) -- Effect of the Error Vector $\bar{e}$ in the $\eta$-plane.

In a previous experiment (ref. 28 ) (Grant No. 05-007-041) a polarimeter was located at the very end of the tail section of the aircraft. However, this arrangement did not satisfy requirement number 1, and because of considerable vibration of the aircraft structure in the tail section, requirement number 4 was not complied with either.

Several design arrangements were studied, proposed, and discussed with the NASA/Ames Research Staff. The design presented schematically in Fig. (3-4) was finally accepted, and the construction executed partially at UCLA and at NASA/Ames Research Center. The scan platform is installed on a "low-boy" supporting structure in the front part of the passenger cabin. It consists of an aluminum (6061-T6) alloy tube, 6 inches in diameter and 5 feet long, mounted between two special ball bearings on the supporting structure. To one end of the tube is attached an enclosure containing the primary electronics for processing of the electronic signals from the polarimeter. On the same end is also mounted a large gear connected by a link chain to a small sprocket of the scan drive motor (Fig. (3-5a)). An angular resolver (5 revolution pot.) is connected to the sprocket shaft. The scan drive motor is mounted on a spring-loaded plate, sliding between two guiding rails (see Fig. (3-5b)) in order to eliminate any slack of the link-chain. The other end of the six-inch tube penetrates through a side window of the passenger cabin and holds by means of a flange, a rotationally symmetrical streamlined fairing. A rotational seal, axially sliding on the six-inch tube, is pressed by the cabin air against the cabin window adapter plate. The polarimeter with bore-sighted TV camera is mounted inside a sealed and electrically heated compartment centrally located in the fairing. Four optical windows (one for each barrel of the polarimeter and one for the TV camera) sealed in the wall of the compartment transmit the radiation to the instruments. The shape and relative size (30 inches in diameter) of the fairing are apparent from Fig. (3-6). Another small, stationary fairing is mounted to the aircraft hull in close proximity to and downstream of the exposed part of the outside penetrating six-inch tube (Fig. (3-4)). As is apparent from Figs. (3-4) and (3-6), the scanning motion is in a vertical plane parallel to the center line of the hull of the aircraft.

Although the scan platform was explicitly designed for use on the Convair 990, its lightness makes it applicable for use on a smaller aircraft, helicopters, and balloons as well.

Scan Platform Control System and Instrumentation. - The scanning motion is provided by a motor-generator (CRS NC-100) and feedback servo-amplifier system (CRS NC-102). By means of a hand-operated potentiometer any scanning speed in forward or reverse direction can be set (constant and independent of the torque) between 0.1 to 100 degrees per second. The monitoring instruments and the electronic data acquisition system are mounted on a "high-

boy" standard instrument rack (Fig. (3-7)). The scan position indicator has scale calibration marks for scan zenity and nadir angles and also for $60^\circ$ backward from nadir positions. The scan speed indicator has scale calibration marks for initial target scan speed, sky scan speed, and return speed values. Two limit switches automatically stop the scanning motion when in either direction the polarimeter approaches horizontal forward (flight-oriented) position (Fig. (3-8)).

The polarimeter line-of-sight view is obtained by means of a bore-sighted TV camera (Sony ACV-3400) displayed on a TV monitor and simultaneously recorded on a video-recorder (Sony AV-3400) for later reference (Fig. (3-7)). The full monitor screen shows the TV camera field of view, and the small circle in the center indicates the polarimeter field of view. The angle of view of the polarimeter is $3^\circ$, while that of the TV camera is $12^\circ$. Therefore, an area linearly four times larger than the target can be surveyed and possible interference by, for example, nearby drifting clouds, identified. For the "sky scan," a neutral density filter (Kodak ND-4) is placed in front of the TV camera lens (Fig. (3-9)). This permits scanning in the sun-vertical "through the sun" without damage to the Videcon tube. This feature also facilitates a double check for accurate determination of the heading of the aircraft. During the ground (target) scan, a rotary solenoid is energized to swing the neutral density filter out of the light path. The sound track of the videotape serves for recording the comments by the flight coordinator or any member of the operating crew as well as for recording of time signals (WWV or from a separate tape recorder) for later identification of the video record with the corresponding data output from the polarimeter.

A rotary solenoid-operated shutter is mounted in front of the three optical barrels of the polarimeter for in-flight calibration (zero signal) check and for the elimination of unusable data which would be acquired during "in between measurements" periods (Fig. (3-9)). Also visible in Fig. (3-9) is a miniature blower which circulates the air (mostly dry $N_2$ supplied continuously from storage bottles) inside the instrument compartment in order to maintain uniform temperature of the instruments and to prevent fogging of the optical windows. The instrument temperature is monitored by means of a thermistor (attached to the body of the TV camera) and recorded multiplexed with the data output from the polarimeter. The temperature level is controlled by four-step switching of the current to the heating strips attached to the walls inside the fairing compartment.

A second auxiliary TV monitor is mounted on top of the instrument rack (Fig. (3-7)) to display the view of the target area as seen by a TV camera located in the nose of the aircraft. This camera is equipped with a remotely controlled zoom lens, and the displayed picture is helpful for identifying the target prior to

the initiation of the ground scan.

Testing and Calibration of the Aircraft Installation. - Upon
the assembly and installation of the scan platform, controls and
data acquisition system on the CV-990, a test flight was performed
to determine whether the scan platform was air-worthy and whether
the fairing affected the performance of the aircraft. Several
accelerometer and pressure pick-ups were placed inside the instru-
ment compartment and on the inside wall of the aircraft cabin in a
downstream direction from the scan platform. Analysis of record-
ings indicated appreciable vibration of the cabin wall, caused
probably by the turbulent flow between the fairing and the aircraft
fuselage. To eliminate this problem, the NASA engineers designed
and additional stationary fairing (Fig. (3-4)) mounted directly on
the window plates and extending from the six-inch tube to the
second window downstream of the scan platform. A second flight
test yielded results indicating an acceptable flow pattern in the
wake of the fairing. The scan platform and the instruments were
entirely vibration-free, as was also indicated by a completely
steady picture on the TV monitor screen.

The scan angle calibration was performed by means of a highly
sensitive precision water level attached to the polarimeter at
four positions of the instrument, as aiming at zenity, nadir, and
head or tail horizon. The calibration curve showed excellent
linearity and accuracy of readout to 0.1° (Fig. (3-10)). The
polarimeter electronics and data acquisition system as well as the
television circuit were tested for interference from the aircraft
power system. No effect on the polarimeter electronics and only
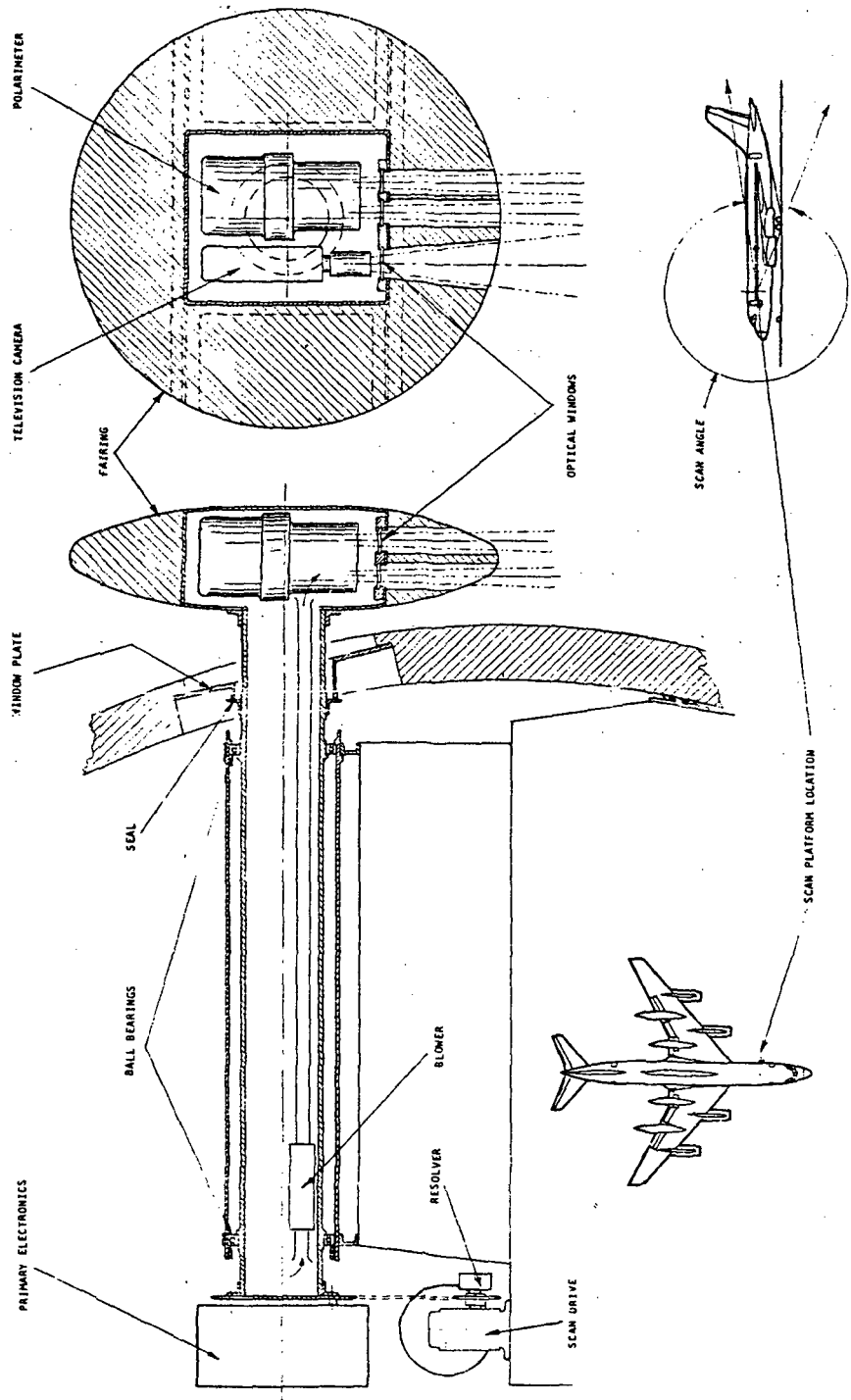a very slight effect on the TV monitor picture were noticed.

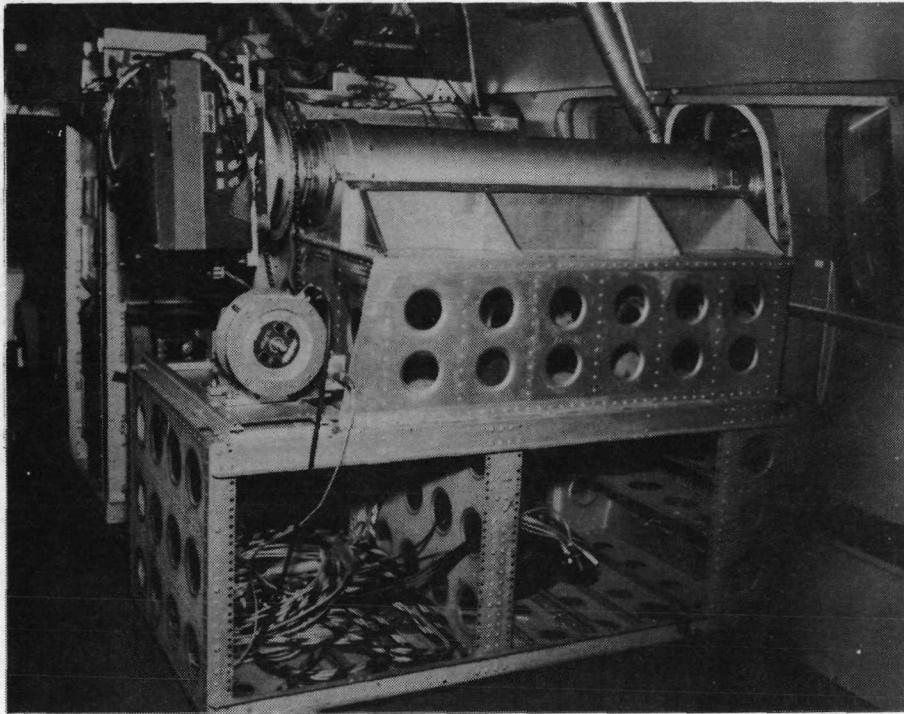Fig.(3-4) -- Schematic of Scan Platform Installation on the Convair 990.

Fig.(3-5a) -- Photograph of the Interior Part of
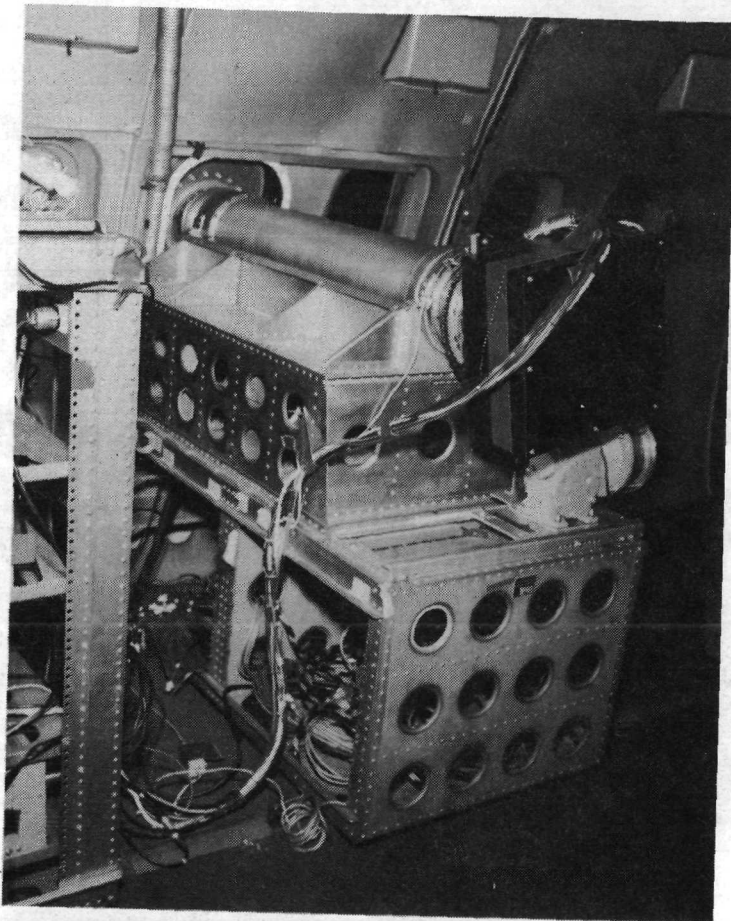the Scan Platform Installation from the Cabin End.

47

Fig.(3-5b) -- Photograph of the Interior Part
of the Scan Platform Installation from the Aft
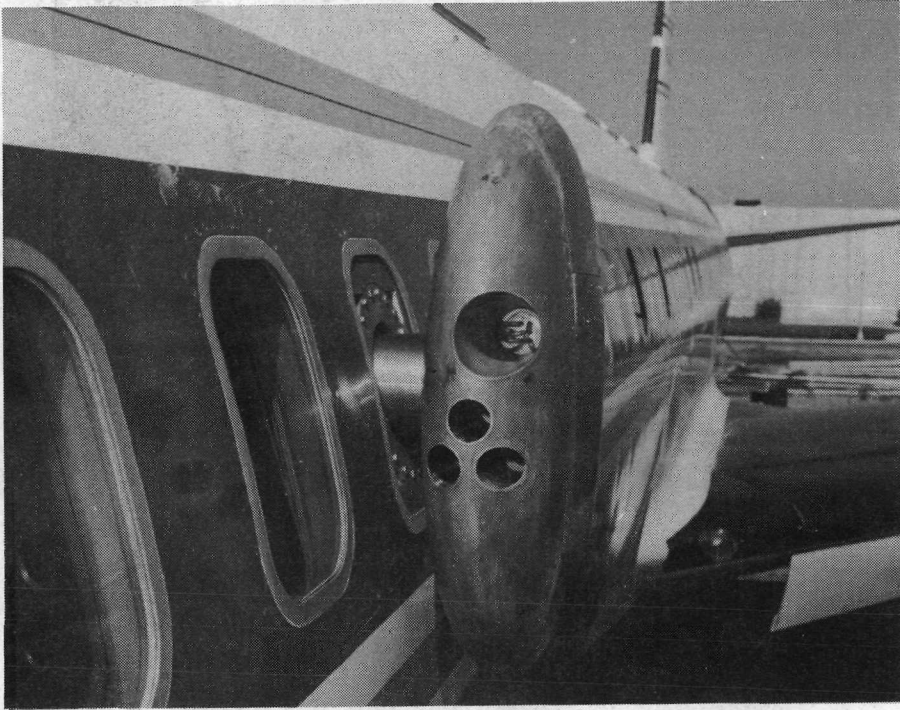End of the Aircraft.

Fig.(3-6) -- Exterior Photograph of the Scan
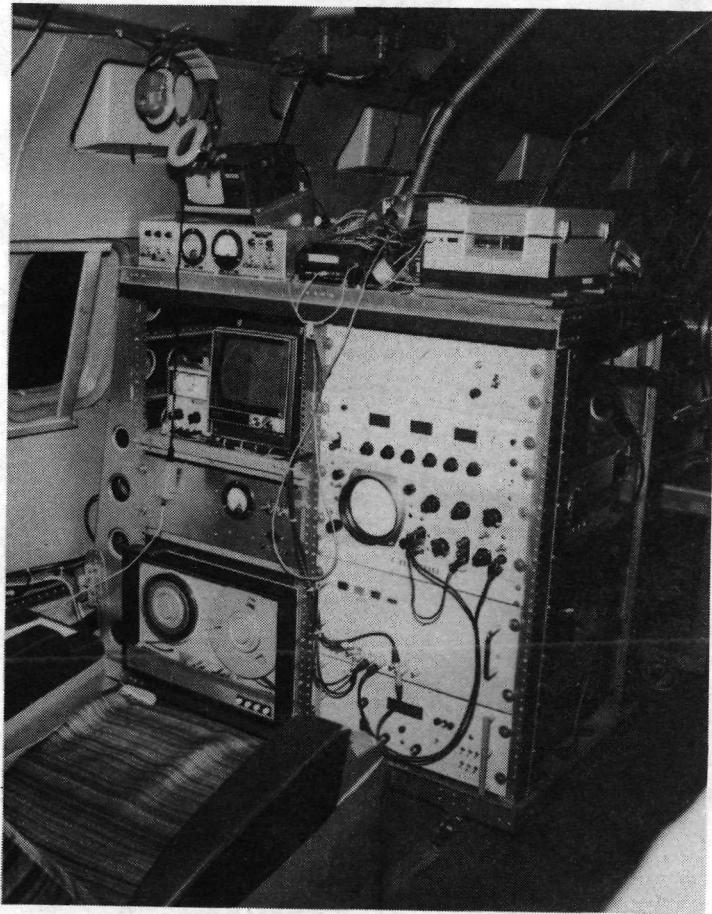Platform Installation on the CV-990.

Fig.(3-7) -- Photograph of the Instrument
Rack and Control Panels for the CV-990
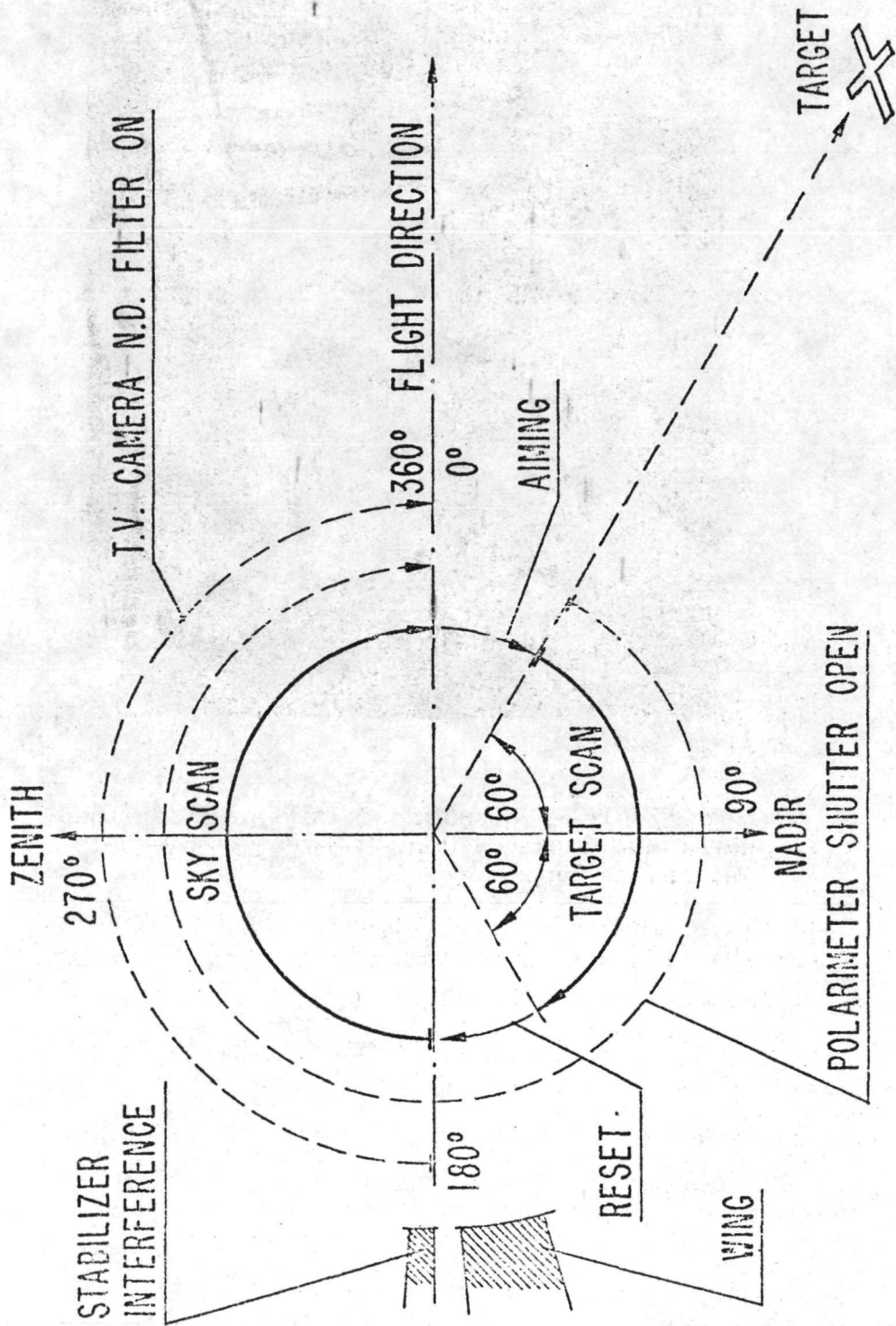Installation.

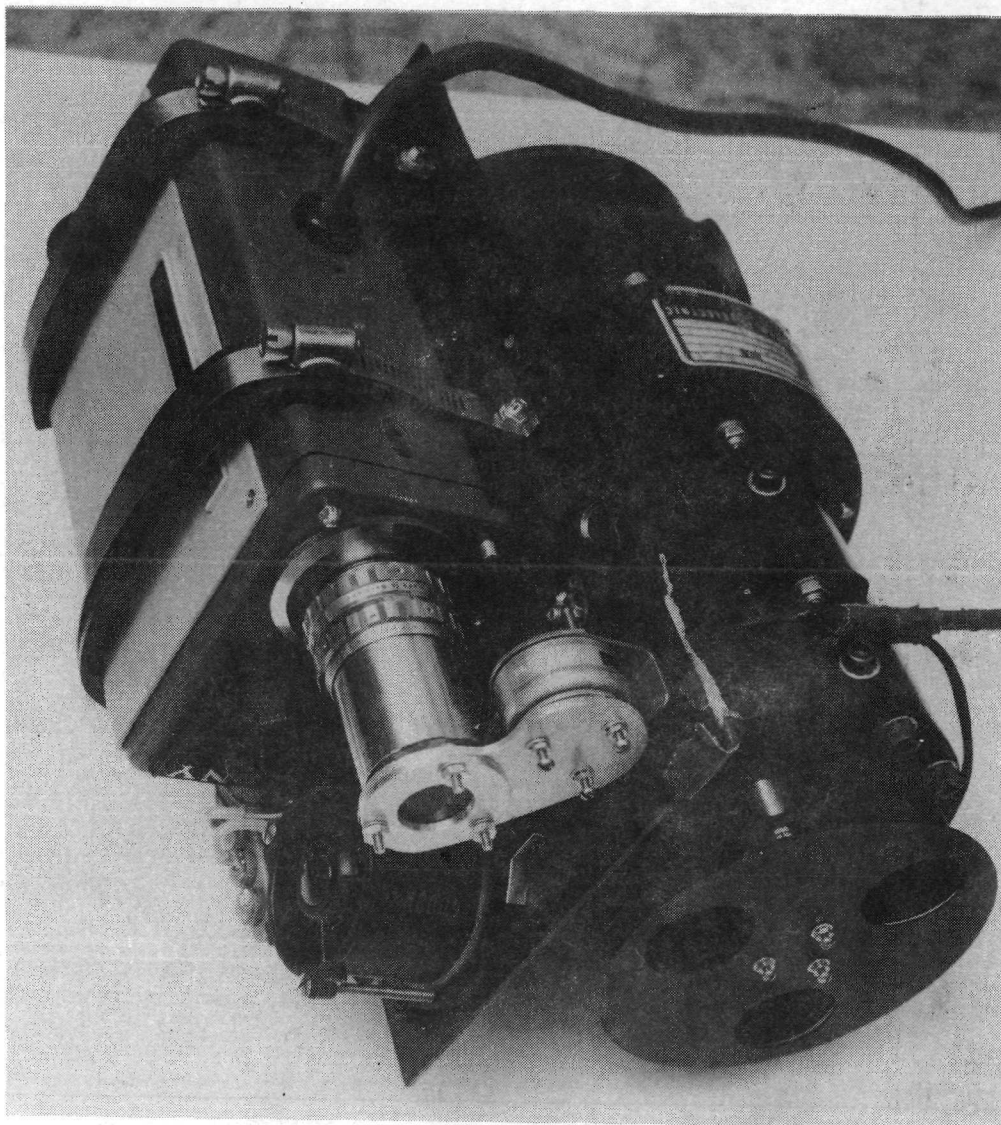Fig. (3-8) -- Schematic Defining Scan Angle and Regions of Scan.

51

Fig.(3-9) -- Photograph of the PPM-TV Camera Boresighted
Package. Note the shutter in front of the camera lens containing
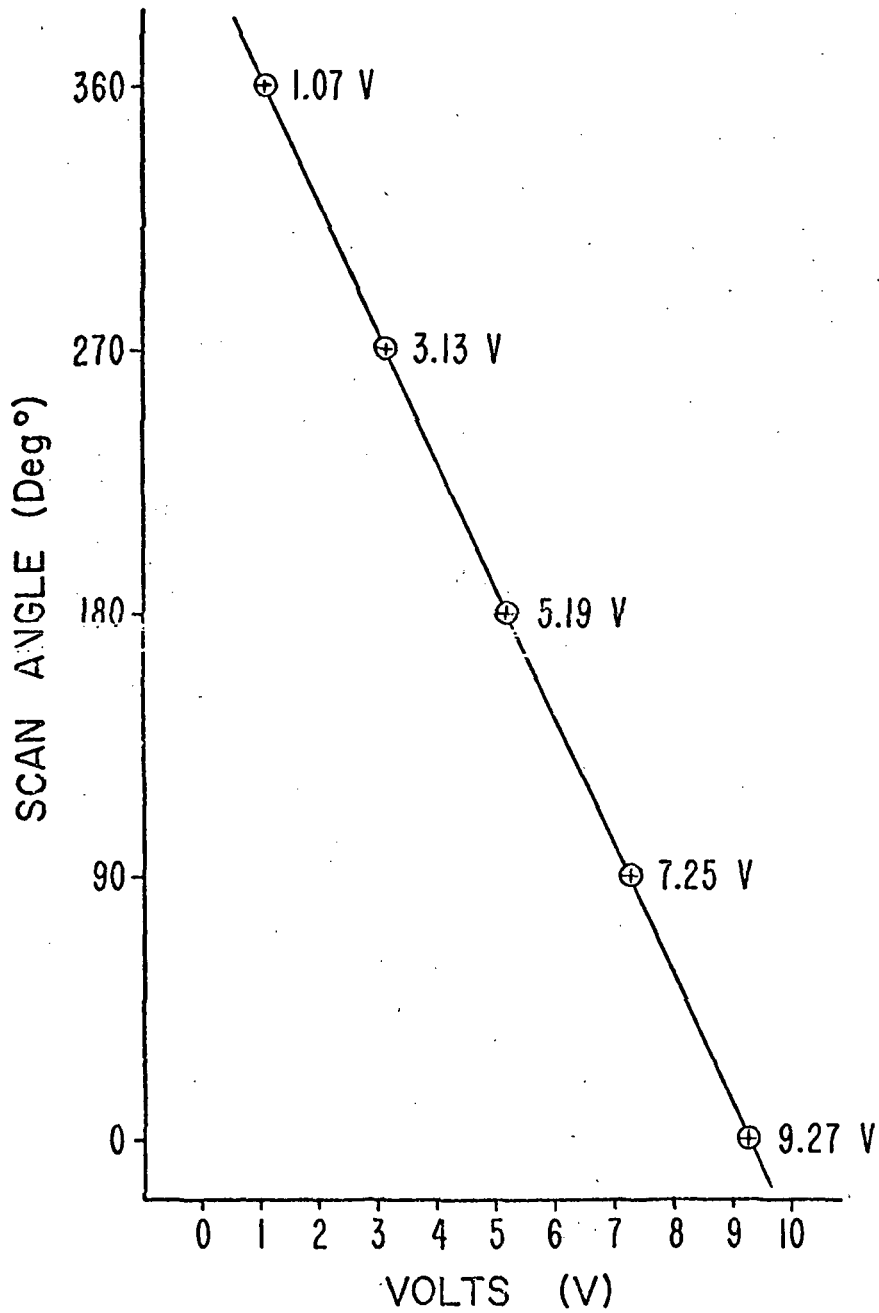an ND-4 filter to protect the vidicon tube.

Fig.(3-10) -- Calibration of Scan Angle Potentiometer.

53

3.1.3  Supporting Data Systems - Direct Sampling of Aerosol
(NCAR). - Direct sampling of the aerosol was carried out under the
direction of Mr. I. Blifford of the National Center for Atmospheric
Research), Boulder, Colorado.  Since previous commitments prevented
Mr. Blifford from being on the flights, his equipment was operated
by Mr. G. Dolan, also of NCAR.

The impactor used by Mr. Blifford has been described in the
literature and its installation on the CV-990 presented no diffi-
culties. (ref. 29 )  In addition, the NCAR workers installed a
filter collection system and an optical counter.  The optical
counter malfunctioned on the Carson Sink flight and despite Mr.
Dolan's efforts, remained inoperable throughout the rest of the
flights.  This instrument would have given a real time indication
of particle densities had it functioned properly.

After the flight the filters and impactor slides were returned
to NCAR for analysis.  The results are presented in Section 3.2.1.

Aircraft Support Systems. - NASA/Ames provided numerous services
and systems which were useful and/or indispensable in accomplishing
the experimental program.  This section does not present a complete
list, but only those which were essential for data reduction and
interpretation both during the CV-990 flights and afterward.

1)  ADDAS - The Airborne Digital Data Acquisition System on
the CV-990 consists of a Hewlett Packard 2116/B/2150B combination
of a general purpose computer with extender plus periphery equip-
ment.  The system was utilized to record the output from the preamp
as well as the scan voltage, etc., as a back-up data recording
system for the experiment.  The system records on a 9-track digital
magnetic tape 800 bpi at 37.5 ips.  Also recorded were the signifi-
cant aircraft parameter outputs from the INS (described below).  A
real line printout of selected aircraft data was made on a Nortec
200 lineprinter every 10 seconds (or during the ring-a-rounds, every
second).  The printouts were presented to us after each flight.
Duplicates of the aircraft tapes covering the time period of data
taking were also provided.

2)  INS - The Litton 51 Inertial Navigation System provided an
update every 1.2 seconds of the following aircraft and navigational
parameters:

| | |
|---|---|
| a)  distance to go | j)  ground speed |
| b)  time to go | k)  track angle |
| c)  cross back distance | l)  true heading |
| d)  desired track | m)  wind speed |
| e)  track angle error | n)  wind duration |
| f)  drift angle | o)  longitude waypoints |
| g)  align status | p)  latitude waypoints |
| h)  present position latitude | q)  roll angle |
| i)  present position longitude | r)  pitch angle |

The INS was also used to determine target acquisition (see Section 3.1.4).

3) Others - Ground-based computers at NASA/Ames were used to spot check the UCLA data tapes immediately after each flight. A belly camera recorded the terrain below during the flight. An on-board Visicorder was used for periodic real-time checks on the PPM preamplifier to verify that the equipment was operating properly.

Other Experimenters. - In addition to the NCAR direct sampling equipment, other experiments were on board and run on some or all of the flights:

1) Stratospheric Sampling Program - J. G. Poppoff, NASA-ARC.

2) Laser True Air Speed Program - R. M. Munoz, NASA-ARC.

3) Infra-Red Water Vapor Measurements - P. M. Kuhn, NOAA-APCL.

3.1.4  The Convair 990 Flights - Review of the Flight Program. -
The UCLA team participated in a total of five flights on the Convair
990 at NASA/Ames, four of which were prime flights for UCLA.  The
original schedule called for the flights to begin on November 16,
but failure of one of the aircraft engines forced a delay in the
schedule.  Simultaneously, a malfunction of the tape recorder was
detected and traced to an open winding in the head.  The tape
recorder was taken to the Kennedy Company for repair, then rein-
stalled on the CV-990.  A summary of the flights is as follows:

December 13, Carson Sink, Nevada. - This site was chosen for
a test site due to poor weather conditions and restrictions at
preferred target areas.  The first target site was abandoned when
low-lying cumulus clouds drifted over the site.  Scattered snow and
high winds at the higher altitudes made it difficult to track a
homogeneous target.

After the flight it was found that tape errors had developed
after about an hour of operation.  The tape was taken to the Kennedy
Company in Altadena for analysis and the following day the tape
recorder and A/D converter were taken to Kennedy, but no instru-
mental malfunction could be found.

December 17, Canada. - The equipment was reinstalled on the
CV-990 and the UCLA experiment rode piggyback with a stratospheric
sampling experiment in order to test equipment.  A test signal
box borrowed from Kennedy was taken along, and alternate recordings
from the test box and data system were made.  From this flight it
was decided that the errors were resulting from overheating of the
A.D converter circuits.  Simultaneously, the programmer came up
with a program to read the bad tapes, but running the program is
not only expensive, but consumes about an hour of supervision for
every minute of CPU time.

December 21, Great Salt Lake Desert. - Again low level clouds
moved in over the target area shortly after our arrival, but the
patterns were continued to test equipment and routines.  The A/D
converter was turned off when not in use and its ventilation improved.
A test also was made wherein the output of the photopolarimeter
processor unit was recorded on the aircraft analog recorder.  On
return to Moffett Field, the analog tape was played back through
the remainder of the UCLA system and transformed to the usual digi-
tal record.  This method was successful, pampering the A/D converter
was also successful and the other data tapes were error free.  The
ventilation was further improved by running a hose from the air-
craft's air conditioning system directly to the A/D converter.

December 29, Mexico. - The weather conditions cleared unexpec-
tedly and permitted a flight to the Mexican desert (Gran Desierto)
just south of Yuma, Arizona.  Again, high winds were encountered at
40,000 feet but the target area was homogeneous over such a large

region that the resultant drift is not expected to be reflected in the data (see Fig. (3-11)). The weather was exceptionally clear with neither cirrus above nor any clouds on the horizon. The horizon view indicated light haziness and the presence of an inversion northward.

December 30, Mexico. - Since weather conditions were much the same, the preceeding day's flight was repeated. Several high cirrus clouds were present over the target area and there was an obvious increase in haziness though it was still light. No cirrus clouds were observed to obscure the sun. The terrain of the Gran Desierto appeared exceptionally flat and homogeneous for an area of about 400 square miles and was superior in this respect to any areas overflown in the United States. For this reason as well as because of the difficulties already related, only data from the Gran Desierto flights have been reduced. These two flights are referred to as Yuma I and Yuma II, respectively, or Y1 and Y2, in the brief notation listed in Table 3-2.
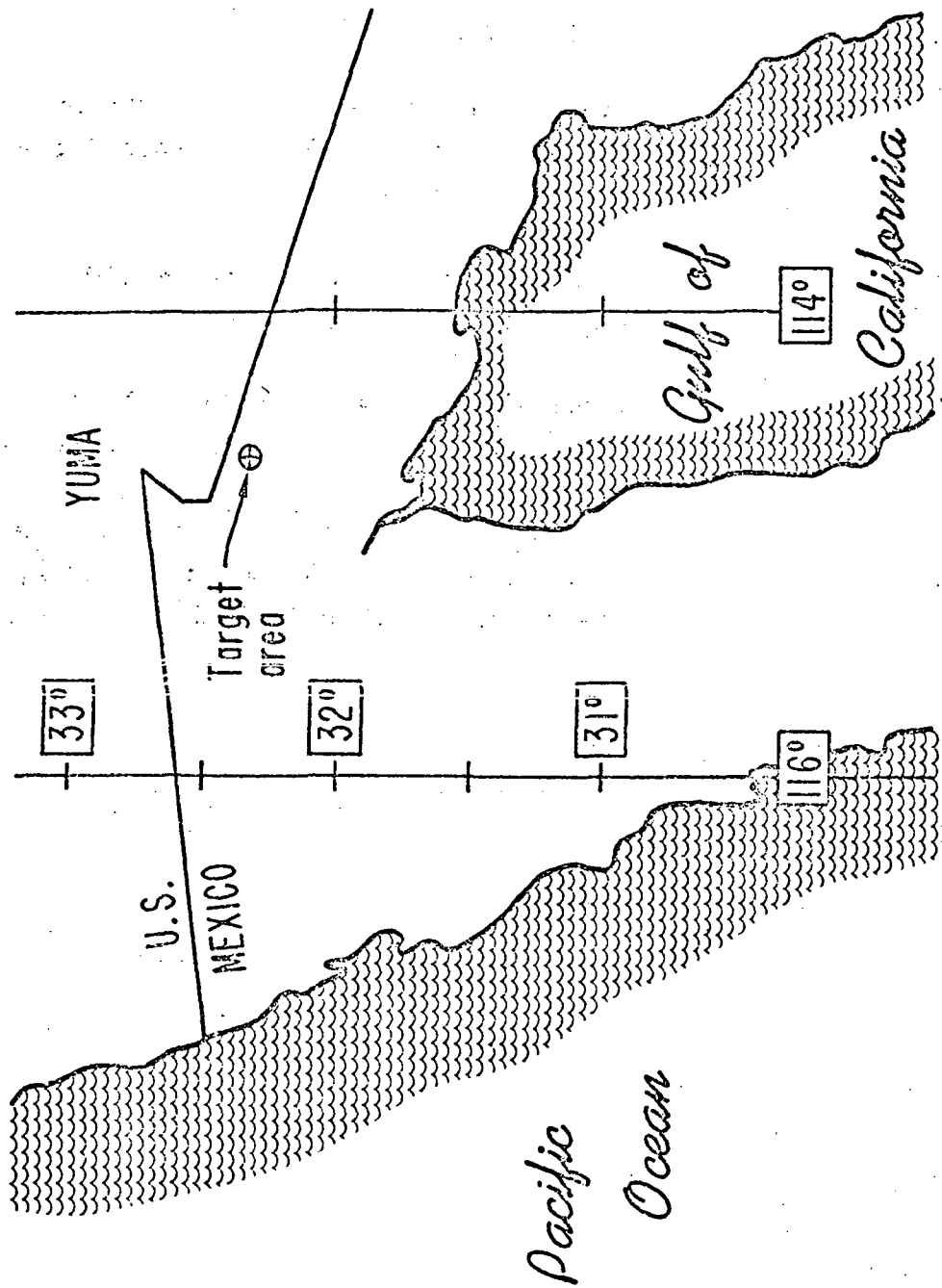
Fig.(3-11) -- Location of Target Area for Yuma I and Yuma II Flights.

Table 3-2     -- Key to Code or Brief Notation

| Symbol | Designation |
|---|---|
| Y1, Y2 | flights over the Gran Desierto on 12/29/71 and 12/30/71, respectively (Yuma I and Yuma II) |
| R1, R2 | rosettes at 10,000 ft and 40,000 ft altitudes, respectively |
| L1, L2, L3, L4 | legs 1, 2, 3, 4 at nominal $0^{\circ}$, $90^{\circ}$, $135^{\circ}$, and $-135^{\circ}$ to the sun, respectively |
| C1, C2 C3, C4 | color channels centered nominally at 3800 $\overset{\circ}{A}$, 4400 $\overset{\circ}{A}$, 5000 $\overset{\circ}{A}$, and 5800 $\overset{\circ}{A}$, respectively (See Table 2 in the Appendix). |

<u>Flight Experiment Procedures</u>. - The flights prior to the Yuma
flights were invaluable for debugging equipment and establishing
suitable flight procedures.  For example, it was found impossible
for the scan operator to recognize and pinpoint the target area
on the TV screen as the plane approached from different directions
at different altitudes.  Instead, for the Yuma flights the INS was
utilized for target acquisition.

The flight procedure sequence used was as follows:

1)  The plane flew over the area at 1,000 feet to select a
suitable target.  When the plane was directly over such a point, a
button was pressed, locking this point into the INS as ground zero.
During this time aerosol samples were collected and after "ground
zero" selection, the plane flew a "racetrack" pattern in the plane
of the sun until sampling was completed.

2)  The plane ascended to 5,000 feet for more aerosol sampling,
again in a racetrack pattern.  During the 1,000 and 5,000 feet
patterns, the photopolarimeter scanned the sky.

3)  The plane ascended to 10,000 feet and began the rosette
pattern shown in Fig. (3-12).  For legs 1, 2, 3, and 4 the desired
relative solar bearings are $0°$, $90°$, $135°$, and $-135°$, respectively.
On the approach to each leg, the scan operator set the instrument
scan angle $30°$ below the horizon ($60°$ forward of nadir).  When the
INS indicated the plane was the desired distance from ground zero,
i.e., when the instrument and TV were centered on ground zero, the
Operations Officer relayed the signal to the scan operator who
began scanning to keep fixed in the center of the TV screen what-
ever was there at the time.  When the INS indicated that the target
was $150°$ below the horizon ( $60°$ back of nadir) the signal was again
relayed and the scan was set to a fixed $2.5°$/second rate, in order
to scan the downward skylight radiation.  Simultaneously the ND4
filter was closed on the TV camera.  The airplane continued a
straight course until the sky scan was completed and then began the
approach to the next leg.  Between data legs the instrument shutter
was closed to record zero levels.  "Zero" and "data" portions of
the tape were separated by file gaps.  (See Fig. (3-8))

4)  After all four legs were completed, the same procedure
was repeated at 40,000 feet, except that area restrictions forced
curtailment of the sky scan on leg 4 at $270°$ (zenith) on 12/29 and
at the horizon on 12/30.

<u>The Ring-A-Rounds (RAR)</u>. - The only feasible method for deter-
mining the calibration factors for the instrument as installed was
to rotate the scan platform until the instrument was pointed at the
zenith and have the CV-990 taxi in a circle on the hangar apron
at NASA/Ames.

Ideally, a clear blue sky was desirable for this purpose but such conditions were never present over Moffett Field during the experiment period. The conditions for the ring-a-rounds (RAR) that were performed were:

1) Salt Lake RAR - prior to flight, with uniform overcast overhead.

2) Yuma I RAR - after flight, clear skies directly above but many scattered clouds immediately surrounding.

3) Yuma II RAR - after flight, conditions similar to those for Yuma I RAR.

The windows were at their cleanest for the Salt Lake RAR, having just been installed the night before. Prior to the Yuma I flight an attempt was made to remove the more obvious dirt particles with a long cotton swab. No attempt at cleaning was made between the Yuma I and Yuma II flights.

After the Yuma II flight, the ports of the scan housing were sealed to preserve the dirt to permit further calibration studies at UCLA.
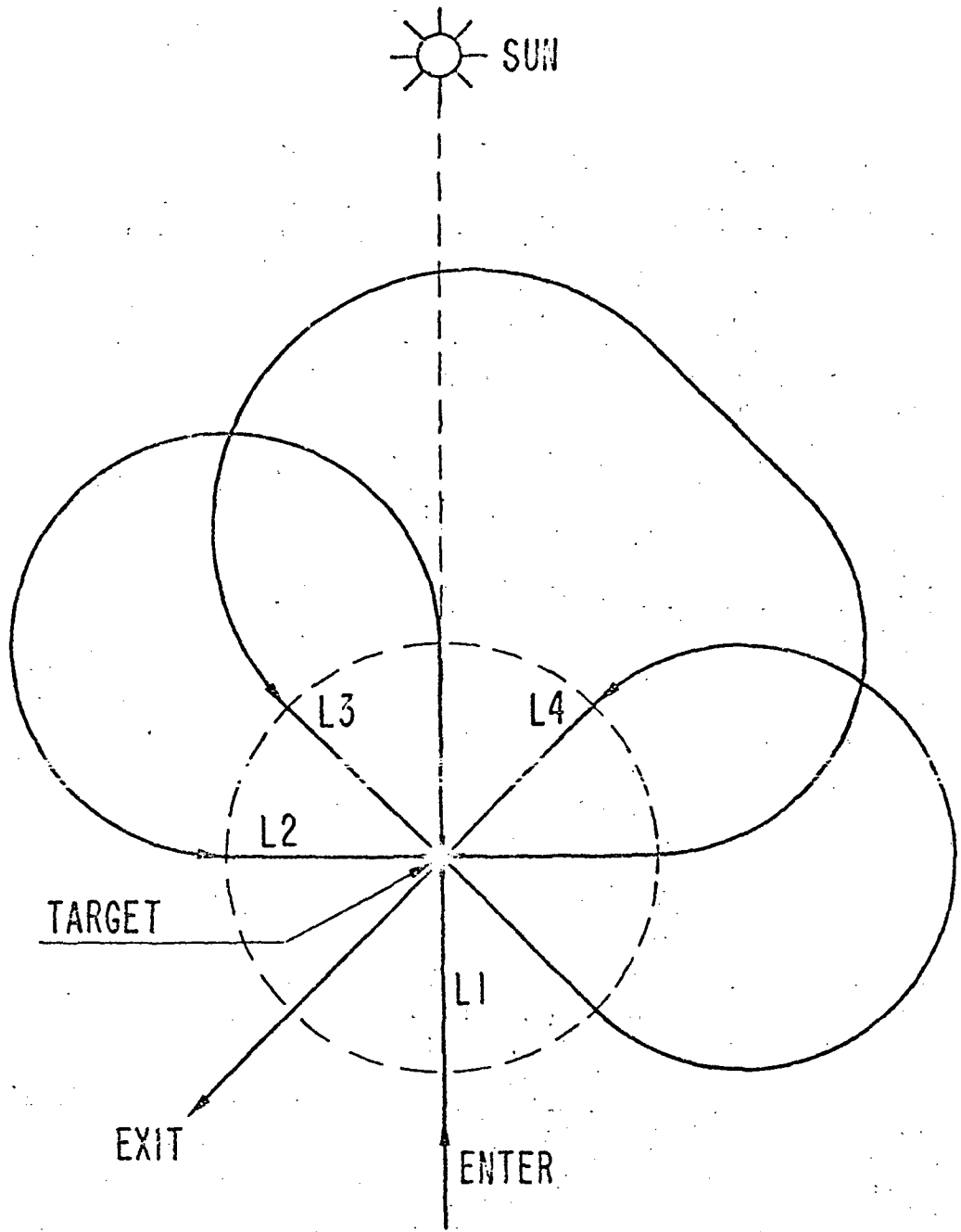
Fig.(3-12) -- Rosette Patterns Executed at 10,000 ft. and 40,000 ft. The Legs of the Rosette Are Defined with Respect to the Sun at $0^o$, $90^o$, $135^o$ ($-45^o$) and $45^o$ for L1, L2, L3, and L4, respectively.

## 3.2  Results of the Flight Experiments

3.2.1  Direct Aerosol Sampling. - In order to have some continuity in the discussion of the reduction of the polarimeter data we present first the results of the direct aerosol sampling.  At the conclusion of the flight programs the slides and filters from the direct sampling experiment were analyzed in Mr. Blifford's labs at NCAR (Boulder, Colorado) and the results of the impactor data transmitted to us.  Only results from the Yuma I and Yuma II flights will be presented here.
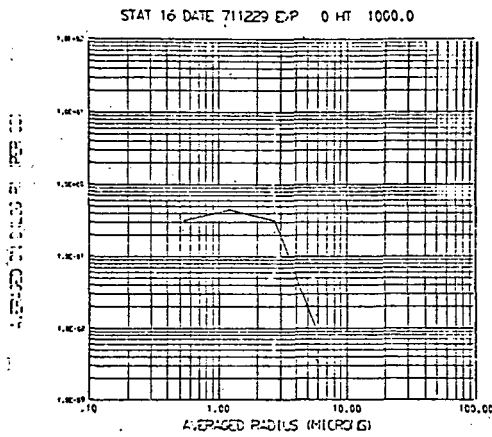
Figs. (3-13, a-h) are computer-produced size distribution curves for all measurements.  Errors are indicated as dots on either side of the curve.  The total number of particles measured in the range of 0.31 to 6.3 $\mu$m was:

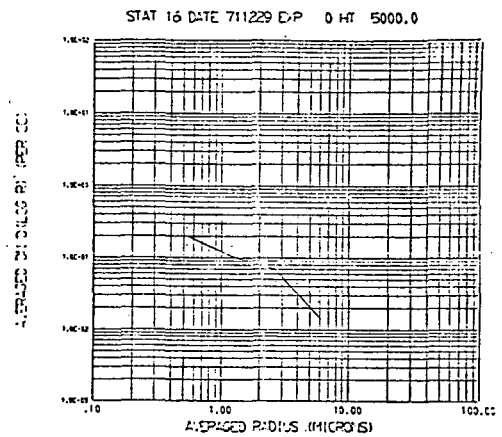| Flight | Altitude (ft.) | Total Particles ($Cm^{-3}$) | % Error |
|--------|----------------|-----------------------------|---------|
| Yuma I | 1,000 | 0.359 | 6.8 |
| | 5,000 | 0.125 | 9.2 |
| | 10,000 | 0.520 | 6.7 |
| | 40,000 | 0.250 | 6.9 |
| Yuma II | 1,000 | 1.03 | 6.3 |
| | 5,000 | 1.37 | 5.4 |
| | 10,000 | 0.252 | 1.3 |
| | 40,000 | 0.319 | 6.1 |

Even though the particle count for Yuma II is significantly higher than for Yuma I, both counts represent one effectively clear atmosphere.

3.2.2  True Heading Problems:  Relative Solar Bearings. - Since the polarization curves are defined with respect to the sun, it is necessary to determine the actual relative solar bearing, i.e., the difference between the true heading of the aircraft and solar azimuth.  The solar azimuth at the relevant time, latitude and longitude, as well as solar elevation may be calculated using standard formulae and data from the Air Almanac for the dates of interest.
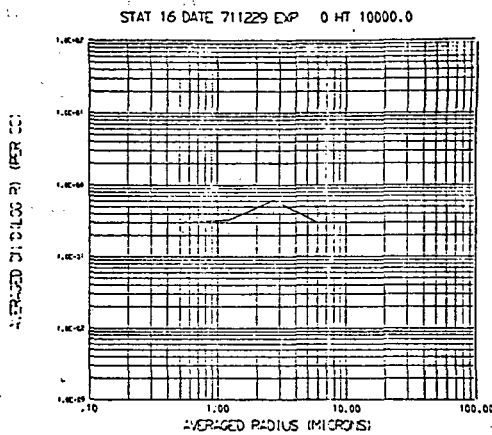
The video tapes contain an accurate record of the aircraft heading relative to the sun as the instrument and TV camera scanned through the sun on the skylight part of Leg 1 scans (1.25" on the screen - 1.5°) and on the skylight scans during the low altitude direct sampling runs.  (The roll of the aircraft and solar elevation must be taken into account in translating the angular position of the sun measured on the TV screen to the relative solar bearing of the aircraft.)
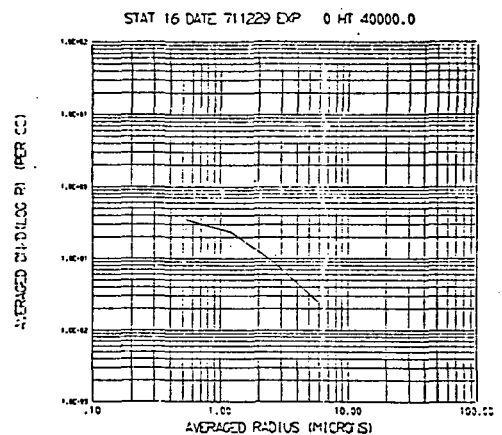
STAT 16 DATE 711229 EXP 0 HT 1000.0

STAT 16 DATE 711229 EXP 0 HT 5000.0

(a)

(b)

STAT 16 DATE 711229 EXP 0 HT 10000.0
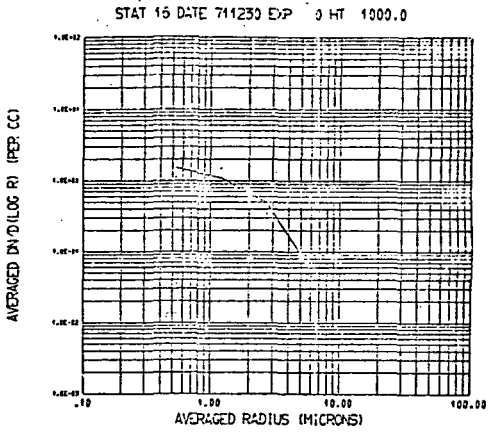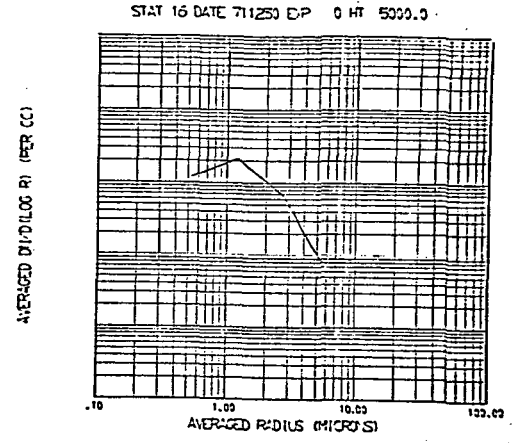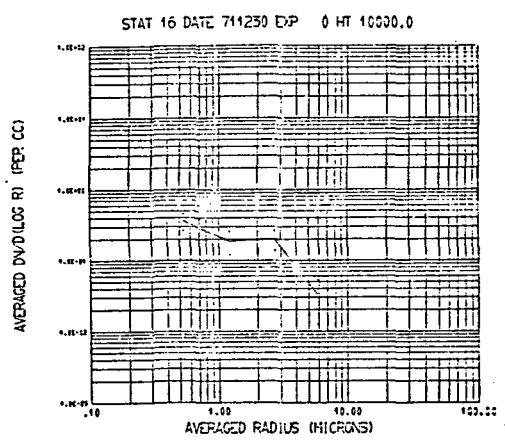
STAT 16 DATE 711229 EXP 0 HT 40000.0

(c)

(d)

Fig.(3-13) -- Direct Sampling Results. The following figures are computer produced plots of the number-size distributions of the collected particulates. (a) through (d) are from Y1 (12/29/71) at 1,000, 5,000, 10,000, and 40,000 ft., respectively. (e) through (h) are from Y2 (12/30/71) at the same corresponding altitudes. The vertical coordinate is dN/d (log R). See next page for (e) through (h).
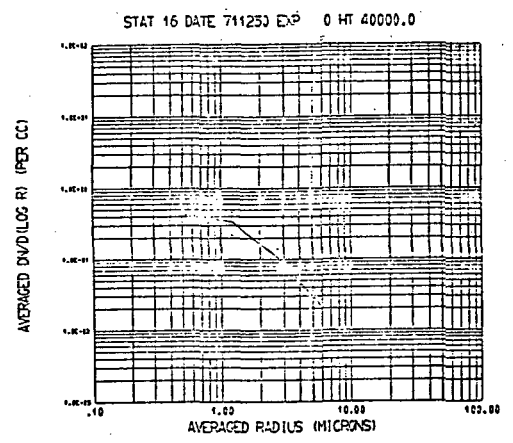
64

STAT 16 DATE 711250 EXP   0 HT   1000.0
(e)

STAT 16 DATE 711250 EXP   0 HT   5000.0
(f)

STAT 16 DATE 711250 EXP   0 HT 10000.0
(g)

STAT 16 DATE 711250 EXP   0 HT 40000.0
(h)

Fig.(3-13) -- continued.

In correlating this information it was noted that there were discrepancies of as much as 6° in the true headings recorded by the ADDAS. Fortunately, the navigator (R. Morrison) had made sextant sightings at the beginning and end of each leg. Comparing his records with the ADDAS printouts revealed discrepancies of an equivalent degree. It was decided to use the average of the navigator's sightings to designate the true heading for a leg, (there appears to be no consistency to the discrepancies) since the printout values were clearly unreliable.

In spite of the skepticism generated by this, we assumed that all other aircraft parameters on the ADDAS printout such as latitude, longitude, roll, and pitch are reliable. The only other parameter which we could check was the pitch angle, which was averaged over the leg and used to calculate the scan angle. (Though the average pitch is recorded on the title blocks of the data curves presented later, it has already been incorporated in the scan angle, the abscissa of the graphs.) The elevation of the sun measured in this manner (only on Leg 1's, of course) is always within a few tenths of a degree of the calculated solar elevation. This verifies not only the accuracy of the pitch, but the accuracy of the scan angle calibrations as well.

Analysis of the solar passes, particularly on the direct sampling runs where the aircraft flew alternately into and away from the sun, indicates that the rotation axis of the scan platform is not normal to the true heading axis of the aircraft, but canted at least one degree to the left (-1°). This has been incorporated in the relative solar bearings recorded on the title blocks of the data graph.

3.2.3 Determination of Calibration Factors - Pre-flight Elliptical Distortion. - Determination of the calibration factors prior to flight were made on the roof of MS using the rotatable collar described in Section 3.3 of the Appendix. The principal factors determined in these experiments are given in Table 3-3(a). The method is essentially (b) of 3.1.1 with the instrument rotated through discrete intervals of 15°.

In the course of these experiments, it was discovered that instead of a circle, the data curve in the $\eta$-plane after taking $f_1$ and $f_2$ into account was distorted elliptically with the major axis in the $2\psi = 135°$ (or $2\psi = -45°$) direction. Also, the angular intervals calculated for $2\psi$ varied by as much as $\pm 2.2°$ from the $30°$ they should have been. As has been shown in Case II of 3.1.1, this type of distortion might be due to prism misalignment. Analysis of the data shows that the distortion can be accounted for by taking $\gamma = 1°11'$. Indeed, using a corresponding calibration matrix restored the curve to a circle and the angular intervals to their proper amount, and such equations were incorporated into the program. (These equations were later removed for reasons to be given.)

66

Attempts to make a direct measurement of the misorientation were undertaken but the error in determining the orientations was $\pm 0.5^\circ$ for the optical bench setup used. It was thought that the measurements, though marginal, ruled out misorientation of the prisms and the next source suspected was the electronic processor. Later tests described in Section 3.0 of the Appendix ruled out this possibility. (In preparation of this report it was discovered that the original calculation, indicating a value of $1^\circ 30'$ was necessary to explain the effect, was in error. The value for $\gamma$ given above restores misorientation as a possibility.)

Ring-a-round at Moffett Field. - Originally, it was planned to use the true heading data from the ADDAS in assessing the ring-a-round data, but all other discrepancies aside, the updating proved inadequate for this purpose. Instead, the data was plotted in the $\eta$-plane and the center of gravity determined graphically, though again some arbitrariness was involved. Examples of the plots for C2 done with the computer are shown in Fig. (3-14). The values deduced from these graphs are given in Table 3-3 (b), (c) and (d). The reliability of the values determined in this manner may be seen by comparing Table 3-3 (d) with (e) and (f) which were determined after returning to UCLA as described below. Note that there is at most 0.3% difference in the same f's and typically 0.2% or less difference.

Unfortunately, as will be seen we cannot believe that these values represent that accurately the value corresponding to the inflight data. This is indicated by comparing the RAR's at Moffett Field. Table 3-3 (b) values are fairly close to (d) values, but the values in (c) contain major differences, particularly in the $f_1$ row and in $f_2$ of C4.

We might explain the differences in $f_1$ as being due to a large piece of dirt on the external window of the B barrel or on the image aperture lens or fibre optic bundle aperture, for B in the chopper compartment, while the singular departure of the $f_2$ of C4 might be due to a piece of dirt (flake of paint on the appropriate sector of the C4 filter).

In the course of these f-value determinations it was realized that the presence of the equations correcting the elliptical distortion was fouling things up (as may be seen from Section 3.1.1 translation must be done first, then rotation or deformation) and the equations were removed.

They were never replaced for two reasons:

1) Due to the uncertainty as to the origin of the distortion it was felt we might be forcing a constant error to replace a random one.

2) If the distortion was caused by misorientation of the prisms, it would have a minimal effect when the polarization was along one of the axes ( $\eta_1$ or $\eta_2$ ) as is the case with the major plane of interest, the sun plane.

In-flight Data Determination. - An attempt was made to obtain information on the calibration factors prevailing during the actual data taking by using method (c) of 3.1.1, the special angle method (SAM). This method relies on the knowledge that the plane of polarization when viewing the zenith is normal to the sun plane. Analysis of the data on this basis yielded inconsistent results.

Although the true heading discrepancies could account for some of the inconsistency (a $1^o$ error in heading can typically result in 1% error in the f-value), it is felt that the presence of dirt in the chopper compartment was the major source of the differences.

Post-flight Studies. - On return to UCLA, the scan platform was mounted on a frame with casters. A pivot point, which could be lowered manually to contact the ground was located near the doorknob (instrument compartment) end. On the few occasions when sky conditions were suitable, the scan platform was taken down to the loading dock behind Slichter Hall for further calibration factor studies. The pivot point was lowered and by slowly pushing the far (electronics box) end of the scan platform, a ring-a-round was performed. Table 3-3(e) shows that even though poor sky conditions prevailed for the Yuma II RAR, the factors determined graphically are consistent with those determined under far better conditions. (The area of the loading dock used was exceptionally flat, deviation from the zenith axis during rotation, excluding pebbles, being less than $\pm0.2^o$.)

The values in Table 3-3(f) were determined using SAM to study the validity of that method. The instrument was oriented at $0^o$, $45^o$, $90^o$, and $135^o$ successively, using the edges of the scan platform as a sundial. This method yields knowledge of the plane of polarization to better than $\pm0.5^o$. Note that the values determined in this manner differ from those in Table 3-3(e) by less than 0.2% on the average, indicating that this method would indeed be useful for determination from in-flight data if the true heading, or better, the relative solar bearing can be measured to a sufficient degree of accuracy while the instrument views the zenith. This method should be kept in mind for future flight experiments.

On only three other occasions were sky conditions suitable for studies on the loading dock though on two days these conditions lasted only for an hour or so, forcing some hurried and curtailed measurements. No conclusive numbers were gained but

68

the following observations were made:

1) What was initially thought to be a dramatic effect of the non-symmetric angular acceptance of the B and D barrels was traced to improper orientation of the instrument so that its axis was not aligned with the zenith.

2) This misalignment came about due to the removal of the instrument package from the compartment and its reinstallation without checking the "level" of the instrument with reference levels on the electronics box. (There are no locating pins to insure accurate orientation on reinstalling.) The error in the direction of scan rotation could at least be the one-half degree observed. It was also noted that the axis of the instrument was off normal to the rotation axis by $0.2^{\circ}$.

3) This uncertainty in orientation mitigated against any study of the maxing of Stokes components due to multiple reflections between the lens of the photopolarimeter and the external quartz windows. Such an effect would be critically angle dependent.

This discussion may seem somewhat lengthy but has been deemed necessary to illustrate the difficulties in determining the calibration factors.

For want of justification in using other values, those in Table 3-3(b) were used for reducing the data of Yuma I and those in (c) were used for reducing the data of Yuma II. It makes no sense to interpolate the f's since they represent ratios of transmissions. Once data plots were obtained, it was easy to see why inconsistencies had occurred in the attempts to obtain good values for the calibration factors.

3.2.4 <u>Experimental Results - Preliminary Discussion</u>. - The reduced data for the rosettes of the Yuma I and Yuma II flights are presented in the following graphs (Fig. (3-15)). These graphs are not assigned individual numbers since they will be referred to by the code (see Table 3-2) in the upper left hand corner, also given in the title block. (A complete set of graphs is presented only for C2 with selected examples for the other color channels. The reasons for this are given in the following remarks.)
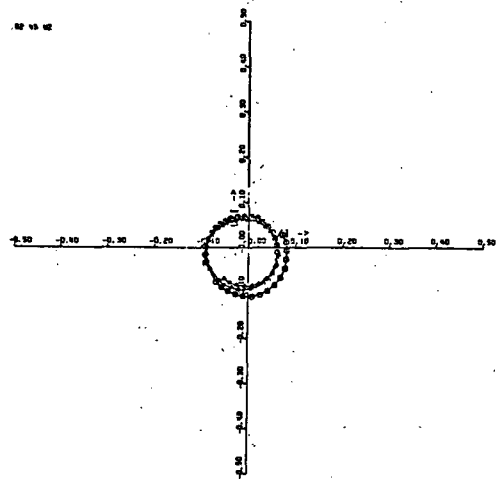
Several main features should be pointed out:

1) The scan is from $30^{\circ}$ below the nose of the plane through the nadir at $90^{\circ}$ to $150^{\circ}$ while tracking the target area. The scan is then moved at an arbitrary rate to the rear horizon ($180^{\circ}$) and set at a uniform rate (about $2^{\circ}$/sec) to scan the skylight passing through the zenith at $270^{\circ}$ and ending at the forward horizon at $360^{\circ}$ (Fig. (3-8)).
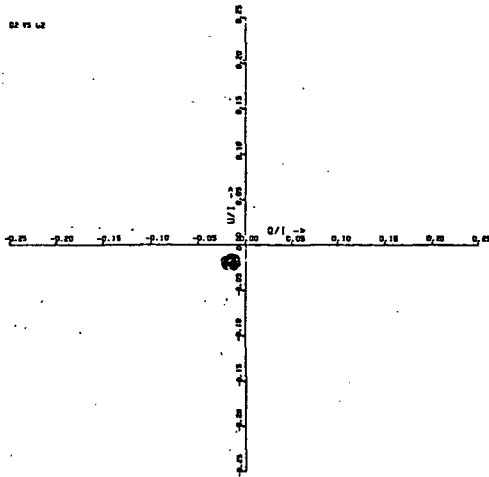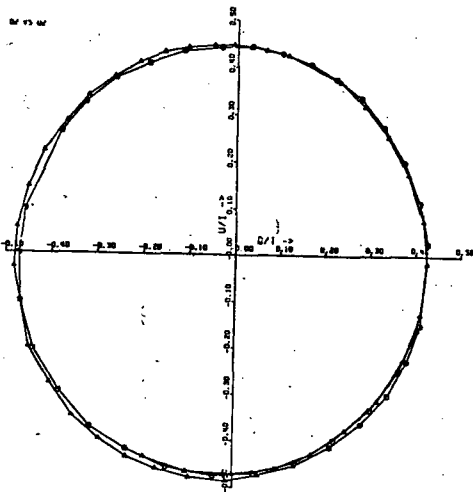
Fig.(3-14) -- Ring-A-Round Data Computer Plots for C2 (4400 Å) from (a) Salt Lake RAR, (b) Yuma I RAR, and (c) Yuma II RAR.

## Table 3.3 -- Calibration Factors

|  |  | | C1 | C2 | C3 | C4 |
|---|---|---|---|---|---|---|
| (a) | Instrument alone prior to flight. | $f_1$ | 0.9123 | 0.9804 | 0.9653 | 0.9701 |
|  |  | $f_2$ | 0.9494 | 0.9868 | 0.9724 | 0.9976 |
| (b)* | Salt Lake RAR | $f_1$ | 0.9200 | 0.9825 | 0.9675 | 0.9750 |
|  |  | $f_2$ | 0.9425 | 0.9825 | 0.9650 | 0.9925 |
| (c) | Yuma I RAR | $f_1$ | 0.8970 | 0.9735 | 0.9565 | 0.9650 |
|  |  | $f_2$ | 0.9420 | 0.9825 | 0.9650 | 1.0020 |
| (d) | Yuma II RAR | $f_1$ | 0.9205 | 0.9863 | 0.9715 | 0.9775 |
|  |  | $f_2$ | 0.9488 | 0.9863 | 0.9713 | 0.9958 |
| (e) | Loading Dock RAR 2/15/72 | $f_1$ | 0.9238 | 0.9888 | 0.9738 | 0.9813 |
|  |  | $f_2$ | 0.9475 | 0.9869 | 0.9706 | 0.9975 |
| (f) | Loading Dock Special Angle, 3/1/72 | $f_1$ | 0.9282 | 0.9918 | 0.9740 | 0.9839 |
|  |  | $f_2$ | 0.9468 | 0.9861 | 0.9698 | 0.9964 |

*(b) to (e) were with the instrument in the scan platform with external windows in place.

2). For convenience in presentation as well as the convenience in data processing, the ground and skylight scans are not separated but presented in one continuous curve.

3) The region of $160^\circ$ to $180^\circ$ represents the scan through the wing and tail section of the CV-990 and no significance can be attached to the peaks in that region.

4) The region from $320^\circ$ to $340^\circ$ in LI curves is where the instrument scans through the sun. Such steep intensity gradients occur in the region of the sun that in a given quarter (color) cycle the I's relating to the outputs $b_0$, $b_1$, and $b_2$ are all different, rendering the values of polarization meaningless.

5) Saturation occurs when passing through the sun, but such singular points are not marked on the graphs. The black stripes that appear on curves for C3 and C4 indicate where saturation occurs for extended periods, rendering the polarization values given meaningless. This saturation is an amplifier saturation (or equivalently exceeds the capacity of the A/D converter) not a detector saturation. The optional preamp gain was not utilized because, first, it was virtually impossible for the operator to know when saturation was occurring (only someone monitoring the visicorder could tell when the system was saturating, and although spot-checks were made on the preliminary flights, there was insufficient personnel on the YI and Y2 flights to man the visicorder continuously) and second, the gain change would have sacrificed C1 and C2.

6) Data taking on L4 of R2's was invariably curtailed due to flight zone restrictions.

7) Dips and irregularities in the skylight portion of the Y2 curves indicate the presence of cirrus clouds on that day.

The major problem in the data indicated on the curve by "A" will be referred to as Type "A" glych. Particularly strong examples are found in Y2R2LIC2, YIR2L3C2, and YIR2LIC2. Not all such glyches are indicated and the reader will be able to identify many for himself. Type "A" glyches are characterized by a sudden break or transition from one continuous curve to another, indicating a sudden change in a calibration factor occurring on one color only. In tracing these glyches in polarization back to the full data printout, it was found that they always correspond to a sudden change in one parameter (of $b_0$, $b_1$, $b_2$) only.

If this glych were the result of a sudden change in the electronics, it would occur in all colors simultaneously, not in one color alone. For the same reason, the sudden appearance of a hunk of dirt on the external windows is ruled out. The only plausible explanation for the behavior of this glych is the

movement of a relatively large piece of dirt, like a flake of paint, onto (or off of) the filter wheel. To verify this, the detector was removed and such a piece of dirt was discovered on one of the filters. The effect of such a hunk would depend on its size and position on the filter, but it is easily seen how the effect occurs in only one parameter if it is remembered that each barrel corresponds to one $120^\circ$ sector of the filter. It was also verified that the dirt remains in place during many cycles of the instrument. While in flight, the vibration and changing orientation of the instrument during scanning could combine to shake it loose.

At any rate, the behavior of the Type "A" glych indicates clearly the origin of difficulties in determining the proper calibration factors at any given moment and severely restricts the reliability of the data. We can, however, make a qualitative assessment of the reliability of a set of curves for a given color rosette, and altitude by observing how close the neutral points in the skylight scan come to zero (or less rigorously the corresponding point in the ground scan) on L1 curves and how well the full set, i.e., L1, L2, L3, and L4, cross over at the nadir and zenith points. Since C2 fares better than the other colors in this respect and shows no saturation, it has been given the most attention.

Before proceeding to the next section, it should be mentioned that the waves in the ground scans of the Y2 curves, particularly noticeable in Y2R2L2, are real ground effects. In reviewing the video tapes for this leg, dark, stripe-like diagonal patches drifted in and out of the photopolarimeter's field of view as the plane drifted right and left. Due to poor contrast and the 400 Hz interference, it is impossible to discern the nature of the patches, i.e., whether they represented shadows due to slopes, vegetation, or some other coloration.

Analysis of the Data. - The dashed curve in Y1R1L1C2 and Y2R1L1C2 is the theoretical internal field calculation for a homogeneous Rayleigh atmosphere. This calculation discussed in the theoretical program report section is for $\lambda = 0.44m\mu$, A = 0.09 at 10,000 ft. altitude and the solar elevation ($34^\circ$) or solar zenith corresponding to that of the experiment. The upward (ground) radiation and downward (skylight) radiation are presented in one continuous curve to conform with the data presentation, even though the calculations were formally separated.

The wavelengths for the computer calculations were chosen in order to make use of existing tabulated information on reflection and transmission matrices. The curve presented is interpolated from those calculations to the 0.44 m$\mu$ wavelength. The albedo of 0.09 was chosen on the basis of the peaks of the data curves. For the given wavelength and type of terrain (dessert) the value is quite reasonable (ref. 30 ).

Fig.(3-15) -- Computer Plots of Polarization vs Scan Angle for
Rosettes of Yuma I and Yuma II Flights.  The following pages
contain computer plots of selected data legs from the flight
experiments.  A complete set (16) of graphs for C2 is presented
followed by one example for each of the remaining color channels.
See text.(Section 2.4.1) for detailed explanation.

UCLA PHOTOPOLARIMETER EXPERIMENT
ON THE NASA/AMES CONVAIR 990

PLOT _P vs θ_s_  CODE _Y, R, L, C_2_  DATE _12/19/71_

LOCATION _Salan Desierto Mojave_ ALTITUDE _10.000 FT_

LATITUDE _32° 19.2' N_  LONGITUDE _114° 38.7' W_

TIME AT NADIR _19: 21: 10_  COLOR _.44 μ_

REL. SOLAR BEARING _-3.1°_  AVG. PITCH _2.8°_

SOLAR ELEVATION _37°_  AVG. ROLL _____
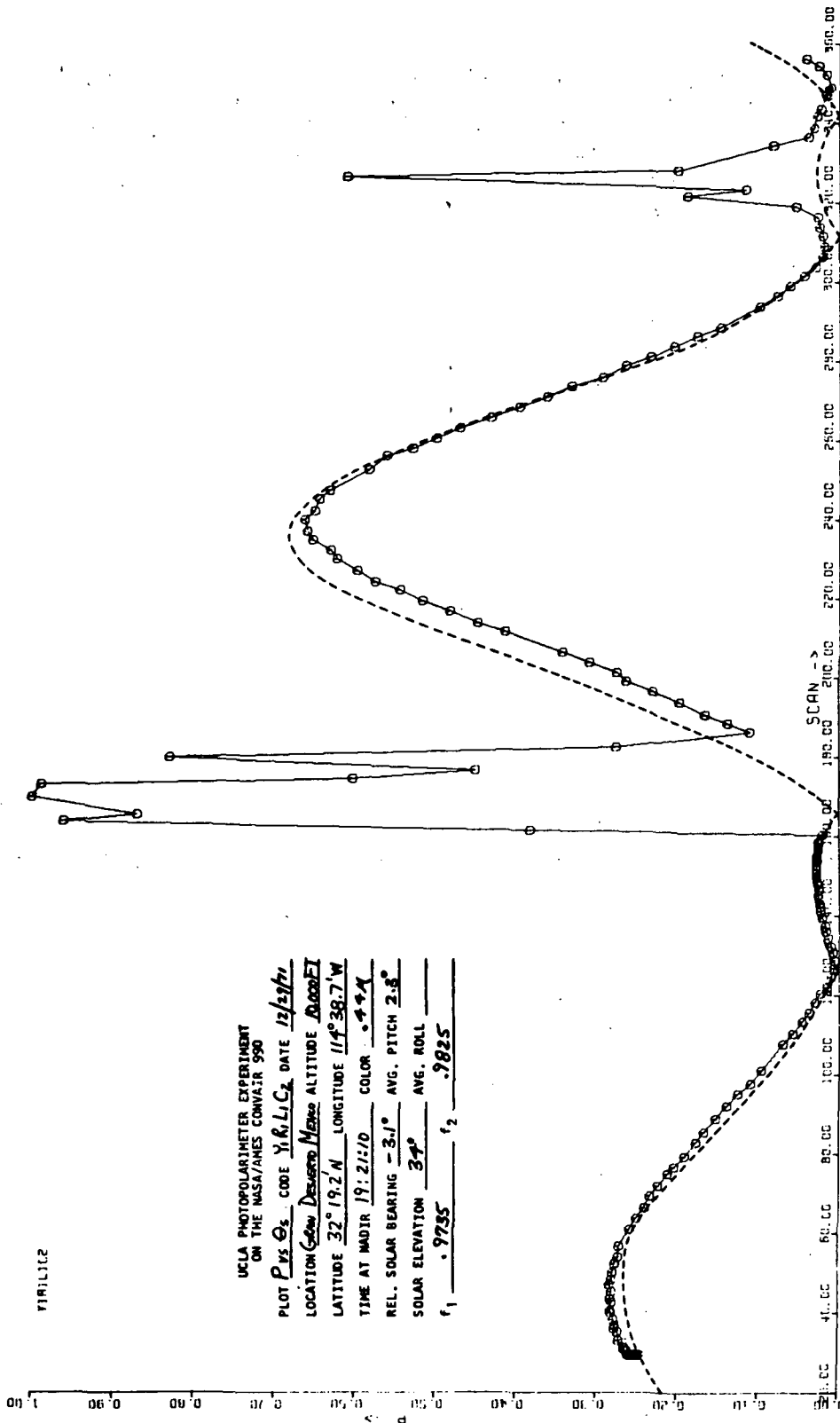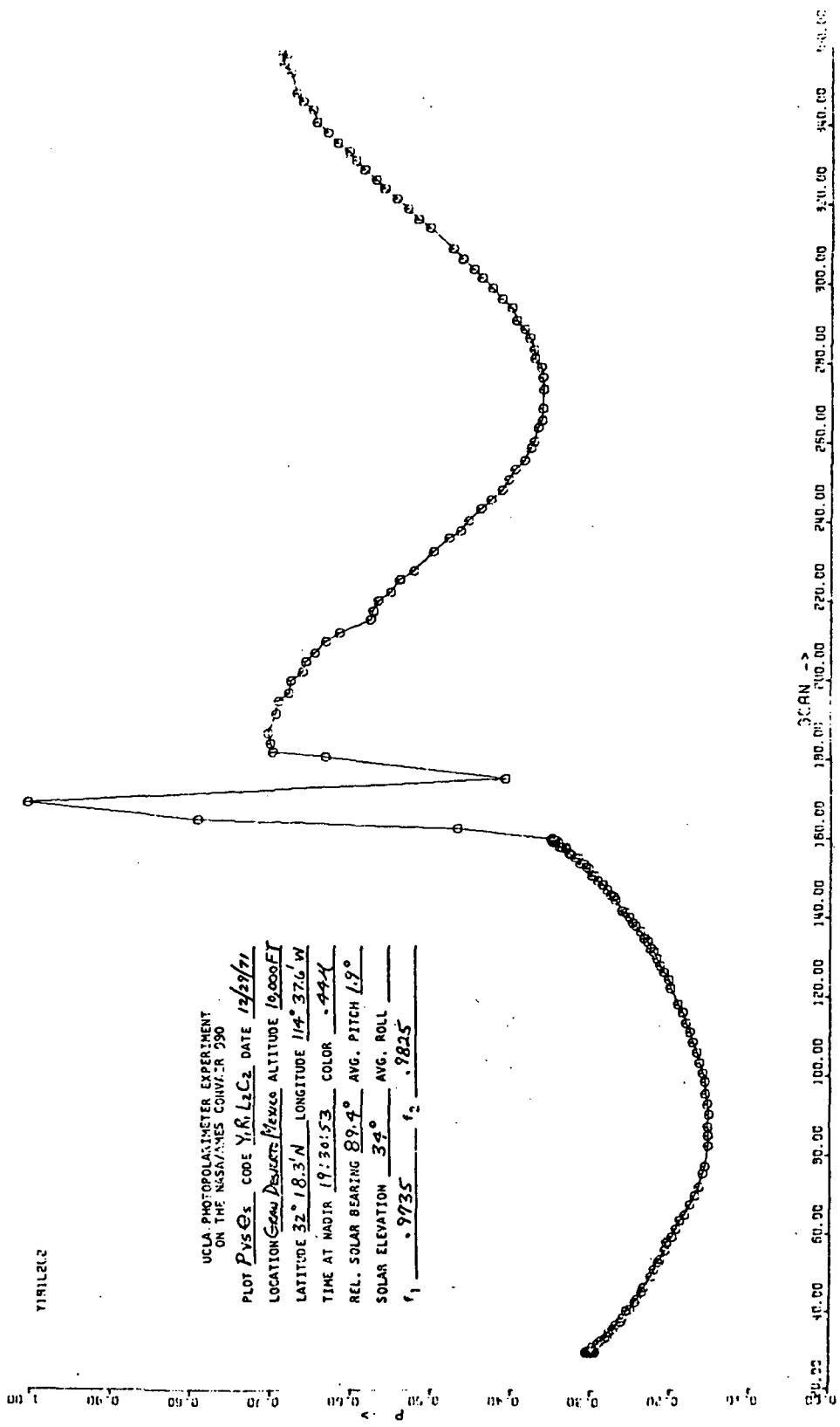
f_1 ___.9735___  f_2 ___.9825___

75

UCLA PHOTOPOLARIMETER EXPERIMENT
ON THE NASA/AMES CONVAIR 990

PLOT $P$ vs $\Theta_s$  CODE $Y_1R_1L_2C_2$  DATE 12/29/71

LOCATION Gran Deserts Mexico  ALTITUDE 10,000 FT

LATITUDE 32° 18.3' N  LONGITUDE 114° 37.6' W

TIME AT NADIR 19:36:53  COLOR .444 μ

REL. SOLAR BEARING 89.4°  AVG. PITCH 1.9°

SOLAR ELEVATION 34°  AVG. ROLL

$f_1$ .9735  $f_2$ .9825

76

UCLA PHOTOPOLARIMETER EXPERIMENT
ON THE NASA/AMES CONVAIR 990

PLOT $P_{15}\,\Theta_S$   CODE $Y_1R_6L_3C_2$ DATE _12/29/71_

LOCATION _Gran Desierto/Mojave_ ALTITUDE _10,000 FT_

LATITUDE _32°18.5'N_   LONGITUDE _114°38.4'W_

TIME AT NOON _19:40:18_   COLOR _.44μ_

REL. SOLAR BEARING _131.7°_ AVG. PITCH _2.1°_

SOLAR ELEVATION _34°_   AVG. ROLL _____

$f_1$ ___.9735___   $f_2$ ___.9825___

YIRILIEZ

77

UCLA PHOTOPOLARIMETER EXPERIMENT
ON THE NASA/AMES CONVAIR 990

PLOT $P$ vs $\theta_s$ CODE Y,R,L4C2 DATE 12/29/71

LOCATION Gran Desierto Mexico ALTITUDE 19000 FT

LATITUDE 32° 17.8' N LONGITUDE 114° 39.7' W

TIME AT NADIR 19:56:19 COLOR .44μ

REL. SOLAR BEARING ~140° AVG. PITCH 1.8°

SOLAR ELEVATION 37° AVG. ROLL _____
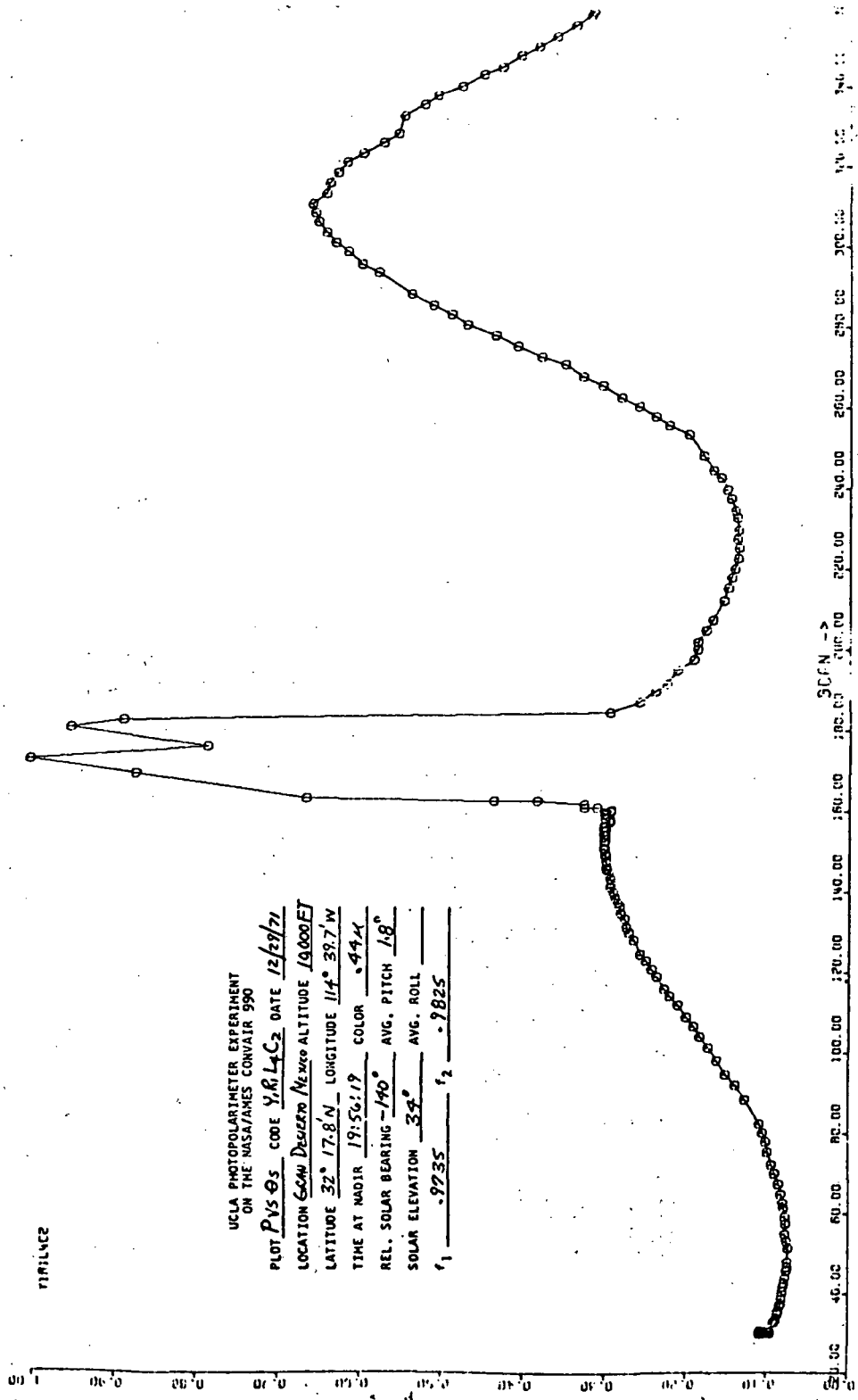
$f_1$ .9735 $f_2$ .9825

SCAN →

UCLA PHOTOPOLARIMETER EXPERIMENT ON THE NASA/AMES CONVAIR 990

PLOT $P$ vs $\Theta_s$ CODE $Y,R,L,C_2$ DATE 12/29/71
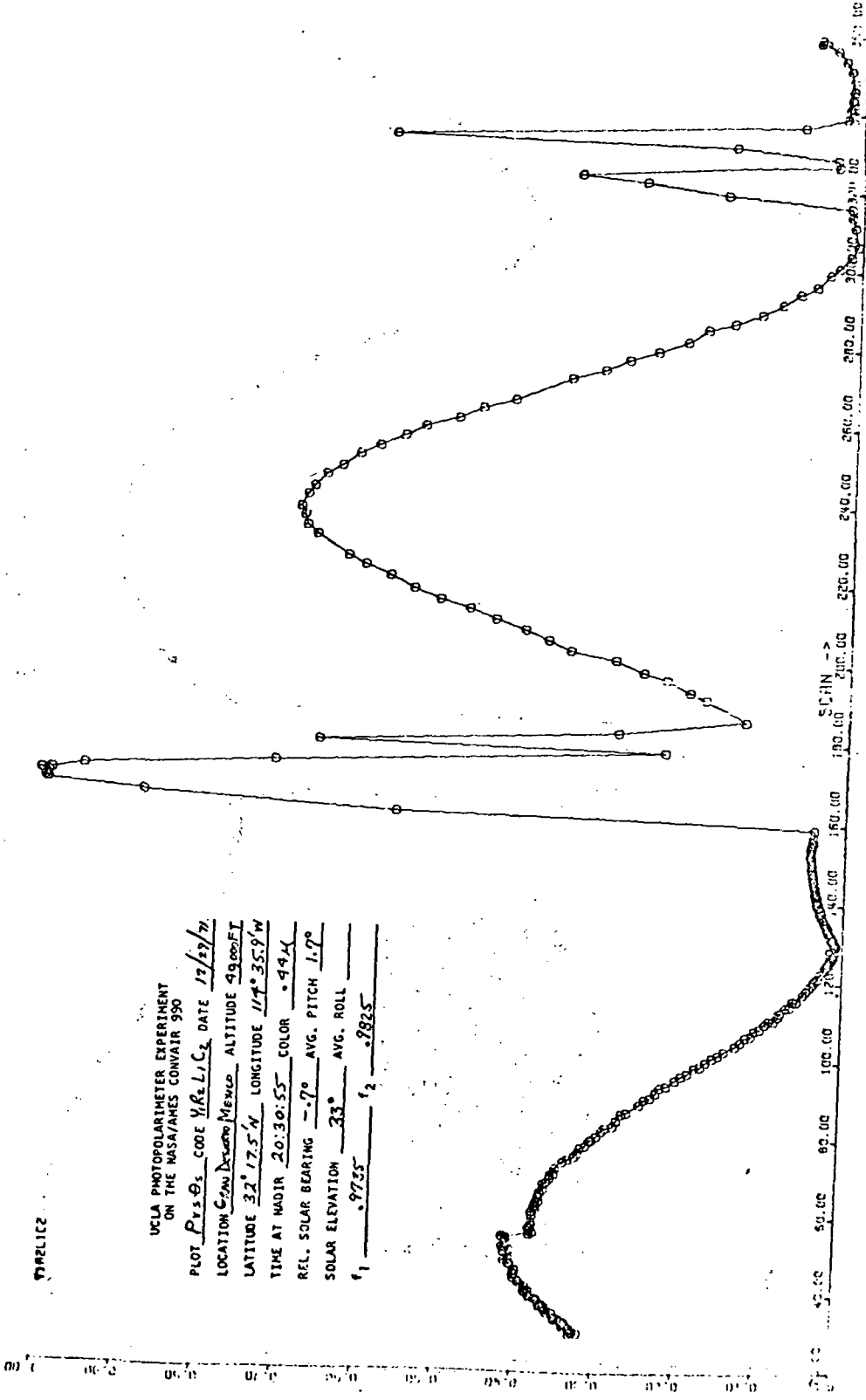LOCATION San Diego Menlo ALTITUDE 49000 FT
LATITUDE 32° 17.5' N LONGITUDE 117° 35.9' W
TIME AT NADIR 20:30:55 COLOR .444μ
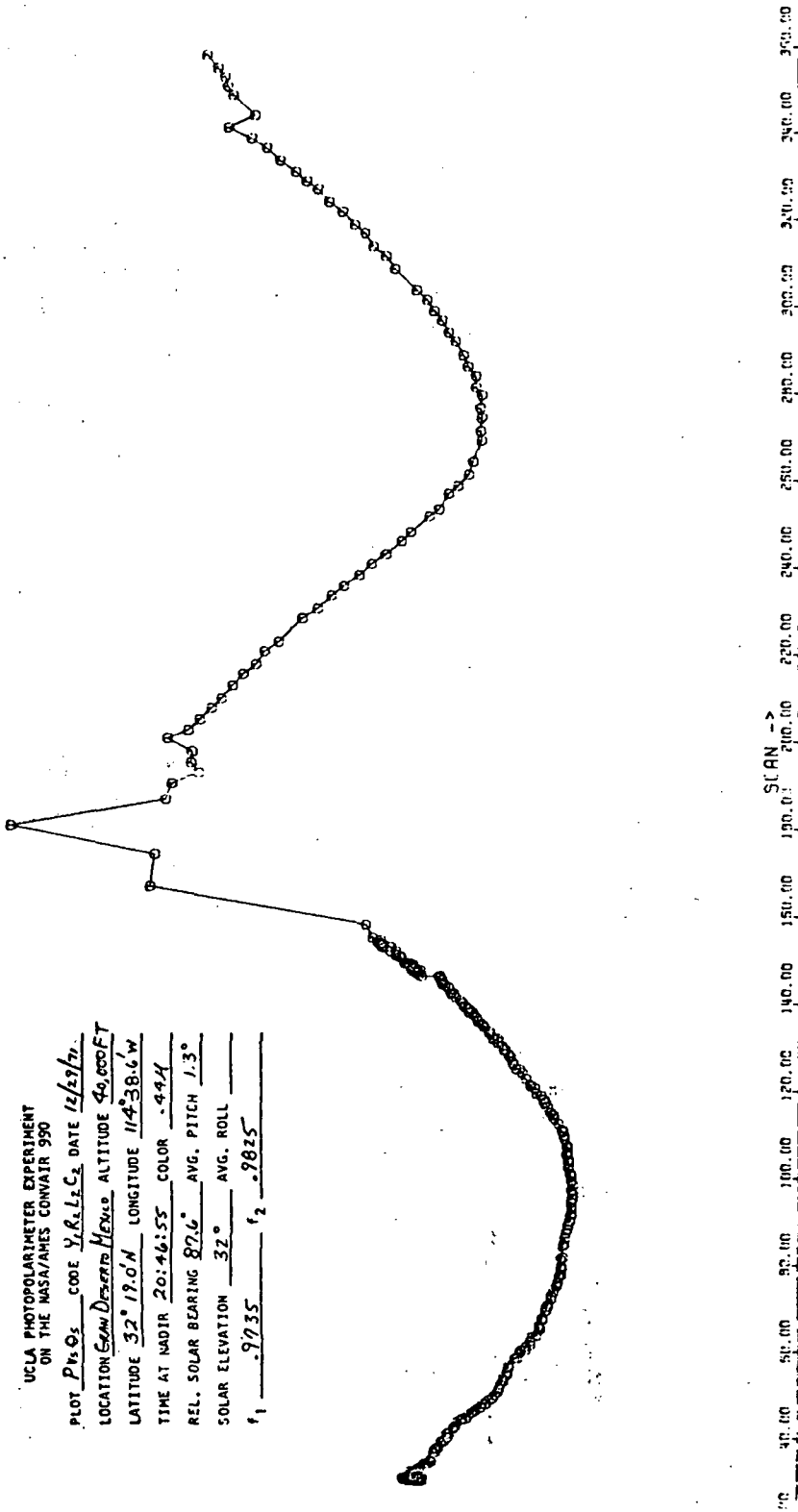REL. SOLAR BEARING -.7° AVG. PITCH 1.7°
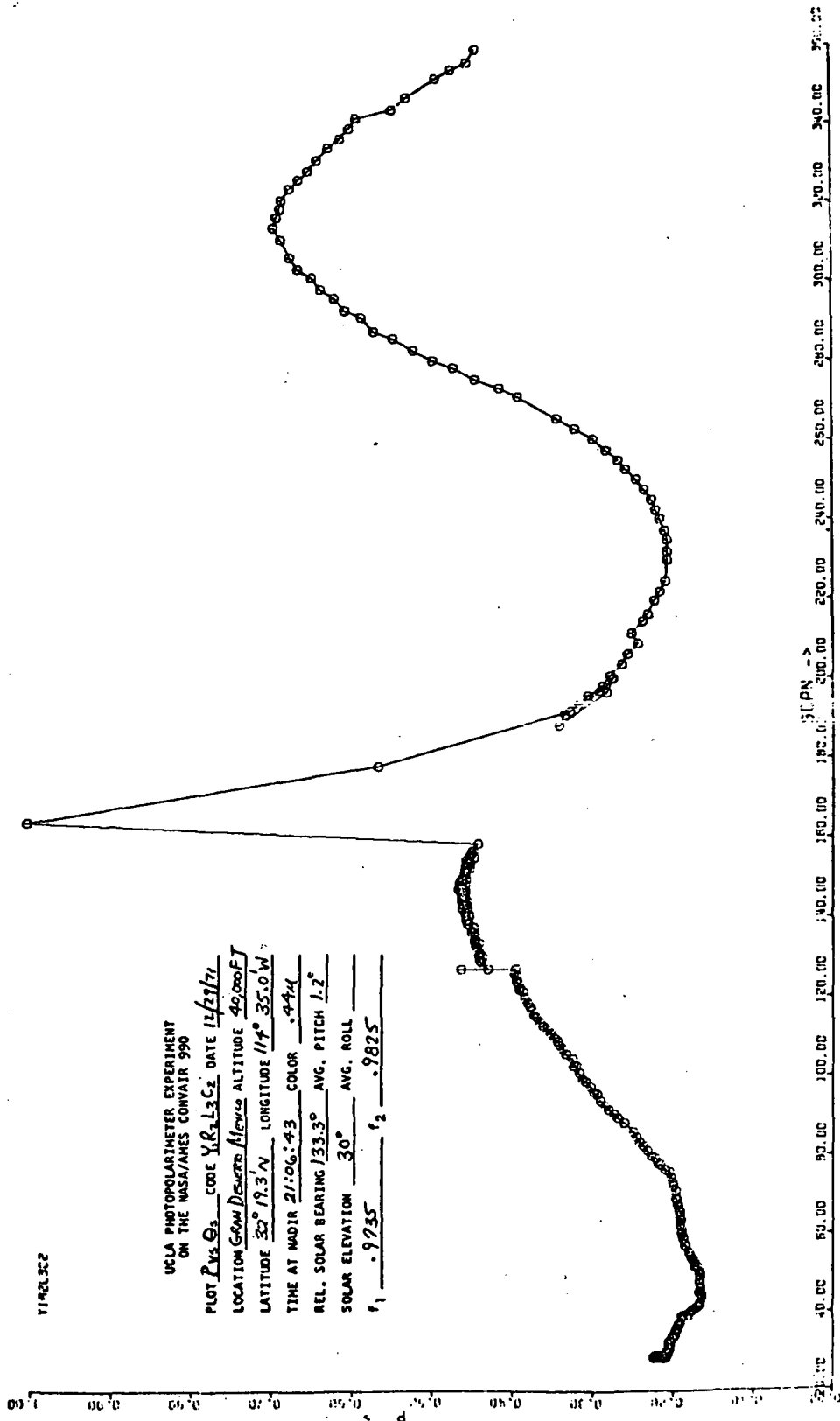SOLAR ELEVATION 33° AVG. ROLL
$f_1$ .9735 $f_2$ .9825

SCAN →

7.9

UCLA PHOTOPOLARIMETER EXPERIMENT
ON THE NASA/AMES CONVAIR 990

PLOT $P_{13}O_5$ CODE $Y_1R_1L_1C_2$ DATE 12/29/71

LOCATION Gran Desierto Mexico ALTITUDE 40,000 FT

LATITUDE 32° 19.6' N LONGITUDE 114° 38.6' W

TIME AT NADIR 20:46:55 COLOR .44 A

REL. SOLAR BEARING 82.6° AVG. PITCH 1.3°

SOLAR ELEVATION 32° AVG. ROLL ____

$f_1$ .9735 $f_2$ .9825

80

UCLA PHOTOPOLARIMETER EXPERIMENT
ON THE NASA/AMES CONVAIR 990

PLOT $P$ vs $\Theta_s$   CODE $Y_1 R_x L_3 C_2$  DATE 12/21/71

LOCATION _Gron Desert Movie_ ALTITUDE _40,000_ FT

LATITUDE _32° 12.3' N_   LONGITUDE _114° 35.0' W_

TIME AT NADIR _21:06:43_   COLOR _.444_

REL. SOLAR BEARING _133.3°_   AVG. PITCH _1.2°_

SOLAR ELEVATION _30°_   AVG. ROLL _____

$f_1$ _.9735_   $f_2$ _.9825_

81

UCLA PHOTOPOLARIMETER EXPERIMENT
ON THE NASA/AMES CONVAIR 990

PLOT _P₁₅ θₛ_ CODE _VR₃ L₃ G₂_ DATE _12/28/71_

LOCATION _Glen Desert Along_ ALTITUDE _49,000 FT_

LATITUDE _32° 12.4 N_ LONGITUDE _114° 32.6 N_

TIME AT NADIR _20:29:12_ COLOR _.44μ_

REL. SOLAR BEARING _-141.2°_ AVG. PITCH _1.4°_

SOLAR ELEVATION _29°_ AVG. ROLL _____
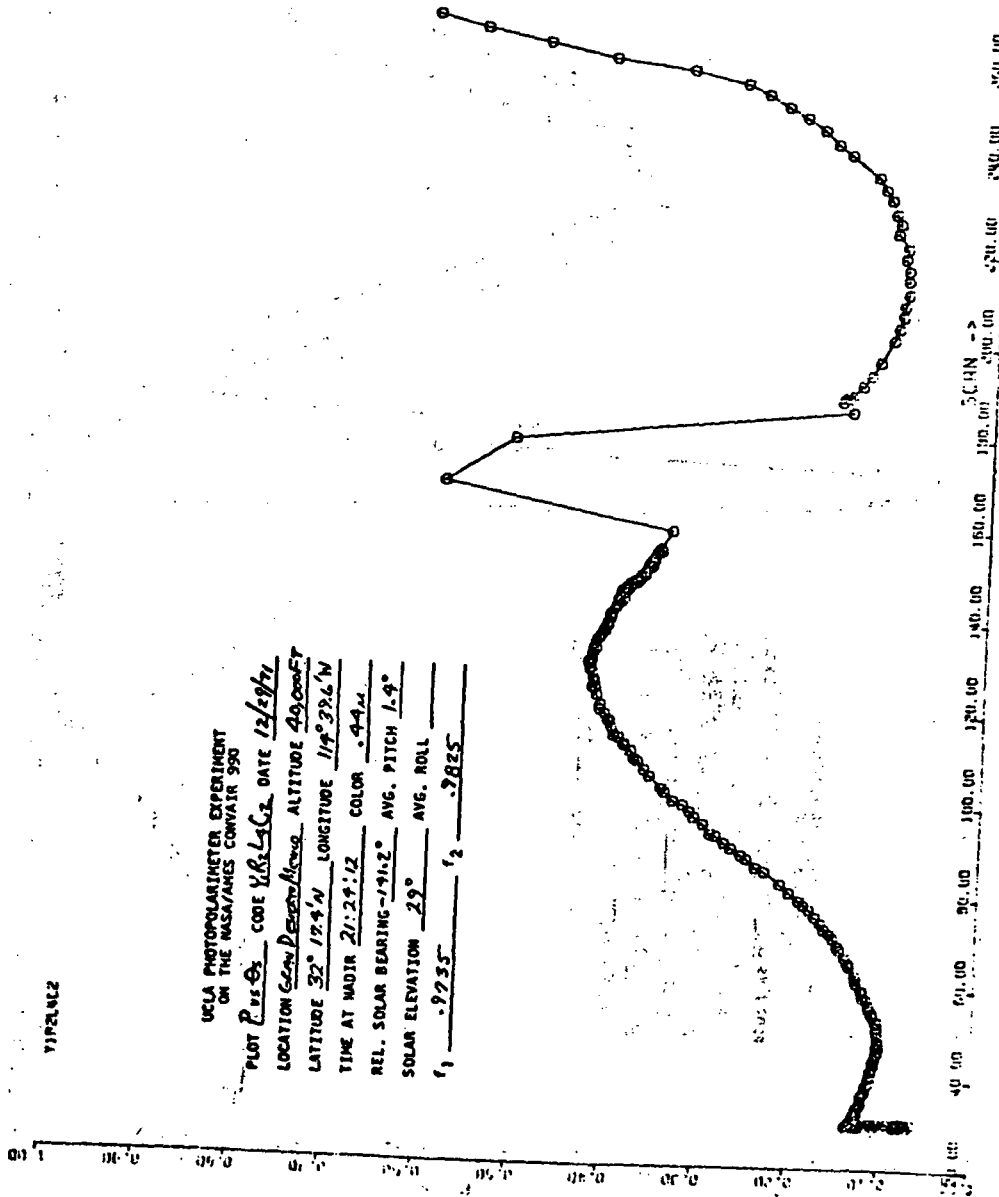
r₁ _.9755_ r₂ _.9825_

UCLA PHOTOPOLARIMETER EXPERIMENT
ON THE NASA/AMES CONVAIR 990

PLOT $P_{15}\theta_3$ CODE $V_1R_1L_1C_2$ DATE _12/30/71_

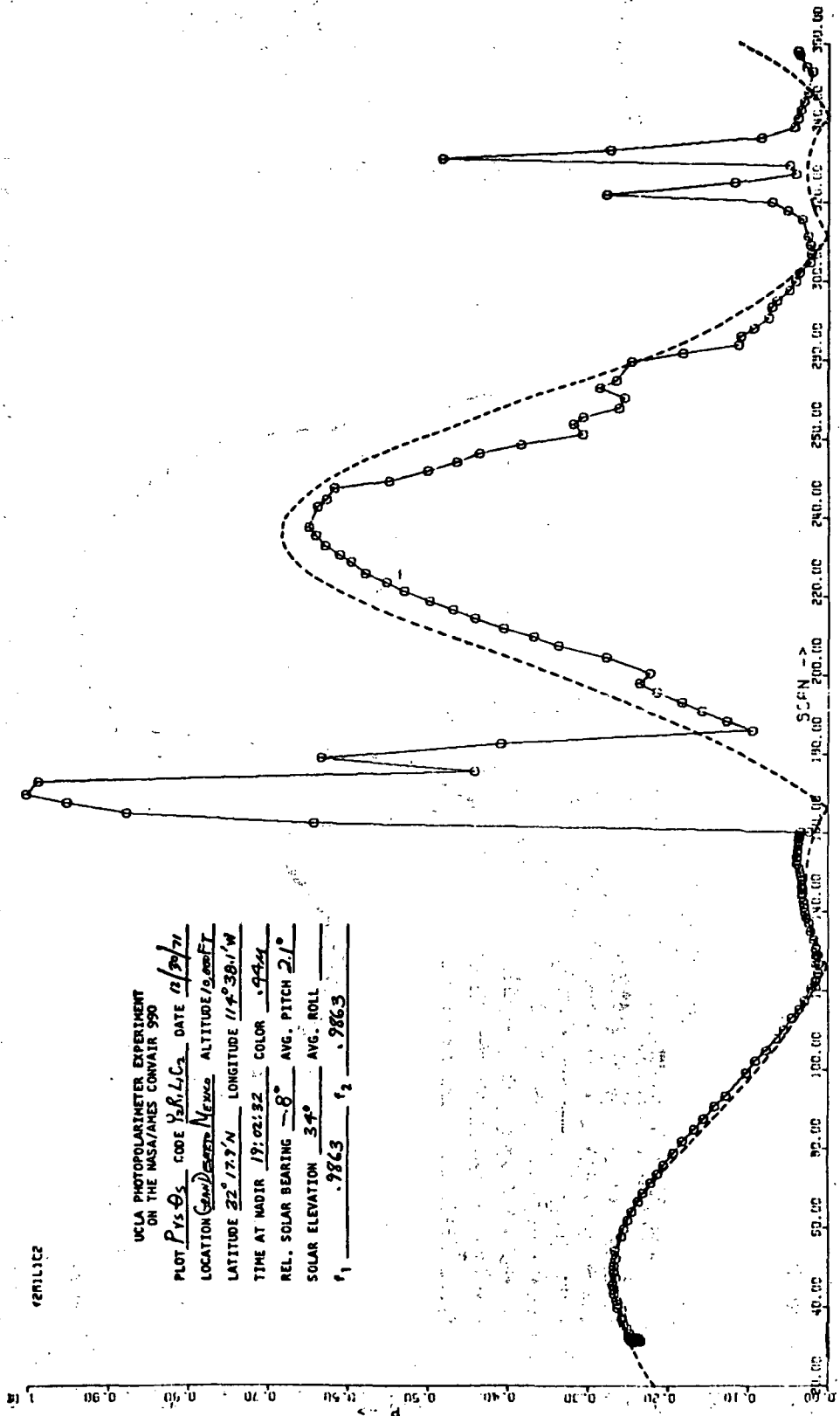LOCATION _(SW)__Gulf__of__Mexico_ ALTITUDE/_9,000_Ft_

LATITUDE _22°17.9'N_ LONGITUDE _114°38.1'W_

TIME AT NADIR _19:02:52_ COLOR _.944_

REL. SOLAR BEARING _-8°_ AVG. PITCH _2.1°_

SOLAR ELEVATION _34°_ AVG. ROLL _____

$f_1$ _.9863_ $f_2$ _.9863_

83

UCLA PHOTOPOLARIMETER EXPERIMENT
ON THE NASA/AMES CONVAIR 990

PLOT $P$ vs $\theta_s$   CODE $Y.R. L_z C_z$   DATE 14/30/71

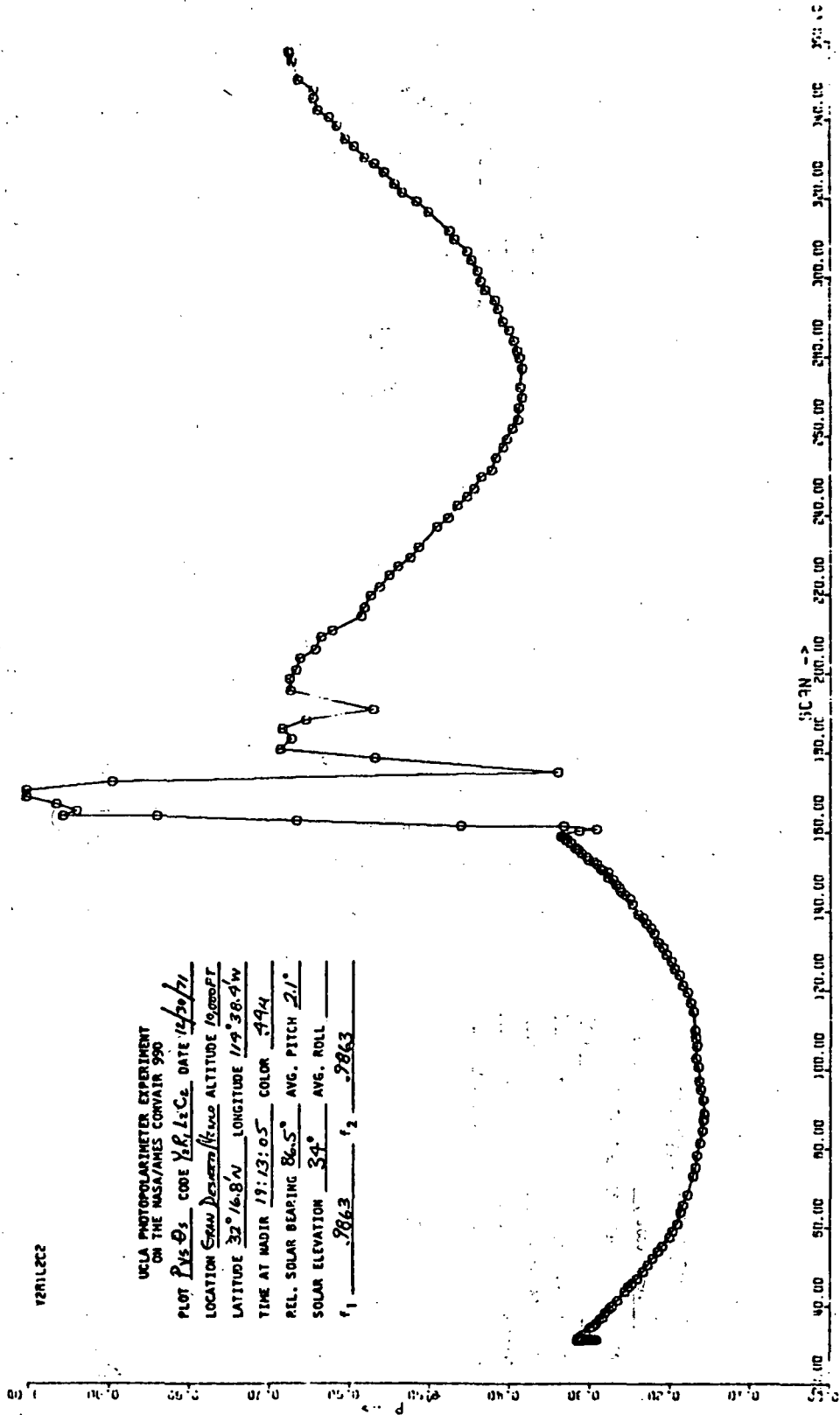LOCATION San Bernadino ALTITUDE 10,000 FT

LATITUDE 32° 16.8' N   LONGITUDE 119° 38.4' W

TIME AT NADIR 19:13:05   COLOR .494

REL. SOLAR BEARING 86.5°   AVG. PITCH 2.1°
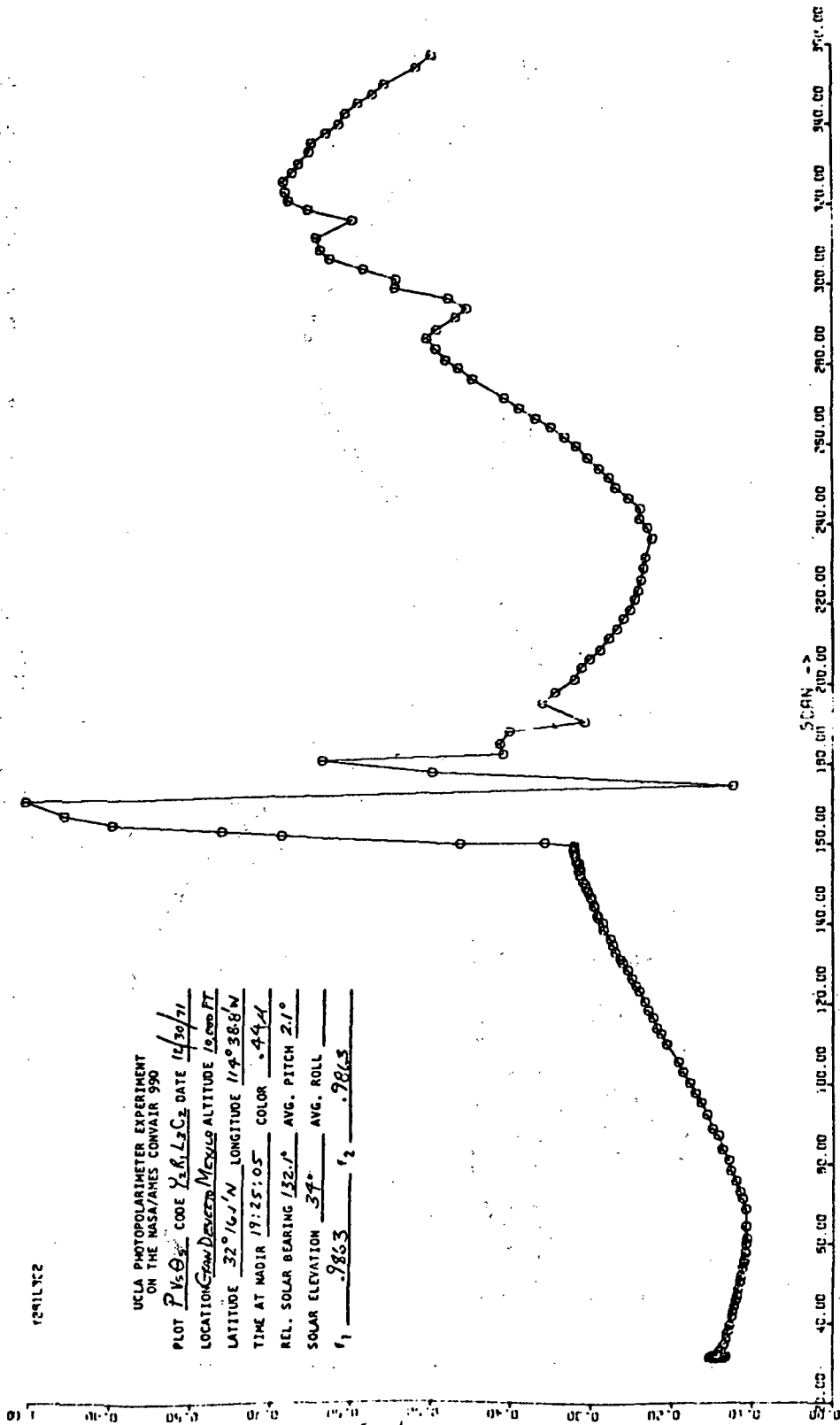
SOLAR ELEVATION 34°   AVG. ROLL _____

$f_1$ ____ .9863   $f_2$ ____ .9863

72AIL2C2

84

UCLA PHOTOPOLARIMETER EXPERIMENT
ON THE NASA/AMES CONVAIR 990

PLOT $P$ vs $\theta_z$ COE $V_1 R_1 L_3 C_2$ DATE 10/30/71
LOCATION Gran Desierto Mexue ALTITUDE 10cm FT
LATITUDE 32°16.1'N LONGITUDE 114°36.8'W
TIME AT NADIR 19:25:05 COLOR .444
REL. SOLAR BEARING 132.1° AVG. PITCH 2.1°
SOLAR ELEVATION 34° AVG. ROLL
$r_1$ .9863 $r_2$ .9863

SCAN →

85

UCLA PHOTOPOLARIMETER EXPERIMENT
ON THE NASA/AMES CONVAIR 990

PLOT $P_{vs}\theta_s$ CODE $Y_vR.I.+C_z$ DATE 11/30/71
LOCATION Gran Desierto Mexico ALTITUDE 10,000 FT
LATITUDE 32°16.7'N LONGITUDE 114°40.5'W
TIME AT NADIR 19:35':31 COLOR .44μ
REC. SOLAR BEARING -138° AVG. PITCH 19°
SOLAR ELEVATION 37° AVG. ROLL _____
$f_1$ .9863 $f_2$ .9863

UCLA PHOTOPOLARIMETER EXPERIMENT
ON THE NASA/AMES CONVAIR 990

PLOT $P$ vs $\theta_s$  CODE $V R_1 L C_2$  DATE 12/30/71

LOCATION (San Dieguito Mesa)  ALTITUDE 40,000 FT
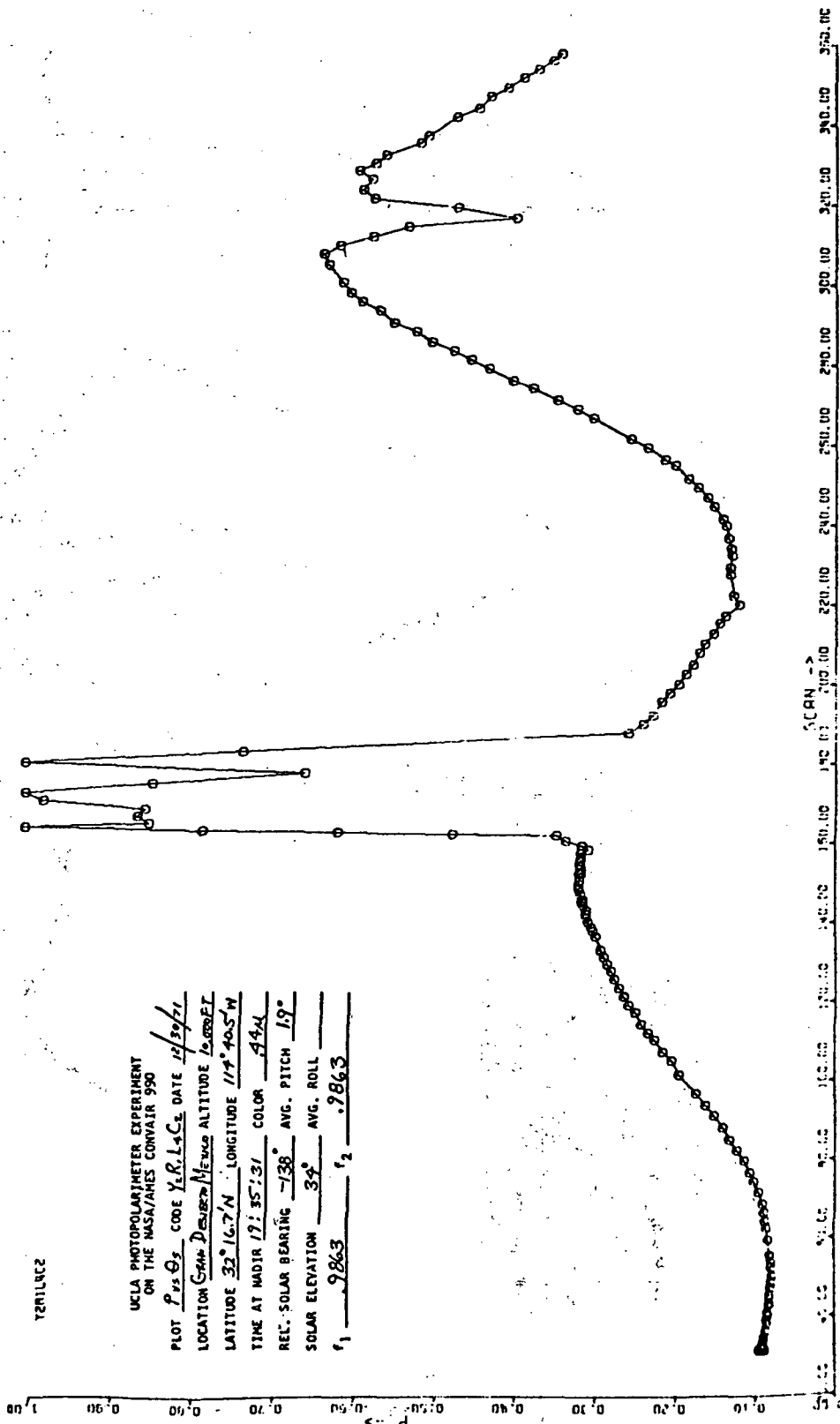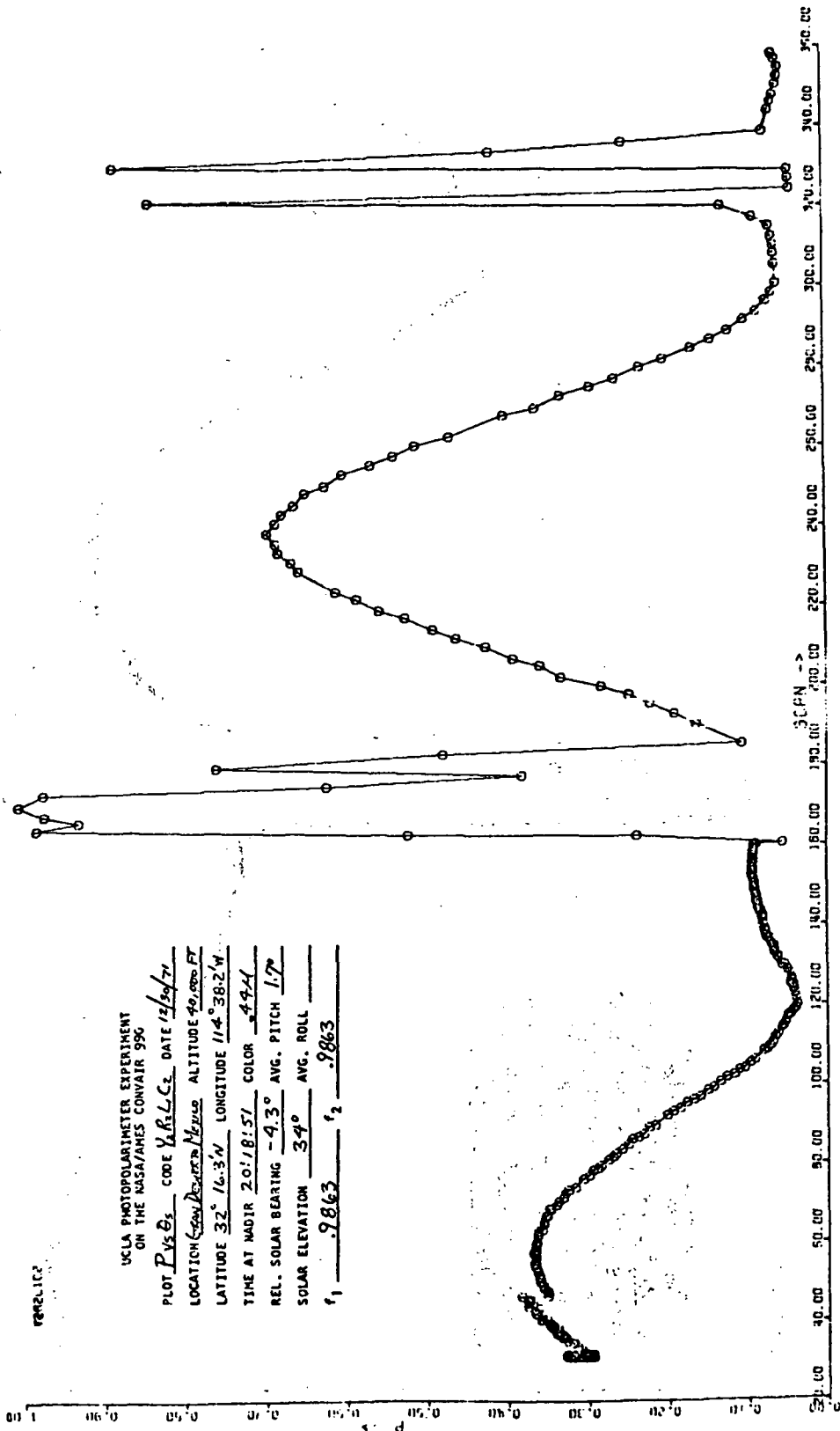
LATITUDE 32° 16.3'N  LONGITUDE 114° 38.2'W

TIME AT NADIR 20:18:51  COLOR 494

REL. SOLAR BEARING −4.3°  AVG. PITCH 1.7°

SOLAR ELEVATION 34°  AVG. ROLL

$\epsilon_1$ .9863  $\epsilon_2$ .9863
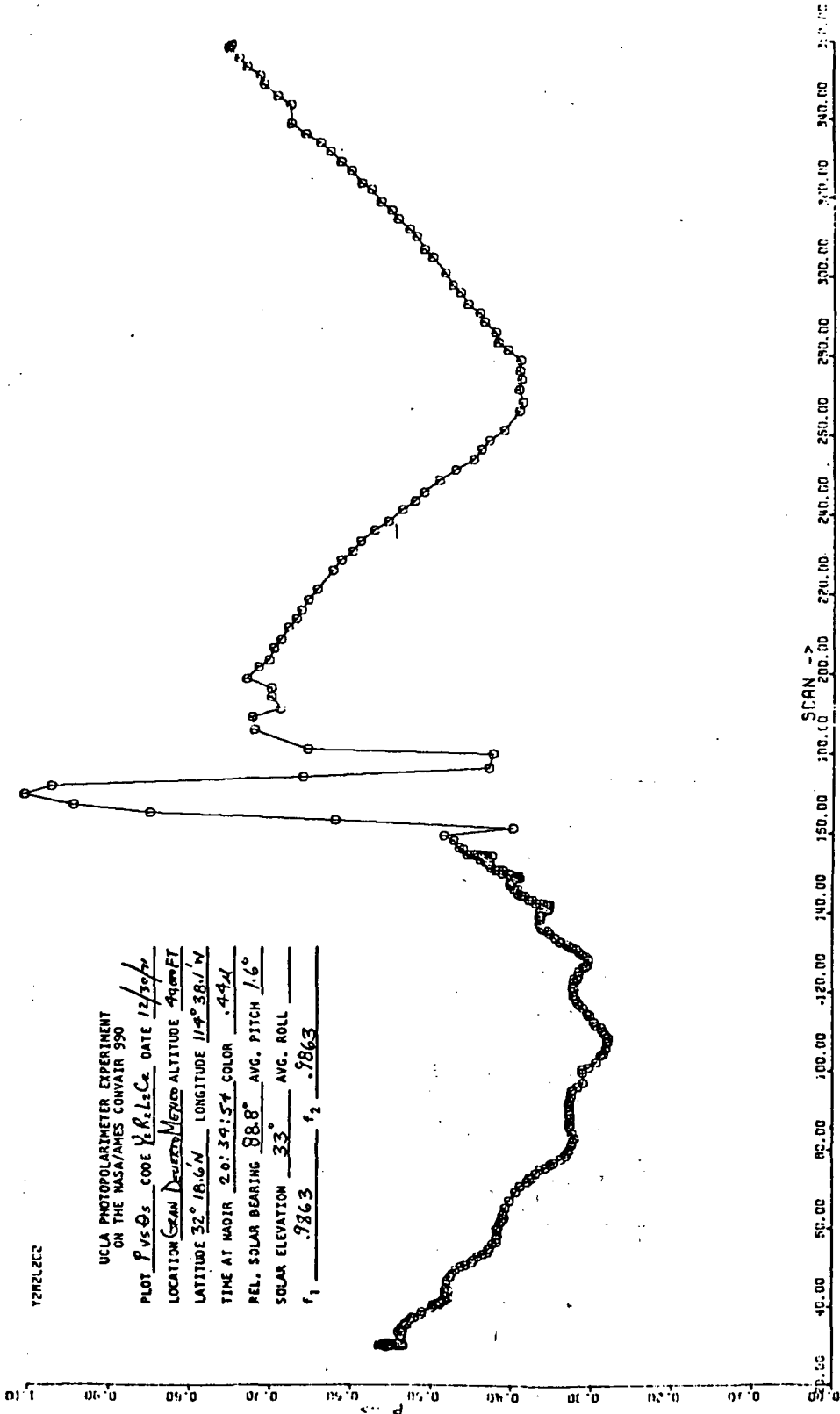
UCLA PHOTOPOLARIMETER EXPERIMENT
ON THE NASA/AMES CONVAIR 990

PLOT _P vs θs_ CODE _½RₗₗₗCₐ_ DATE _12/30/__

LOCATION _Gran Desierto Mexico_ ALTITUDE _49000 FT_

LATITUDE _32° 18.6′ N_ LONGITUDE _114° 38.1′ W_

TIME AT NADIR _20:34:54_ COLOR _.444_

REL. SOLAR BEARING _88.8°_ AVG. PITCH _1.6°_

SOLAR ELEVATION _33°_ AVG. ROLL _____

f₁ _.9863_ f₂ _.9863_

SCAN →

UCLA PHOTOPOLARIMETER EXPERIMENT
ON THE NASA/AMES CONVAIR 990

PLOT $P$ vs $\theta_s$ CODE $Y_2 f_1 l_3 C_2$ DATE 12/30/71

LOCATION Son Desert Mexico ALTITUDE 19,000 FT

LATITUDE 32°15'N LONGITUDE 114°38.3'W

TIME AT NADIR 20:52:00 COLOR .444

REL. SOLAR BEARING 131.3° AVG. PITCH 1.4°

SOLAR ELEVATION 32° AVG. ROLL ___
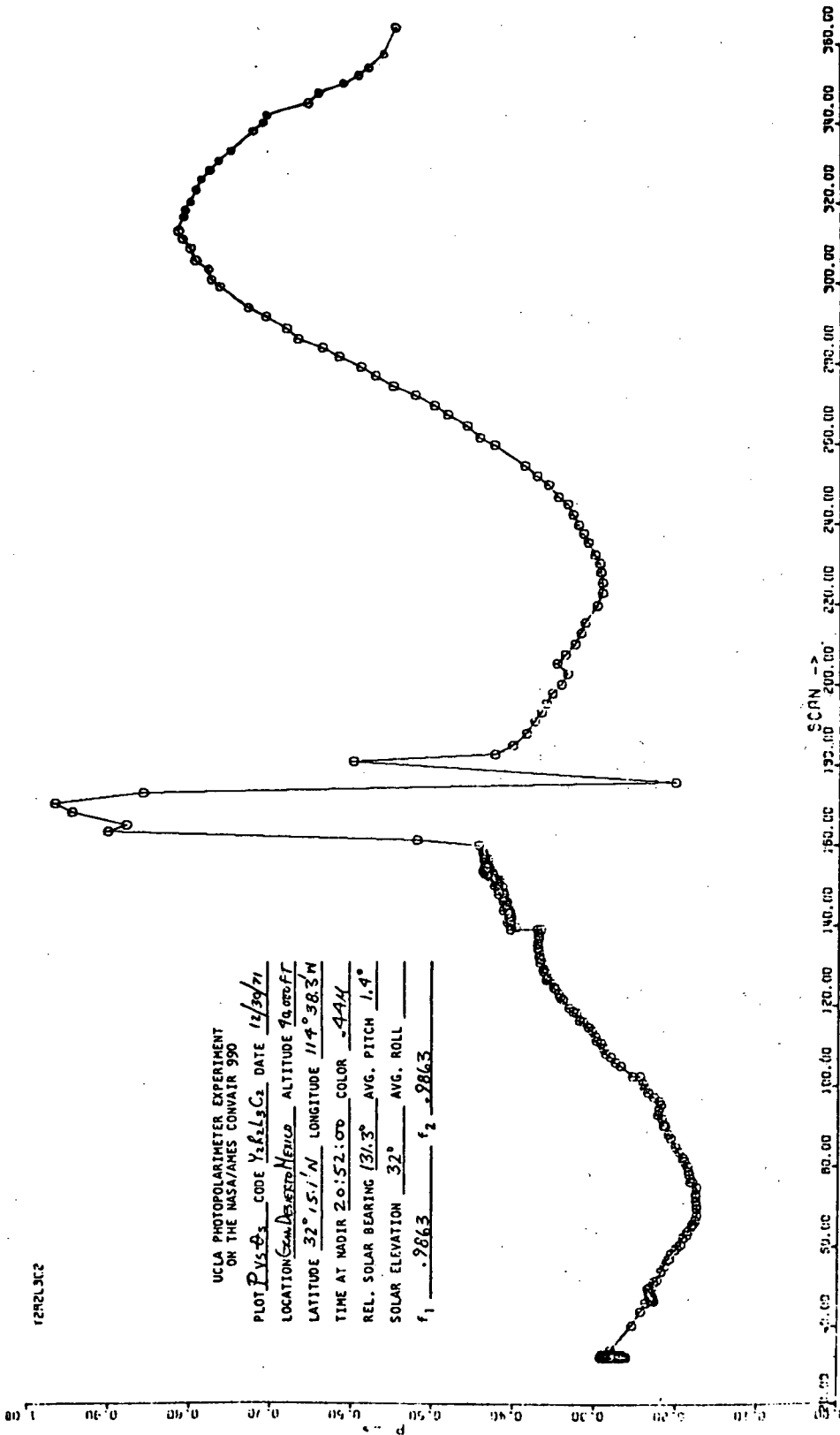
$f_1$ .9863   $f_2$ .9863

r2n2L3C2

SCAN —>

P

89

UCLA PHOTOPOLARIMETER EXPERIMENT
ON THE NASA/AMES CONVAIR 990

PLOT $P$ vs $\theta_3$ CODE $V_2 R_3 L_4 C_2$ DATE 12/30/71
LOCATION Salton Desert M, E-W ALTITUDE 39,000 FT
LATITUDE 32° 18.6'N LONGITUDE 114° 41.1'W
TIME AT NADIR 21:08:52 COLOR .44$\mu$
REL. SOLAR BEARING -136.9° AVG. PITCH $\wedge$4°
SOLAR ELEVATION 30.7° AVG. ROLL
$f_1$ .9863 $f_2$ .9863

UCLA PHOTOPOLARIMETER EXPERIMENT
ON THE NASA/AMES CONVAIR 990

PLOT $P$ vs $\Theta_s$ CODE $Y_6 L_6 C_6$ DATE 12/29/71

LOCATION _Sean Devoto Hoque_ ALTITUDE _19,000 FT_
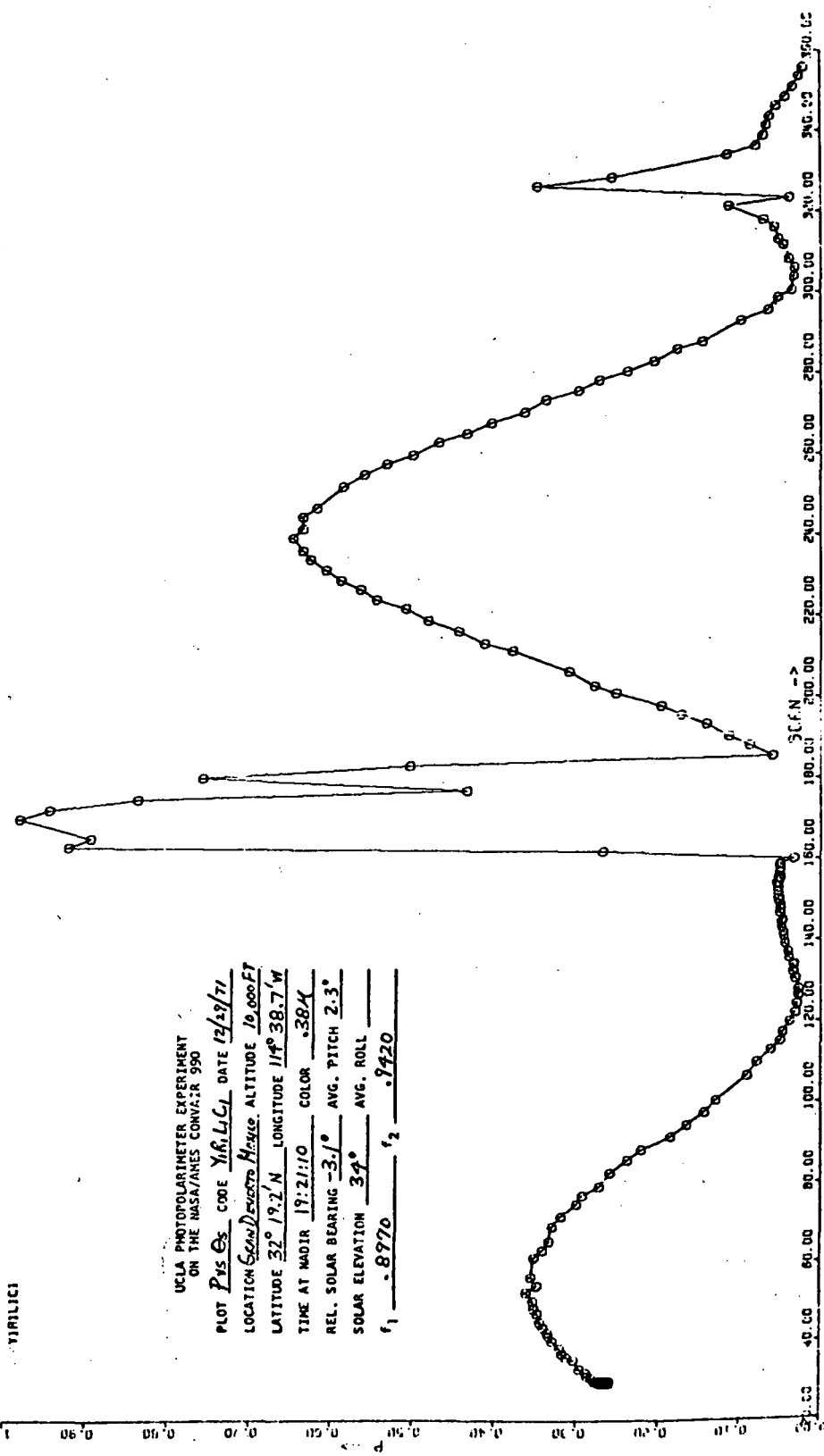
LATITUDE _32° 19.2' N_ LONGITUDE _114° 38.7' W_

TIME AT NADIR _19:21:10_ COLOR _.384_

REL. SOLAR BEARING _-3.1°_ AVG. PITCH _2.3°_

SOLAR ELEVATION _34°_ AVG. ROLL _____

$f_1$ _.8976_ $f_2$ _.9420_

91

UCLA PHOTOPOLARIMETER EXPERIMENT
ON THE NASA/AMES CONVAIR 990

PLOT _P vs θs_ CODE _Y,R,L,C₃_ DATE _12/29/71_

LOCATION _Cow Desert House_ ALTITUDE _10,000 FT_

LATITUDE _32°18.2'N_ LONGITUDE _114°38.7'W_

TIME AT NADIR _19:21:10_ COLOR _.50 M_

REL. SOLAR BEARING _-3.1°_ AVG. PITCH _2.3°_

SOLAR ELEVATION _34°_ AVG. ROLL _____

f₁ _.9565_ f₂ _.9650_

92

UCLA PHOTOPOLARIMETER EXPERIMENT
ON THE NASA/AMES CONVAIR 990

PLOT $P$ vs $\theta_s$ CODE $V_1R_1L_1C_4$ DATE 12/30/71

LOCATION Gran Desierto Mexico ALTITUDE 10,000 FT

LATITUDE 32° 17.9' N LONGITUDE 114° 38.1' W

TIME AT NADIR 19:02:32 COLOR .584

REL. SOLAR BEARING -8° AVG. PITCH 2.1°
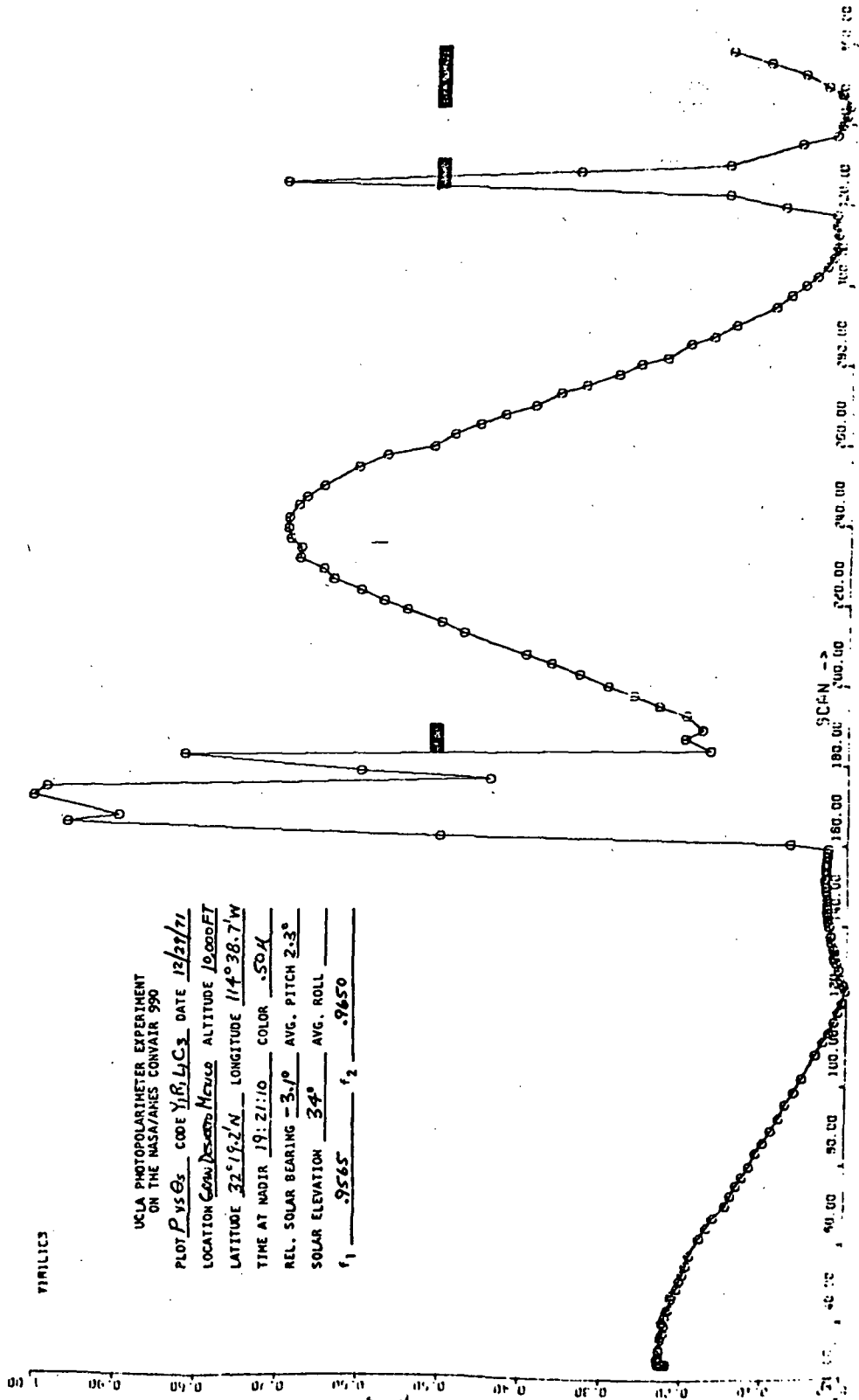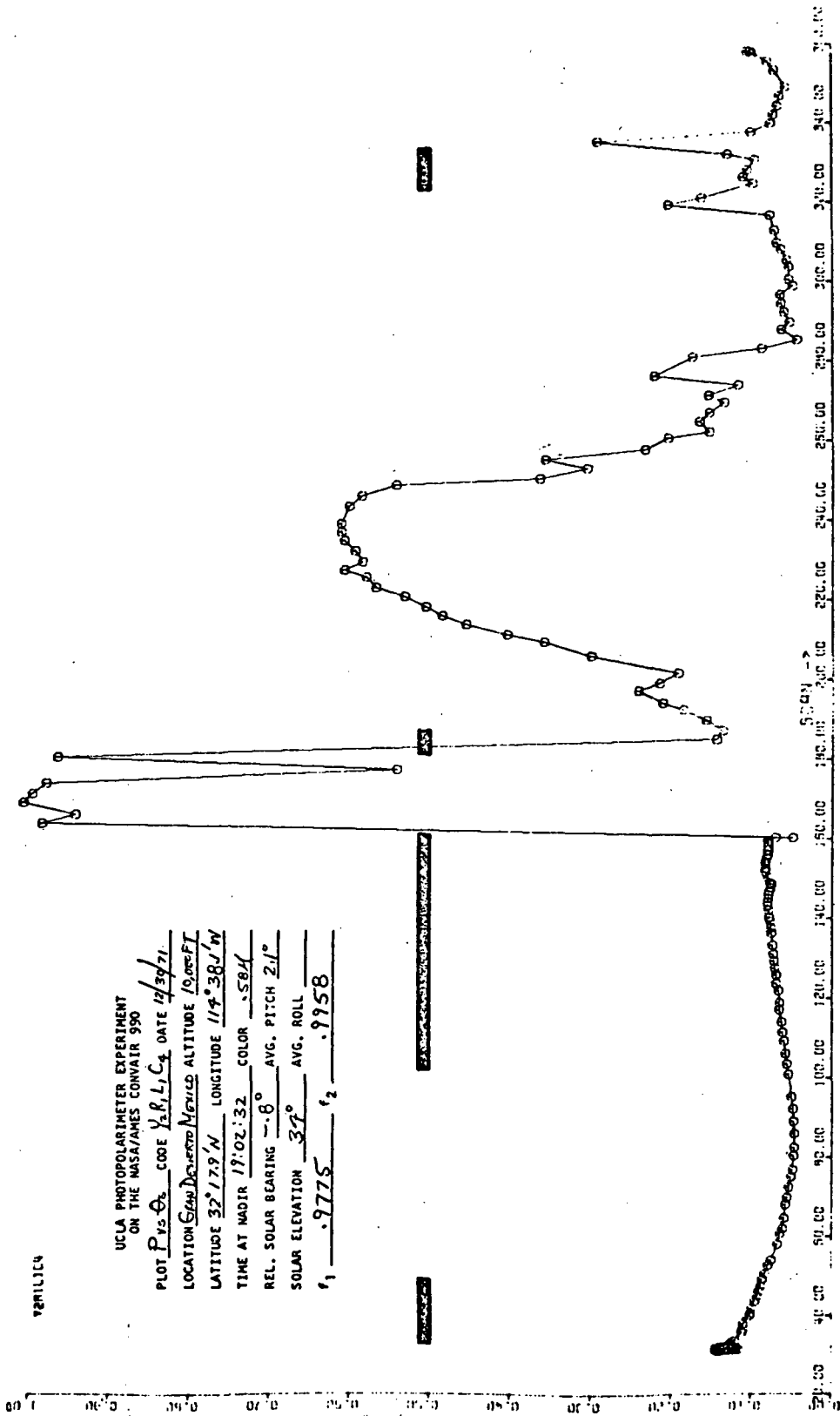
SOLAR ELEVATION 37° AVG. ROLL

$\epsilon_1$ .9775 $\epsilon_2$ .9958

Note the excellent agreement, particularly on the ground scan portions for both days showing that the aerosol has an insignificant effect on the polarization as would be expected for the particle counts presented in Section 3.2.1. The departure of the theoretical curve on the left hand side of the peak in the skylight portion is not understood at present. It should be noted, however, that the skylight data from both Y1 and Y2 are in excellent agreement with each other except for the cirrus cloud dips. The agreement might be even better were it not for the occurrence of a Type A glych at $200^O$ in Y2R1L1C2.

Though not shown here, curves calculated for the radiation emerging from the <u>top</u> of the atmosphere do not yield the same agreement, illustrating the importance of the internal field calculations. It was hoped that Dr. Takashima would be able to calculate some curves for relative solar bearings other than $0^O$, but his hasty departure for Japan precluded this. Further calculations will require both more time and money, both of which are exhausted at present.

The entire set of curves from Y1 and Y2 are presented here in the hope that workers either here or elsewhere will be able to make further analysis of them.

## 4.0 SUMMARY AND RECOMMENDATIONS FOR FURTHER WORK

4.1 Instrumentation. - A detailed critique of the instrument is presented in the appendix and in Section 3.2.3 of this report. To summarize those comments, the instrument requires refurbishing before it can be used for further experiments, some of which is desirable and some of which is necessary. Once the sources of systematic error are eliminated or reduced to an accountable state, the system will be capable of the high quality measurements desired. Evidence for this is seen in the low scatter of the data presented in the previous section, in which point-to-point connection results in a remarkably smooth curve.

In many of the laboratory and field experiments the accuracy of the measurements was found to be limited by the three digit capacity of the A/D converter. Since both the converter and tape recorder are presently outmoded and were the source of major problems, it is advisable to replace these two components for future experimental work.

The results of the flight experiment have demonstrated the validity of the instrumental system and techniques, and the feasibility of using a similar system for satellite measurements though some modifications may be necessary. A considerable practical advantage was gained in using the solid-state detector, thereby eliminating the need for a precision high-voltage photomultiplier power supply. If, however, it is decided to use a substantially decreased field of view for the satellite instrument, it may be necessary to return to a photomultiplier as a detector. If the field of view is decreased by one order of magnitude or less, the solid state detector may be retained by operating in a biased mode. Though this would result in an increase in statistical errors, it would still be preferable to a photomultiplier.

A common pitfall of experimental science is improper or inadequate calibration of the instrumentation. Calibration problems peculiar to the multi-barrel polarimeter as well as the general lack of polarimetry standards have been discussed. The need for exhaustive testing and calibration of the instrument prior to launch as well as methods for calibration checks in space (see, e.g., SO46FR (32)) cannot be overemphasized.

4.2 Experimental Results. - For reasons already presented, the experiments were conducted under zero turbidity conditions. The comparison with the Rayleigh atmosphere calculation demonstrates the excellent agreement between theory and experiment that may be obtained with good instrumentation and good experimental procedures. As always, it is important to study first the simplest situations before haphazardly attacking the most complex situations. In this case, it means exhaustively studying

tracked homogeneous target areas such as the Gran Desierto primarily in the sun plane, under a variety of turbid conditions with simultaneous direct sampling. If this is not done, there is small hope of understanding results from a satellite where of necessity the "targets" may not be homogeneous (except of course over oceans, extensive cloud cover, or large desert areas) and the scanning plane may not be normal to the earth much less the sun-plane.

As it was impossible to fly the instrument under turbid conditions, we have relied on the recent work of Rao and Takashima to demonstrate that a total atmospheric turbidity may be determined from the polarization of emergent radiation. The tracking procedure and improved instrumentation developed under this contract should lead to greater accuracy and confidence in the turbidity determination.

4.3 Theoretical Advances. - The theoretical work conducted under the current program has produced two major advances in treating scattering by turbid atmospheres.

The first and most general result is the equivalent characterization of the number-size distribution of polydispersions. This eliminates the multiplicity of distributions formerly used and reduces the number of parameters needed to characterize hazes or aerosols. It is clear that this represents both a conceptual and computational advantage in compiling a model library.

The second significant result is the separation of the forward peak which will result in a more tractable formulation of the computational problem leading to speedier and therefore cheaper calculations. A corollary result is that the number-size distribution may be determined by study of the solar aureole from the ground. Though not directly applicable for the satellite experiment currently envisioned, this result may be used for ground based experiments in support of the satellite experiment. The result might also be used in a satellite experiment studying the aureole through the atmospheric limb to determine stratospheric particulates. Such an experiment does not require polarimetry but a polarimeter may be used if the field of view may be reduced to a size much smaller than the solar disc ($\sim\frac{1}{2}^{o}$). In this case, there would be no problem with signal strength since the intensities involved would be many orders of magnitude greater than those involved in the earthward-looking polarimetry experiment.

4.4 Further Work. - The current state of the project suggests several avenues to be pursued in the near future. The outline below is somewhat arbitrary but is constructed to present those items which should receive the most immediate attention. Some of the items may be approached concurrently, others of necessity consecutively.

96

## OUTLINE FOR FUTURE WORK

A. Theoretical

    1) Incorporation of the theoretical results (separation of the forward peak) into model calculations.

    2) Formulation of plans for the model library including types of aerosol distribution and ground reflection characteristics as well as computational methods to be used.

    3) Compilation of tables and graphs to constitute a library.

B. Experimental

    1) Further flight experiments on the Convair 990 with the photopolarimeter over a particular area under various turbidity conditions with concurrent direct sampling.

    2) Ground-based aureole studies to determine number-size distribution. Since direct sampling would also be useful here, it would be advantageous to conduct such an experiment concurrent with the Convair 990 experiment or with the other experiments in which direct sampling is being conducted.

C. General

    1) Formulation of requirements for the satellite experiment including orbit, field-of-view, tracking accuracy, preferred target areas, etc.

    2) Development of the satellite photopolarimeter and calibration methods.

    3) Formulation of plans for rapid reduction and assessment of satellite data (data management).

## 4.5 CONCLUSION

One of the original motivations for this study was the problem of whether or not increased industrial activity in recent years is causing an increase in particulate concentrations in the atmosphere on a global scale over and above that produced by naturally occurring processes. It is clear from the material presented here that it is entirely feasible to monitor global turbidity from a satellite photopolarimeter on a long term basis to provide an answer to this question.

Application of the satellite data to yield information on the surface state of oceans, ground moisture, and crops, the nature of cloud cover (ice or water clouds, etc.) as well as more detailed information on aerosols and ground reflection characteristics will depend upon further theoretical work and the availability of satellite data for analysis.

## APPENDIX

### Test Reports on the UCLA/GE Photopolarimeter

1.0 <u>Introduction.</u> - The important experimental objective of this project has been the development of instrumentation suitable for satellite installation (at least in principle) and capable of obtaining reliable data of sufficient accuracy. For this reason as well as for contractual ones, details of tests and analysis of the photopolarimeter's behavior are separated from the body of the report into this appendix. Some redundancy occurs and is desirable; it is hoped that this procedure will underscore rather than minimize the role of the PPM in the flight experiments and data interpretation.

The instrument used in the current phase (i.e., contract) is based on ideas and prototypes originated at UCLA by T. A. Hariharan and W. L. Stevens under NASA grant No. NGR 05-007-041. (ref. 28) The current design was developed in cooperation with the General Electric Space Science Laboratories at Valley Forge, Pennsylvania in breadboard form under an earlier subcontract (S046) and the model used in the flight experiments is a refinement of that model constructed by GE under subcontract in the current contract.

The final report on the S046 subcontract (S046FR) ref. 31) contains elaborate descriptions of the photopolarimeter design which will not be repeated here. (The phenomenological design principles have been discussed in the body of this report.) A number of design changes were incorporated in the engineering model, however, the most significant being the incorporation of a solid state detector (United Detector Technology, Inc., PIN-10) instead of a photomultiplier. This resulted in an improvement in ruggedness, eliminated the need for a highly stable high voltage supply, and reduced space and weight requirements for both detector and power supply.

Other significant differences are:

1) A calcite compensating block in the I barrel with optic axis oriented similar to that in the Glan-Thompson prisms in the B and D barrels, i.e., normal to the optical axis of the barrel. This is either parallel or normal to the polarization transmission plane of the B prism.

2) The fibre optics are not mixed at the detector or exit end of the bundle as in the S046FR studies. Each input occupies a $120^\circ$ segment of circular exit aperture.

3) The gains of the AGC (Automatic Gain Control) are 1, 10, 100 in the nomenclature of the UCLA workers where the signals are

called I, 2B, and 2D. The GE workers refer to the signals as $\frac{1}{2}$, B, D and the gains as 2, 20, 200. In the reports by the GE workers transmitted here, their own nomenclature is preserved. It is hoped there will be no confusion on the reader's part.[a]

4) The Glan-Thompson prisms contain an interface layer of a new epoxy glue rather than the traditional Canadian Balsam. This was done to enable the instrument to endure lower environmental temperatures.

5) An optional (lower) gain in the preamplifier was included.

Section 2 of this appendix presents tests and results performed at GE both prior to and after assembly, with the names of the responsible GE workers appended. For the sake of coherence, miscellaneous reports have been edited and compiled. Section 3 includes comments by UCLA workers on tests observed at GE in May 1971, (These are referred to as "acceptance tests" though in reality they were only demonstrations) as well as reports on pre-flight, post-flight, and in-flight behavior of the instrument.

Before presenting these reports it is essential to point out some of the difficulties in evaluating photopolarimeters in general, and this instrument in particular. First, there are no standard polarization sources. Textbook definitions of polarization parameters involve procedural prescriptions in terms of the measurement apparatus. Instruments such as this one may become the polarization standards of the future. Even sources for zero polarization do not exist; for some instruments the sun might be adequate, but only for those with fields of view less than half a degree. Devices for magnifying the angular field may well introduce residual polarization and could only be evaluated in terms of a reference photopolarimeter or must satisfy some rigid theoretical conditions. Integrating spheres such as those used by both GE and UCLA described in detail in SO46FR in Section 2.6 may be suitable if the observations are strictly on axis, but observations off center may detect a residual polarization. (A figure of merit for these spheres might be defined as the ratio of the area of the aperture to the hemispherical area, and degrees of polarization of this order can be observed off center.)

A unit polarization source can be defined by passing an arbitrary source through a Glan-Thompson prims. (Note: Older definitions of polarization included use of Nicol prisms, but it is now

---

[a]For convenience, the original Q, U, I, etc., notation used in SO46FR is retained in this appendix instead of the more complex generalized notation intruduced earlier.

known that Glan-Thompsons are superior, the non-normal surfaces of Nicol permitting residual elliptical polarization.) For some purposes high quality polaroid sheets may be used, but the transmission of polaroid can vary significantly over the areas involved.

This particular instrument has three independent and physically separated optical barrels. Even assuming perfect boresighting and identical fields of view ($3^\circ$) the fields of view do not overlap at laboratory distances. Thus, in tests involving integrating spheres, each barrel is viewing well separated portions of the target surface, and when a polaroid sheet is used, each barrel looks through a different portion of the sheet. Similarly, all three barrels cannot look through the same (external) polarizing prism simultaneously. Rotating or translating the instrument to permit each barrel to look through the same prism or portion of polaroid or portion of the integrating sphere target* is limited in accuracy by the accuracy with which the movements can be accomplished and by the stability of the light source. Also, laboratory sources have not provided sufficient intensity in the short wavelength channels and skylight observations have been necessary for studies of those channels. Certain evaluations have been made only for the 5000 Å and/or 5800 Å barrels and the results must be extrapolated to the others.

Another significant problem in working with the instrument is that the system is not designed to give real-time readouts of data. Methods used for real-time readouts (quantitative) were limited by the equipment available as well as by peculiarities of the system itself and generally required measurements of one parameter at a time with significant time required to move the sampling pulse to another parameter (i.e., one Stokes parameter of one color, etc.). It was found that measurements recorded on tape and then reduced via the computer were more reliable and accurate, but this required excessive time delays , usually a minimum of three days. This presented severe limitations in working with the instrument. For example, if the skylight measurements were being made and the results indicated either correction of some malfunction or alteration of experimental procedures, it was necessary to wait until the weather was again amenable for measurements. This was an extreme limitation in post-flight experiments. In the period from the beginning of January 1972 to the beginning of April it was possible to make skylight measurements on only two days. In order to begin preparation of this report, further experiments were abandoned.

Not all of the tests performed either by GE or by UCLA are reported. In most cases, tests deleted were superceded by later tests or performance of the instrument in the flight experiments.

---

*See Section 3.1 for a detailed description of such tests.

101

Even though the flight worthiness of the instrument has been demonstrated, the environmental tests performed at GE were an important part of the subcontract and essential for pre-flight tests. The letters and graphs verifying these tests are included as they were transmitted to us.

The laboratory of the Atmospheric Radiation Group at UCLA does not have adequate facilities for performing or verifying many of the tests involved, not only the environmental tests but those such as calibrated sensitivity, angular response of the barrels, etc. Thus, the inclusion of the pertinent GE reports is essential.

Table 1 -- Optical Component Tests

| Component | F.l. | Color-%T | Disp. | Biref. |
|---|---|---|---|---|
| Objective "B" | 98 | 1-93<br>2-93<br>3-93<br>4-96 | (2.9mm) | $\delta < 10^{-2}$ |
| Objective "D" | 100 | 1-91<br>2-94<br>3-94<br>4-96 | (2.9mm) | $\delta < 10^{-2}$ |
| Objective "I/2" | 100 | 1-91<br>2-94<br>3-94<br>4-96 | (2.9mm) | $\delta < 10^{-2}$ |
| Ap. Im. "B" | 13 | 1-96<br>2-97<br>3-95<br>4-95 | | |
| Ap. Im. "D" | 13 | 1-96<br>2-97<br>3-95<br>4-95 | | |
| Ap. Im. "I/2" | 13 | 1-96<br>2-96<br>3-95<br>4-95 | | |

| Component | | Color-%T | FOV(6328Å) | Reject. |
|---|---|---|---|---|
| Prism "B" | | 1-35<br>2-42<br>3-42<br>4-46 | $16.3^{\circ}$<br>$(16.7^{\circ})$ | $< 10^{5}$ |
| Prism "D" | | 1-36<br>2-43<br>3-43<br>4-46 | $15.3^{\circ}$<br>$(15.2^{\circ})$ | $< 10^{5}$ |

103

Table 1 -- (cont.)

| Component | F.l. | Color-%T | FOV(6328Å) | Reject. |
|---|---|---|---|---|
| Compensator "I/2" | | 1-73 | | |
| | | 2-81 | | |
| | | 3-90 | | |
| | | 4-94 | | |
| Fiber Bundles | | 1-66 | | |
| | | 2-66 | | |
| | | 3-66 | | |
| | | 4-63 | | |

2.0 Tests at General Electric: 2.1 Preassembly Optical
Component Tests (T. Wise). - Table 1 is a summary of the various
parameters of the components. The leftmost column groups the
components: Objective lenses, aperture imaging lenses, calcite
prisms and compensator block, and the fiber bundle. Following this
there are tabulated the transmissions of the components at the
four different wavelengths. The "Dispers" column lists the chrom-
atic and polarized dispersion, in terms of change of focal length,
for the lenses and compensator block, respectively. Under "Biref"
there is listed a maximum value of birefringence for the objective
lenses. This is given in terms of the induced optical phase shift
$\delta$; the following formulas relate $\delta$ to the residual birefringence
($\Delta$n) of a component and to the light intensity transmitted by the
second of two crossed analyzers.

$$ I = 4A^2 \sin^2\theta \cos^2\theta \sin^2 \delta/2 $$

Where $\theta$ is the angle between optic axis of material and the axis
of the first polarizer, A is the amplitude of the incident radi-
ation, and $\delta = 2\pi \gamma d \Delta n$ is the phase difference introduced by a
birefringent material of thickness $d$. This intensity will be a
maximum for $\theta = 45^\circ$ where $I = A^2 \sin^2 \delta/2$. $\delta$ less than $10^{-2}$ repre-
sents induced spurious polarization of less than one part in $10^4$
at P = 5%. The "Fov" column in the data sheet gives the measured
polarized fields of view of the two calcite prisms. The values
given, however, relate only to the normal input face of the prism.
As we learned later, the angles should have been referenced to the
optical axis rather than to the mechanical axis. The prisms have
a half degree deviation which makes the actual polarized field of
view larger than this data would indicate. The column labeled
"Reject" gives a maximum value for a passage of the ordinary ray
in the calcite prisms. My tests indicated that the prisms were
at least as good as specified in this respect, possibly better.

The basic set up of the test bench is as follows: An 11-inch
refracting collimator was used to check the collimation of the light
coming from a 3 inch f/1 mirror. All of the component testing was
done with light from a grain-of-wheat lamp at the focal point of
this mirror. Ahead of the lamp was an aperture which restricted
the light bundle to the diameter of the component under test and
ahead of this was a filter holder. I was able to get sufficient
illumination at 3800 Å by consuming several lamps at 20% over volt-
age. To determine the dispersion of the lenses and of the compen-
sator block, the same basic set up was used with a needle point
and a microscope. A UV image converter was used for the 3800 Å
test. Placing the needle at the focal point of the lamp filament
image removed chromatic effects in the microscope.

To check the component transmissions in addition to the mirror and the light source, a remotely operated aperture and shutter were used which permitted easy subtraction of noise present at low signal levels and hence provided accurate ($\pm$1%) values of light transmission. Readout was via a Schottky detector, opamp, digital voltmeter combination. A HeNe laser whose output was fed through the two Glan-Thompson prisms and onto a detector was used to determine the prism rejection and polarized field of view. The dynamic range of the signal levels went from 0.1 millivolt to 10 volts, thus permitting resolution of 1 part in $10^5$ when the uncrossed polarizer signal level was set at 10 volts.

Figs. 1 - 4 are the filter transmission curves provided by Baird-Atomic. In the instrument, the 5800 Å filter has been modified by the insertion of a No. 8 Wratten filter to eliminate the UV wing in the Baird-Atomic filter.
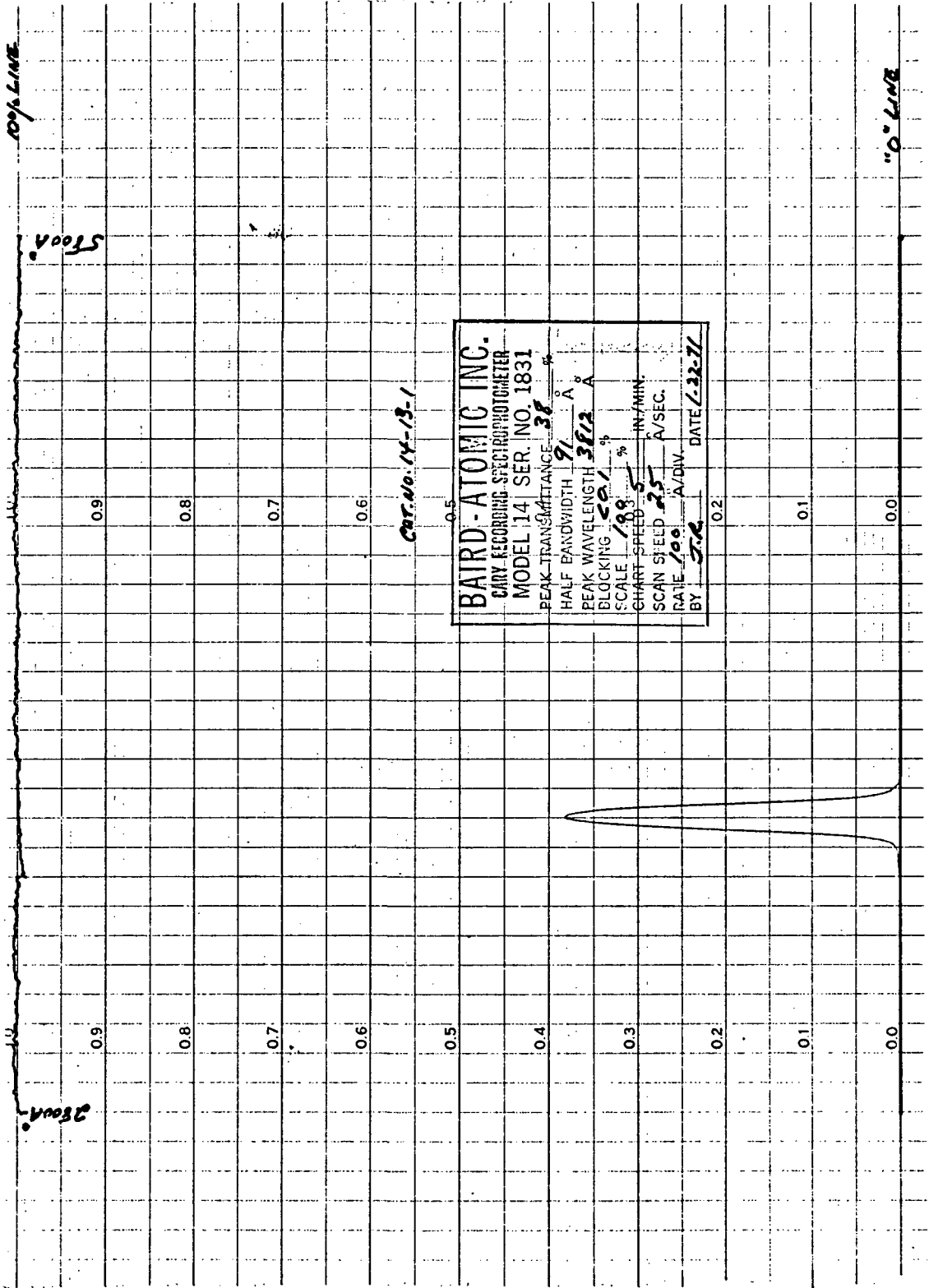
Fig. 1 -- Transmittance of Interference Filter for Color Channel One (C1) Nominally
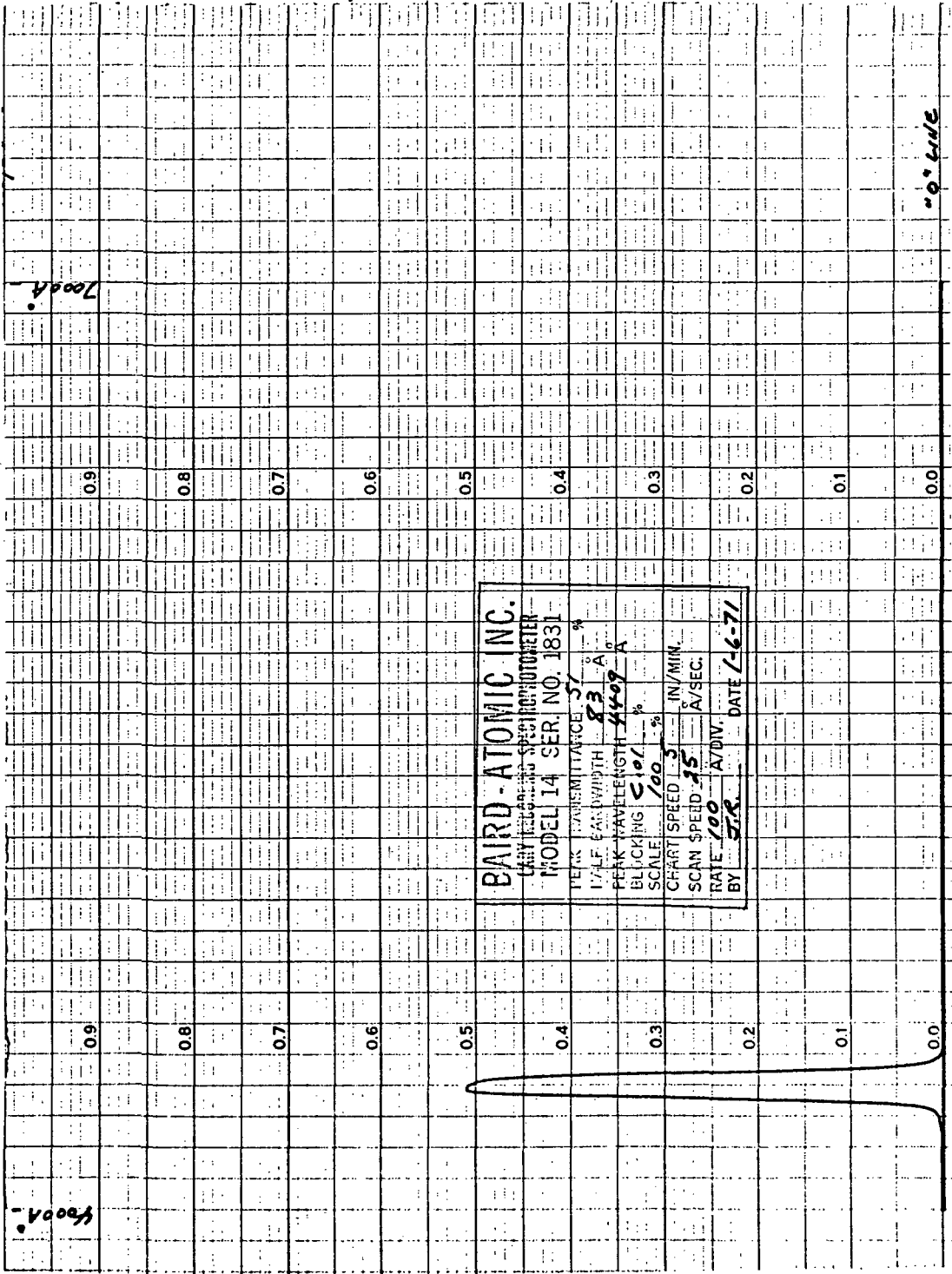Centered at 3800 A.

Fig. 2 -- Transmittance of Interference Filter for Color Channel Two (C2) Nominally Centered at 4000 A.
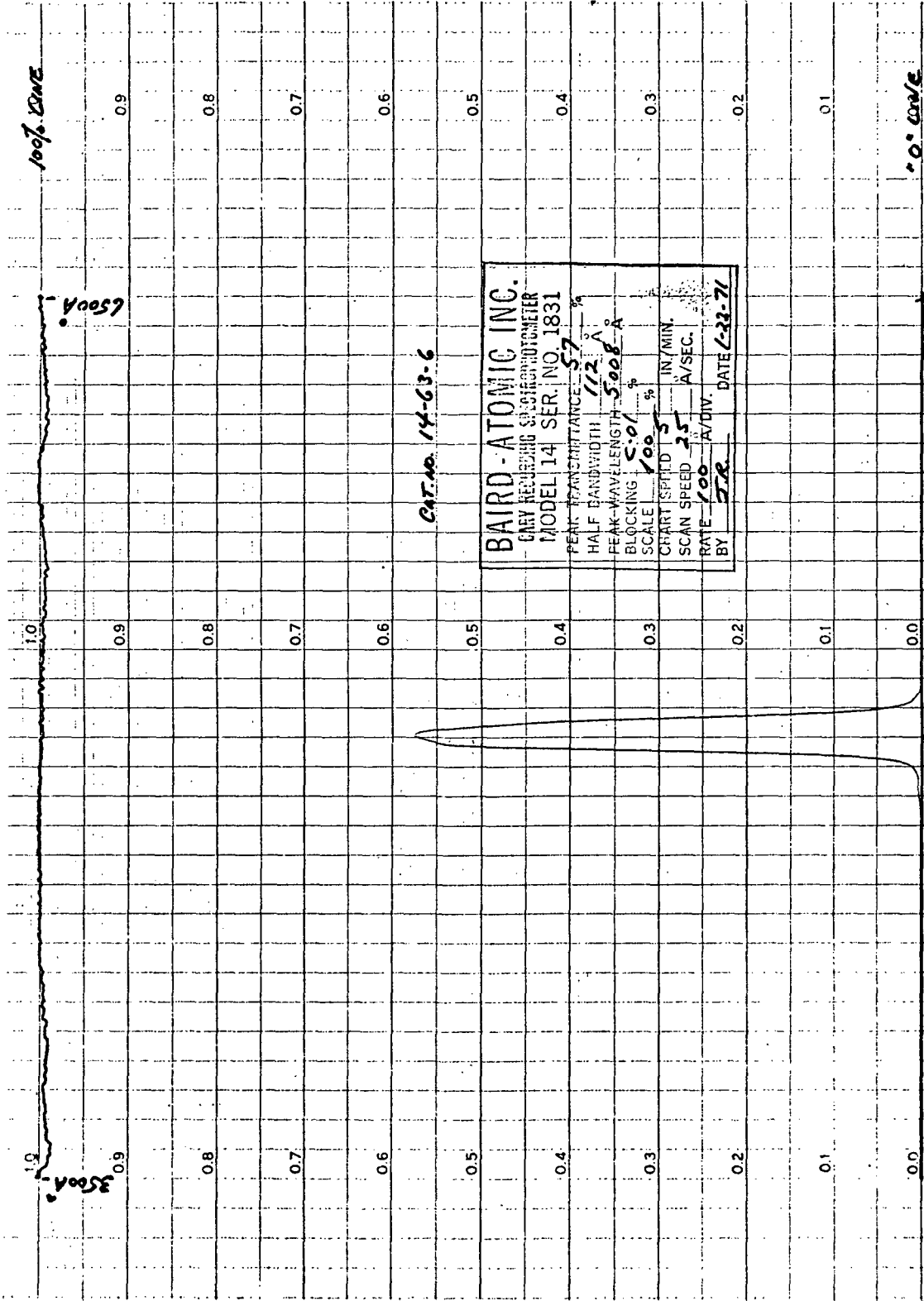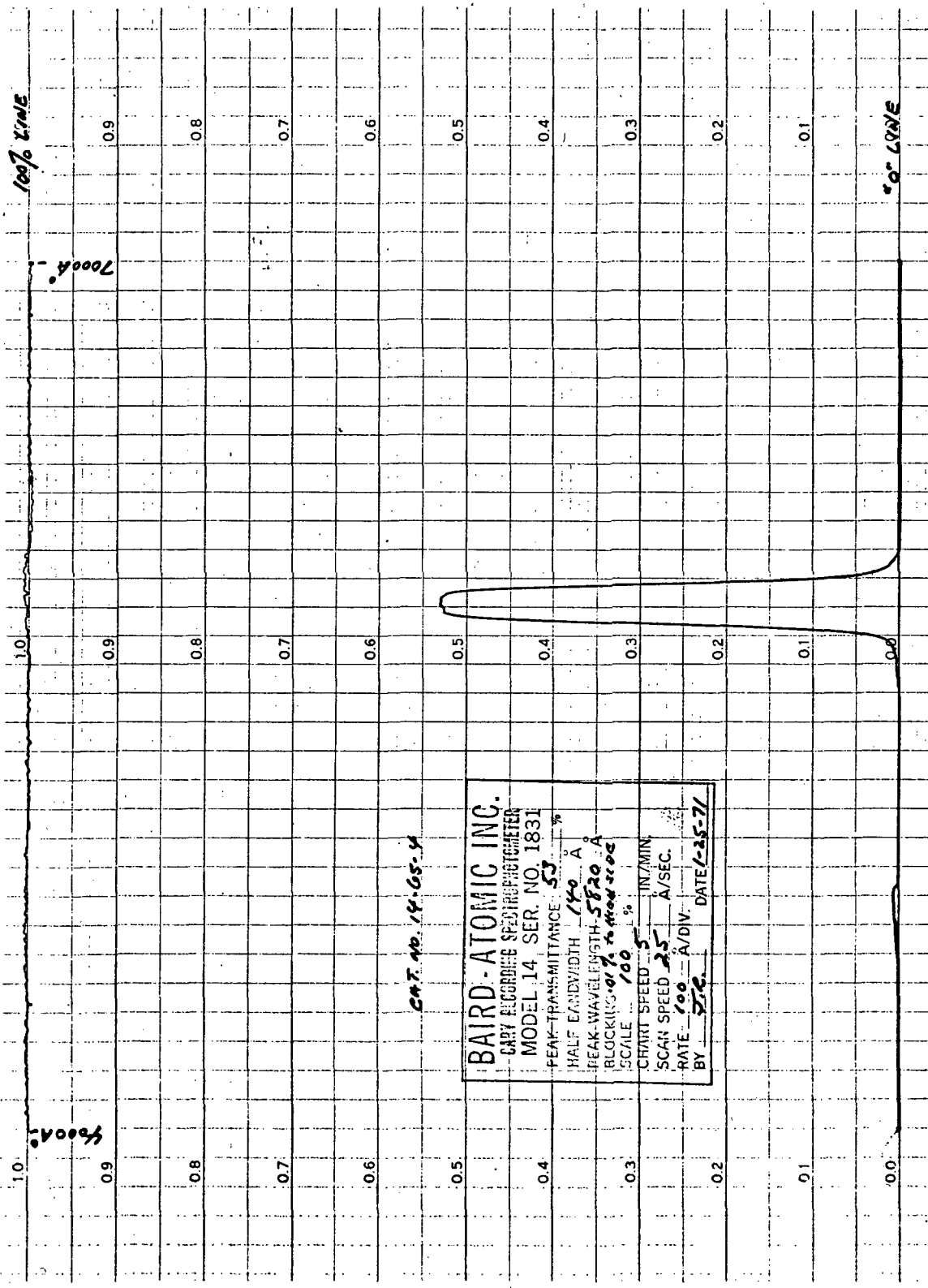
BAIRD-ATOMIC INC.
INFRARED SPECTROPHOTOMETER
MODEL 14 SER. NO. 1831

PEAK TRANSMITTANCE _57_ %
HALF BANDWIDTH _83_ Å
PEAK WAVELENGTH _4407_ Å
BLOCKING _<.01_ %
SCALE _100_ %
CHART SPEED _5_ IN./MIN.
SCAN SPEED _15_ Å/SEC.
RATE _100_ Å/DIV.
BY _J.R._ DATE _1-6-71_

108

Fig. 3 -- Transmittance of Interference Filter for Color Channel Three (C3) Nominally Centered at 5000 A.

BAIRD-ATOMIC INC.

CARY RECORDING SPECTROPHOTOMETER

MODEL 14 SER. NO. 1831

PEAK-TRANSMITTANCE _53_ %

HALF BANDWIDTH _140_ Å

PEAK-WAVELENGTH _5820_ Å

BLOCKING 0.1 % TO 11000 ICS

SCALE _100_ %

CHART SPEED _5_ IN/MIN.

SCAN SPEED _25_ Å/SEC.

RATE _100_ Å/DIV.

BY _S.C._ DATE _1-25-71_

CAT. NO. 14-65-Y

Fig. 4 -- Transmittance of Interference Filter for Color Channel Four (C4) Nominally Centered at 5800 A.

2.2 Field of View:  Boresighting and Angular Response of the B, D, and ½ Barrels. - On June 7, (1971) the instrument was set up in front of the 100" collimator with a pinpoint of light as a probe to determine the boresight, cut-off, and uniformity characteristics of the instrument's field of view.  The results of the first test, when graphed, indicated that the individual fields of view were within a tenth of a degree of the specified three degrees and were boresighted with each other to within a tenth of a degree. Also, cut-off was as expected at the 5000 Å wavelength (Fig. 5).

However, two oddities appeared in the B channel in particular. First of all, its overall signal level was 20 to 30% higher than either of the other two barrels.  Secondly, it had a notable tail-off of the signal on one side.

In an effort to understand what these effects were, the test was repeated with the ½ barrel at the $135^\circ$ position, which has the effect of orienting the prism in the D barrel precisely as the prism in the B barrel had been oriented in the previous test. Although this data appears in the notes, it was not graphed since we found that one of the difficulties in the measurement of the B barrel was a 10% residual polarization effect in the collimator favoring a greater signal for that channel.  We concluded that the data as originally taken was still valid for the determination of boresight, cut-off, and size of the fields of view.  However, uniformity was in doubt.

With the purpose of checking the uniformity of field alone, the integrating sphere was set up 30 feet from the instrument and closed down to a 3 inch opening.  The instrument was then scanned across this target with the I barrel at the $180^\circ$, $135^\circ$, $90^\circ$, and $45^\circ$ positions.  This data appears in graphical form (Fig. 6) and indicates that a small light source does indeed produce a larger signal in the B channel; however, the difference now is only 10%. This 10% difference may be accounted for by the slightly restricted field of view of the B barrel, causing the downward trimming of the other two barrels in order to match integrated responsivity of the three channels.  In addition, the tail-off of the signal in the B channel appears as much as it did in the previous test. In fact, there is a similar, but lesser effect in the D barrel when the D prism is oriented as the B prism was oriented in the previous test.

The physical significance of this effect may be stated as a characteristic of the Glan-Thompson prism and its small changes in refractive index across the interface.  Internal reflection of the extraordinary ray increases as its incidence angle on the interface increases.  This explanation has been confirmed by the actual orientation of the prisms in each of the barrels and by the direction of

111

scan of the point light sources in these tests. The operational significance of this is the greater contribution to the overall signal that a target on one side of the field of view makes relative to a target on the other side of the field of view. Since proper operation of the instrument demands uniform targets, this should be no problem at all.
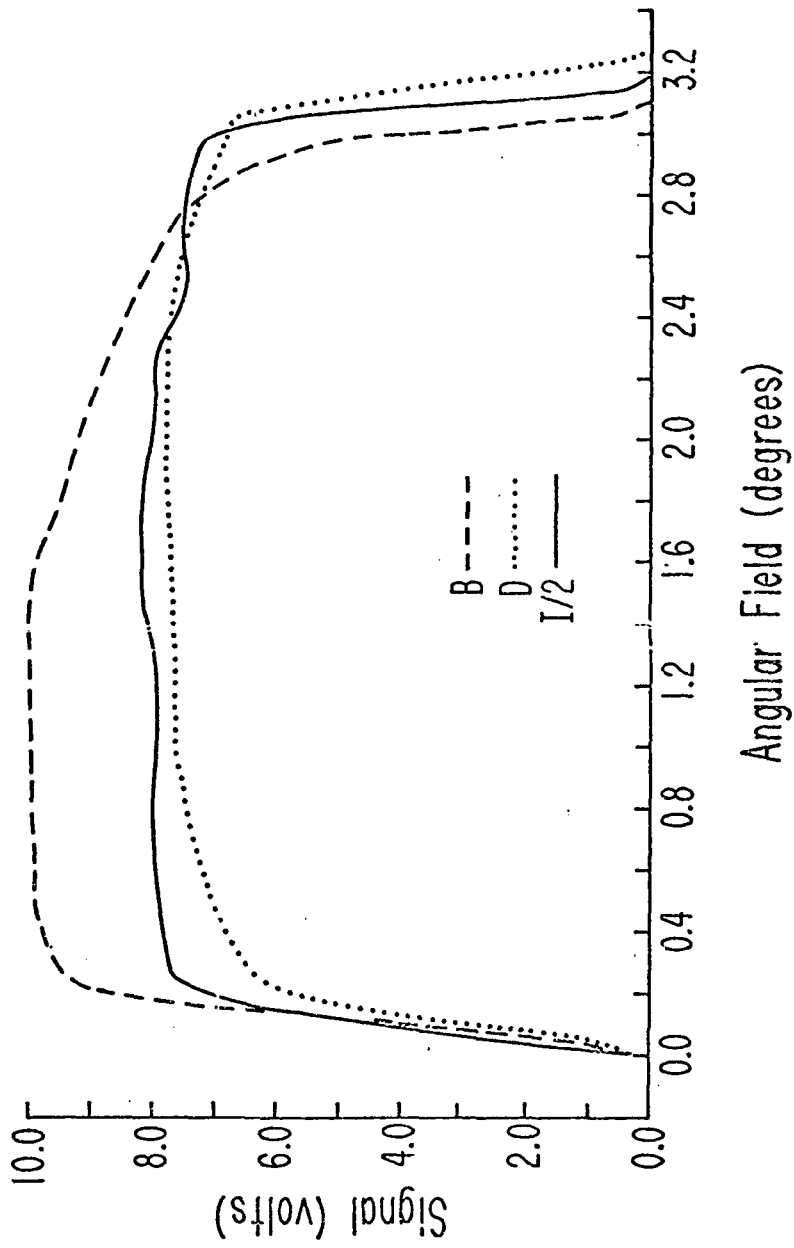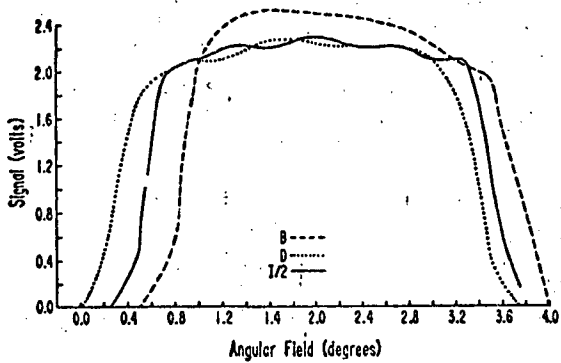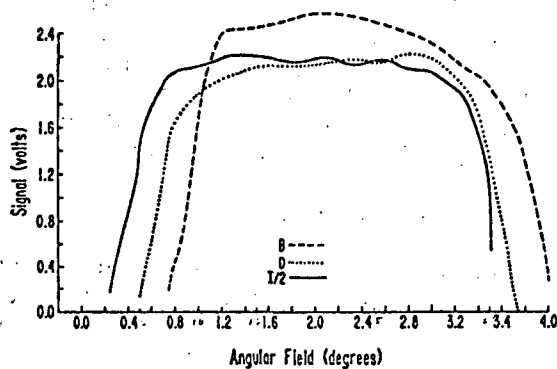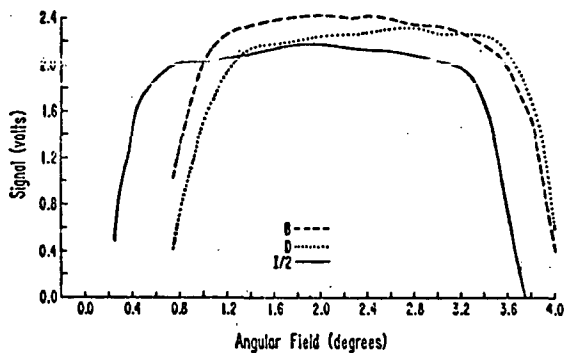
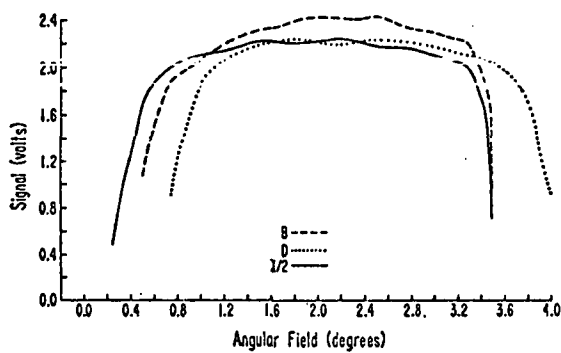Fig. 5 -- Results of Field of View Studies Using a Pinpoint Light Source and the 100" Collimator.

113

Fig. 6 -- Results of Angular Response Studies Using the Integrating Sphere with 3" Opening 30 feet away with the I Barrel Set at (a) 180°; (b) 135°; (c) 90°; and (d) 45°.

## 2.3 Sensitivity: Linearity and Intensity Calibration of the 1/2 Barrel.

- The sensitivity tests which were carried out early in June determine the system responsivity at each wavelength, the linearity over one decade in any one color, and linearity over several decades among all colors. A pleasing aspect of the responsibility information is that the system at 3800 Å performs three times as well as originally predicted by the minimum system design. This has the effect of contracting the overall dynamic range of the output signals, since the signal at 5800 Å is no more than predicted.

Fig. 7 shows the results of these tests with the output of the photopolarimeter in volts plotted vs. the reading in amperes of the calibrated E, G, & G radiometer (E, G, & G High Sensitivity Detector Head, Model #585-66 S/N 78). Table 2 gives the resultant calibration of the 1/2 readings taking into count the calibration of the radiometer.
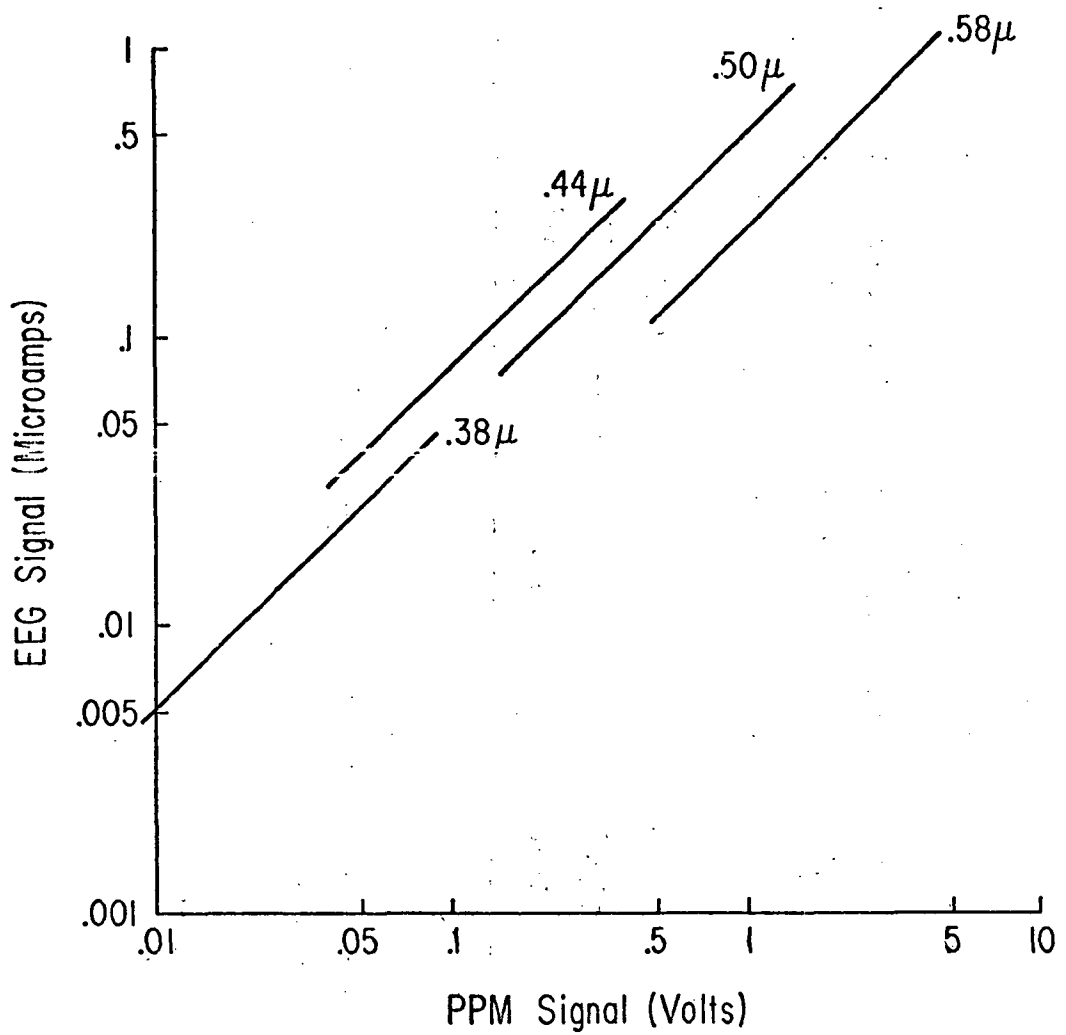
Fig. 7 -- Calibration of the Photopolarimeter Against the
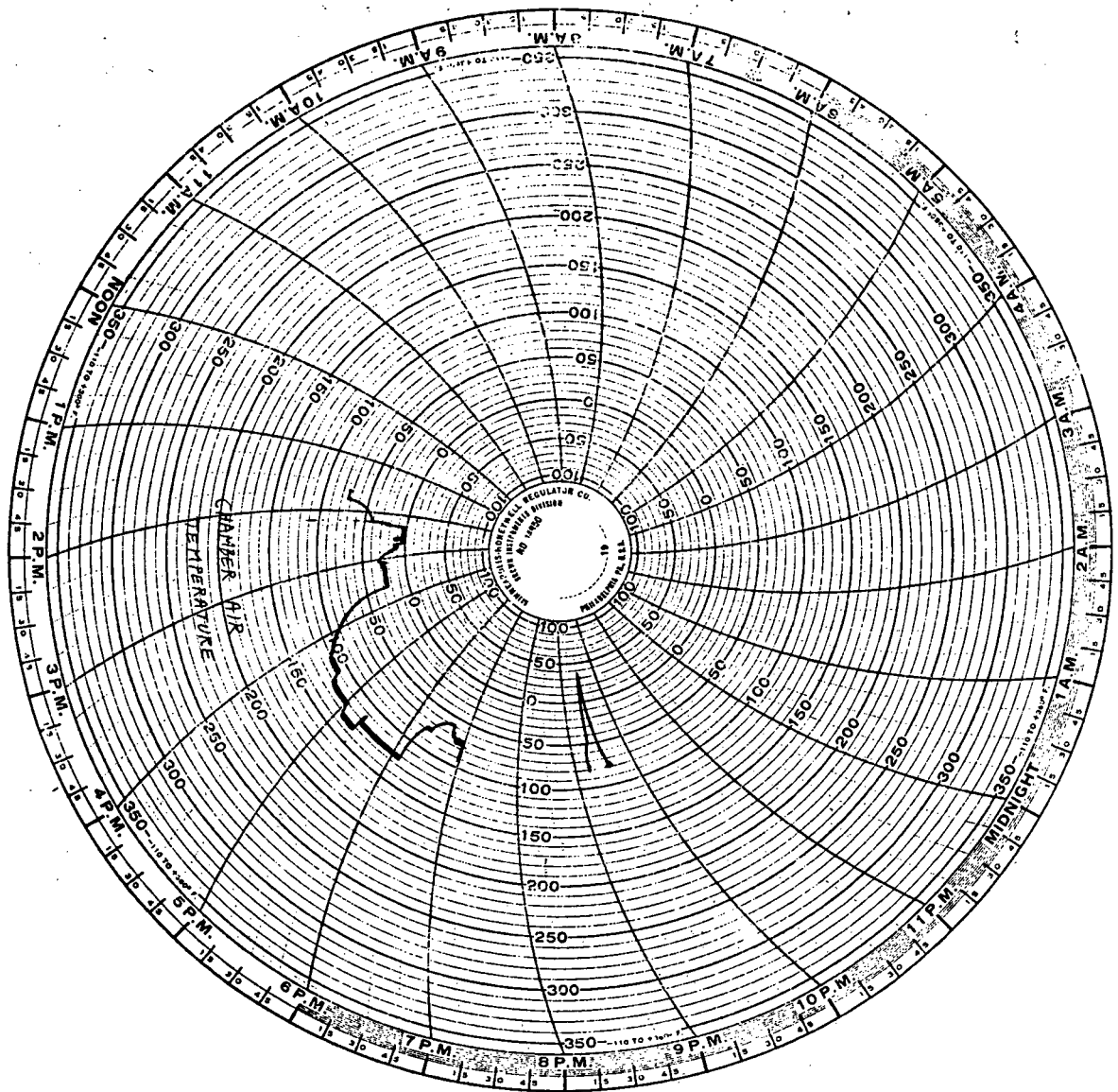Calibrated E, G, & G Radiometer.

Table 2 -- Color Channel Characteristics

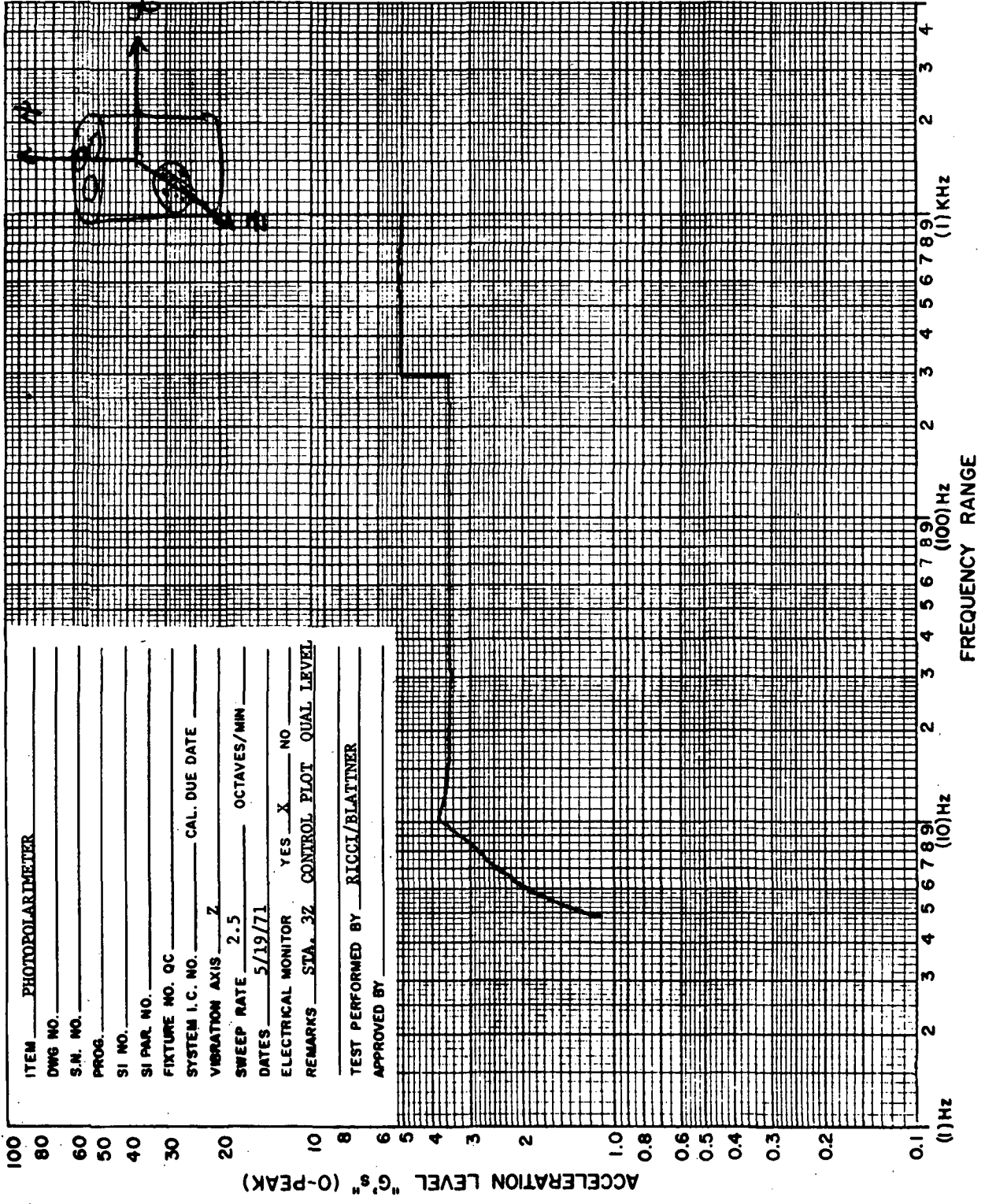| Channel | Peak Wavelength ($\overset{\circ}{A}$) | Bandwidth (m$\mu$) | Calibration (I/2) $\dfrac{v}{\text{w/cm}^2\text{-m}\mu}$ | External (I/2) Window Transmission* |
|---|---|---|---|---|
| 1 | 3812 | 9.1 | $2.152 \times 10^8$ | .927 |
| 2 | 4409 | 8.3 | $2.304 \times 10^8$ | .929 |
| 3 | 5008 | 11.2 | $4.364 \times 10^8$ | .929 |
| 4 | 5820 | 14.0 | $6.149 \times 10^8$ | .931 |

*The calibration factor for the flight data is the product of the entries of the last two columns.

2.4 <u>Environmental Tests (L. Napaluch and T. Wise)</u>. - On May 19 and 21, 1971 the instrument and electronics box were subjected to temperature and altitude, and vibration tests certified by the letters and graphs immediately following. During both tests, a light source was arranged and output from the processor was monitored (see Fig. 8). There was considerable ripple in the lamp and its intensity varied as various units in the vicinity cycled on and off. In addition, the data was very noisy due to disturbances from the refrigeration unit heaters and the low altitude and high altitude pumps. Because the instrumentation must be grounded, neither electronics box nor optical assembly were insulated from the chamber, and a ground loop was established through the instrumentation ground. For these reasons, nothing conclusive can be drawn from the data observed during the environmental test except that no inexplicable or grossly aberrant behavior was observed, i.e., the instrument and electronics behaved well during the test. No difficulties were encountered in stopping and restarting the motor at $0^{\circ}$C.

Measurements taken with the integrating sphere before and after the environmental test were compared, the E, G, and G radiometer being used to set up identical intensities in the sphere. The intensity signals changed very little; in fact, there is a uniform half percent increase in the post-environmental test studies. This is within the previously determined long term stability of the instrument. In many cases there were no discrepancies for the Q and U readings and where there were they represent maximum changes of 25% of the signal voltage. This is very good considering the fine balance that exists in the Q and U outputs. Moderate changes in the instrument and in the testing of the instrument will produce voltage changes on the order of decades.

Subsequent to (1) specified vibration levels up to 5 G's and residual levels up to 9 G's (2) temperature soaks at $0^{\circ}$C and $50^{\circ}$C, and (3) vacuum levels down to 100 torr, there was no detectable mechanical instability greater than 0.5%.

CHAMBER AIR TEMPERATURE

MINNEAPOLIS-HONEYWELL REGULATOR CO.
BROWN INSTRUMENTS DIVISION
PHILADELPHIA, PA.

119

ITEM   PHOTOPOLARIMETER

DWG NO.

S.N. NO.

PROG.

SI NO.

SI PAR. NO.

FIXTURE NO. QC

SYSTEM I.C. NO.   Z           CAL. DUE DATE

VIBRATION AXIS   2.5

SWEEP RATE   5/19/71          OCTAVES/MIN

DATES

ELECTRICAL MONITOR   YES   X   NO

REMARKS   STA. 3Z   CONTROL PLOT   QUAL LEVEL

TEST PERFORMED BY   RICCI/BLATTNER

APPROVED BY

ACCELERATION LEVEL "G's" (0-PEAK)

100
80
60
50
40
30
20
10
8
6
5
4
3
2
1.0
0.8
0.6
0.5
0.4
0.3
0.2
0.1

(1)Hz   (10)Hz   (100)Hz   (1)KHz

FREQUENCY RANGE

121

ITEM PHOTOPOLARIMETER ELEC. PKG. (UCLA)

DWG NO.

S.N. NO.

PROG.

SI NO.

SI PAR. NO.

FIXTURE NO. OC

SYSTEM I.C. NO. _____ CAL. DUE DATE

VIBRATION AXIS X

SWEEP RATE 2.5 OCTAVES/MIN

DATES 5/21/71

ELECTRICAL MONITOR YES ____ NO X

REMARKS CLOSED LOOP PRIOR TO RUN

TEST PERFORMED BY RICCI/BLATTNER

APPROVED BY

ACCELERATION LEVEL "G's" (O-PEAK)

FREQUENCY RANGE

(1)Hz (10)Hz (100)Hz (1)KHz

ITEM PHOTOPOLARIMETER ELEC. PKG. (UCLA)

DWG NO.

S.N. NO.

PROG.

SI NO.

SI PAR. NO.

FIXTURE NO. QC

SYSTEM I.C. NO. CAL. DUE DATE

VIBRATION AXIS Y

SWEEP RATE 2.5 OCTAVES/MIN

DATES 5/21/71

ELECTRICAL MONITOR YES NO X

REMARKS CLOSED LOOP PRIOR TO RUN

TEST PERFORMED BY RICCI/BLATTNER

APPROVED BY

ACCELERATION LEVEL "G's" (0-PEAK)

FREQUENCY RANGE

(1)Hz    (10)Hz    (100)Hz    (1)KHz

126

ITEM PHOTOPOLARIMETER ELEC. PKG.
DWG NO.
S.N. NO.
PROG.
SI NO.
SI PAR. NO.
FIXTURE NO. QC
SYSTEM I.C. NO. _____ CAL. DUE DATE
VIBRATION AXIS Z.
SWEEP RATE 2.5 OCTAVES/MIN
DATES 5/21/71
ELECTRICAL MONITOR YES NO X
REMARKS CONTROL ACCEL.
TEST PERFORMED BY R. RICCI/K. BLATTNER
APPROVED BY

ACCELERATION LEVEL "G's" (0-PEAK)

FREQUENCY RANGE

127
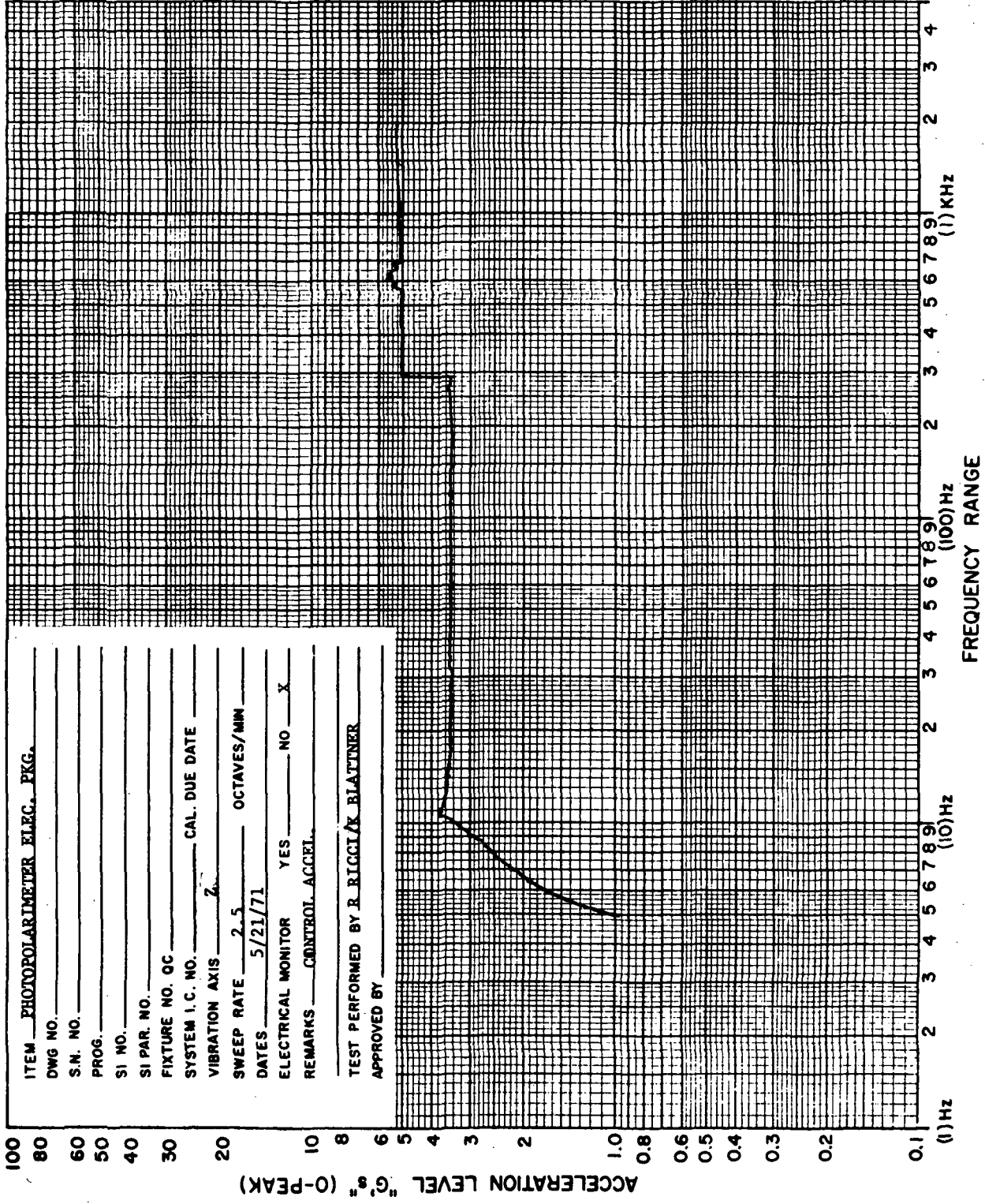
ITEM PHOTOPOLARIMETER ELEC. PKG. (UCLA)
DWG NO.
S.N. NO.
PROG.
SI NO.
SI PAR. NO.
FIXTURE NO. QC
SYSTEM L.C. NO. _____ CAL. DUE DATE
VIBRATION AXIS ____ X
SWEEP RATE ____ 2.5 ____ OCTAVES/MIN
DATES ____ 5/21/71
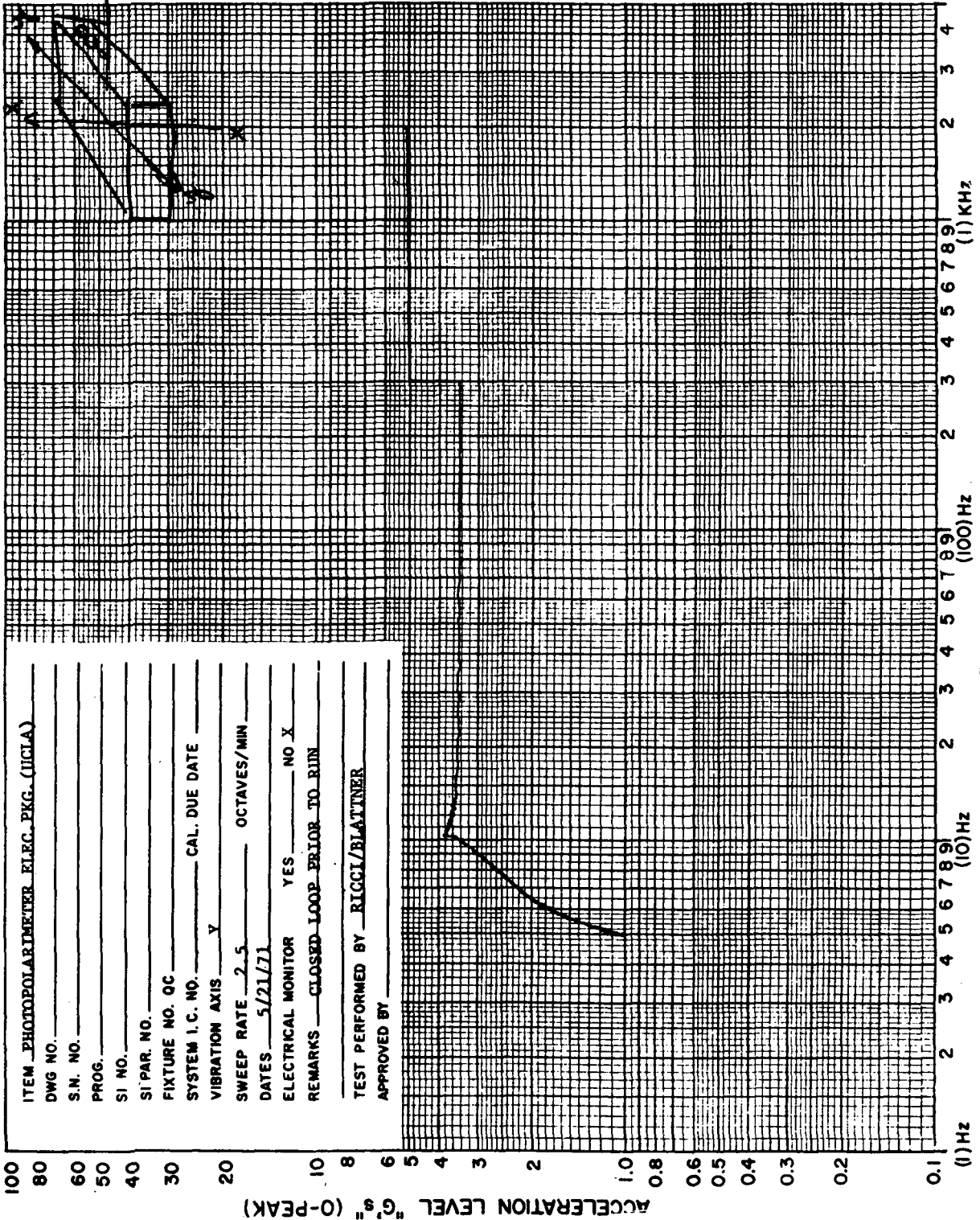ELECTRICAL MONITOR ____ YES ____ NO X
REMARKS ____ CONTROL ACCEL PLOT

TEST PERFORMED BY
APPROVED BY

ACCELERATION LEVEL "G's" (O-PEAK)

100
80
60
50
40
30
20
10
8
6
5
4
3
2
1.0
0.8
0.6
0.5
0.4
0.3
0.2
0.1

(1)Hz          (10)Hz          (100)Hz          (1)KHz

FREQUENCY RANGE
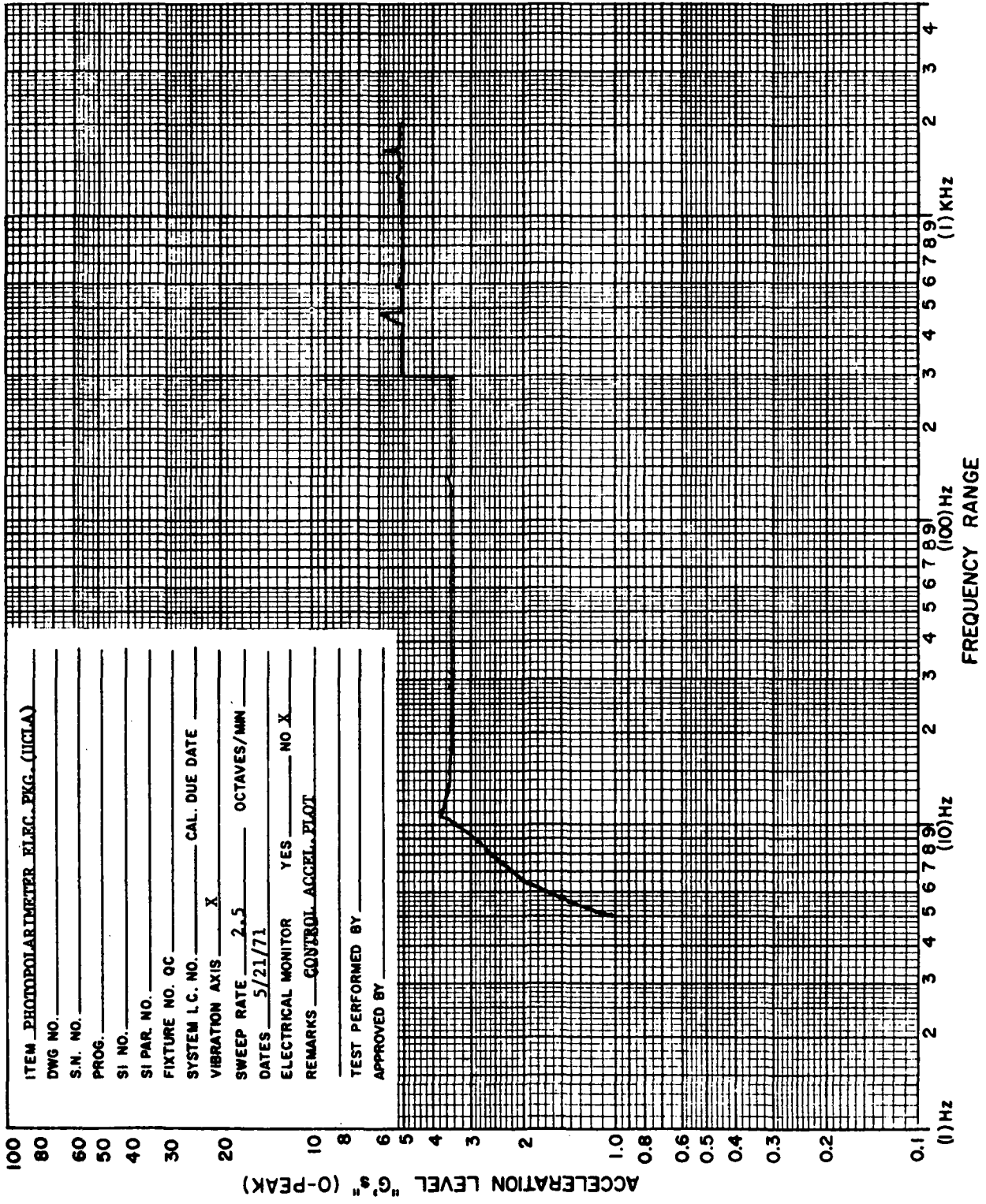
Fig. 8 -- Photograph Showing a Typical Set Up of the Photopolarimeter During the Vibration Tests at General Electric, Valley Forge Space Center.

2.5 Sources of Extraneous Noise (L. Napaluch). - (From May 26 to May 28, 1971 Mr. Kopa and Dr. Bradbury witnessed acceptance tests of the instrument at the General Electric Space Sciences Laboratory.) During the data gathering phase of the acceptance tests a considerable amount of noise or signal output variation was evidenced with the instrument looking into the integrating sphere at essentially low polarization light. This variation was greatly in excess of that expected from the known pre-amp noise, so further exploration was indicated.
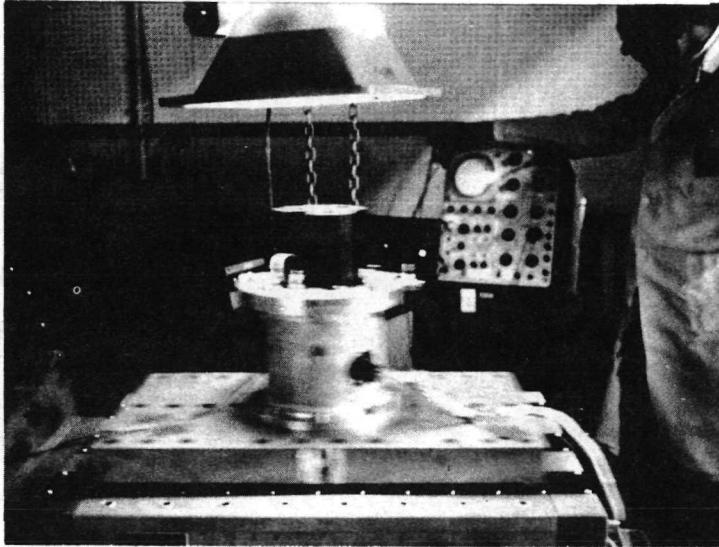
The noise can be broken down into the following list:

1) Ripple on the light source in the integrating sphere

2) Pre-amp noise

3) Pre-amp input cable noise (microdot)

4) Photodiode noise

5) Processor drift

6) False triggering of the data system

Item 1. - The light source ripple arises because the excitation is a full wave rectified output from an A.C. regulator. The light intensity ripple of 120 Hz is less than 1% and is somewhat attenuated by the 3.6 millisecond time constant of the photopolarimeter leaving a residual of about 0.2%.

This source of disturbance is inherent in the instrumentation and makes it difficult to read the processor output accurately. To eliminate it, a new regulator, battery powered, has been built and tested. All further instrument tests with the integrating sphere will use this new regulator and hence will be free from ripple.

Item 2. - The pre-amp noise was the same as it had been when measured and calculated previously. This constitutes a limitation in photopolarimeter performance at the highest gain, the gain with an open circuit link. This gain provides full output of 10 volts with $5.2 \times 10^{-7}$ amps input. When the pre-amplifier gain is set for 10 volts at $5.2 \times 10^{-7}$ amps, the design point for the instrument, this noise will be only 10% of what it is at the highest gain. At the nominal design gain, the pre-amp noise will not be significant in determining instrument performance.

Item 3. - With the cable alone placed on the pre-amp input, there may or may not be an increase in noise, depending on the level of vibration the cable sees. When cable and pre-amp were on a table near the masonry wall, there was no significant increase

in noise.  When they were placed on the test table near the center
of the floor, a place of known high vibrational level, the noise
went up by a factor of two at the pre-amp output.  As noted in
Item 2, this would contribute to a limitation in photopolarimeter
performance at the highest gain.  Likewise, noise contribution
of the cable at the nominal design point would not be significant.

Item 4. - The photocell contributed sufficient noise to
triple the noise output of the pre-amp when connected through the
microdot cable.  Further, during the high temperature test a
rather large increase of about 8 to 10 times was seen in the noise
at +50°C.  The photodiode was probably contributing most of this
increase but this has not yet been established.  Although at the
nominal design gain this noise would be much reduced, it would
be significant in limiting photopolarimeter performance.

Item 5. - From the specifications of the processor amplifiers,
an expected drift is about $\pm 0.5$ millivolts at the input.  When
the barrels were closed and this residual voltage (an intercept
error and not a slope error) was observed, it was consistently
below this level.  However, under varying temperature conditions
such as initial turn-on stabilization, it can exceed 0.5 milli-volts.
The use of 40K amplifiers in place of 40J units (Analog Devices,
Inc.) helped keep this error to less than 0.5 millivolts as measured.

This drift error can be a limitation in photopolarimeter
performance particularly at the nominal design gain.  At the high
gain pre-amp setting it contributes about equally with the noises.

Item 6. - The open breadboard of the sample-hold circuit and
its driver used to obtain data at a point in the processor output
was subject to false triggering whenever certain equipment was
operating in the vicinity.  This caused a problem only when trying
to average mentally many successive readings.

3.0  Tests at UCLA - 3.1  Comments on the Acceptance Tests*
at GE (R. Bradbury). - The source for the tests observed was a
quartz-iodine tungsten lamp mounted in a four-foot integrating
sphere.  The source as actually observed by the instrument was a
5 or 6-inch diameter plane target painted with the same material
as was the interior surface of the sphere.

Many of the problems involved in evaluating the data are
related to the source, e.g., for any one measurement, each barrel
of the photopolarimeter is looking at a different area on the
target.  Additionally, there are short term temporal variations
of intensity of about 0.08% and long term variations within $\pm 0.5\%$.

The short term fluctuations do not appear in the G.E. data
records, since T. Wise recorded the average of a number of suc-
cessive readings on the digital voltmeter.  My own observations

of these fluctuations are summarized in the following typical data, taken with 0% polarization, 0° rotation of the photopolarimeter:

| Color | Fluctuation | Gain | Parameter |
|-------|-------------|------|-----------|
| 5800 Å | ±0.003 v | 2 | for I(4.29v) |
|  | ±0.6 | 200 | for Q and U |
| 5000 Å | ±0.002 v | 2 | I(1.360 v) |
|  | ±0.3 | 200 | Q and U |
| 4400 Å | ±0.020 | 20 | I(2.725 v) |
|  | ±0.20 | 200 | Q and U |
| 3800 Å | ±0.09 | 200 | I(3.04 v) |
|  | ±0.10 | 200 | Q and U |

The fluctuations in the 3800 Å signals represent 2 mv peak to peak noise which is signal independent, since the intensity is too low in this color channel to see the effect of the source fluctuations. This noise, illustrated in Fig. 9, which shows oscilloscope traces of ten consecutive cycles of the photopolarimeter, currently represents the limiting error source, far above the expected 0.5 mv error due to the processor electronics. The sources of the noise have been discussed further by Napaluch in Section 2.5. It is, however, small compared to the source ripple which in turn is small compared to discrepancies due to the spatial inhomogeneity of the source.

The signals in both the 4400 Å and 3800 Å channel are too weak to make any meaningful assessment of the operation of the instrument at those wavelengths, so my main concern in this report will be the 5000 Å and 5800 Å channels. Another source, possibly skylight, must be used to evaluate the short wavelength channels.

Fig. 10 shows five consecutive traces of the output of the processor with the signals identified above. (The signal sequence is the same in all similar photos to follow.) The sampling pulse of the test circuit rather than the gain circuit is shown. The signal at this point (I in the 4400 Å channel) is read out of the digital voltmeter. The situation is the same as for the table above.

The effect due to the source ripple may be seen clearly in the Q and U signals in the 5800 Å channel, where in both cases at lease four different values for both signals may be discerned.

---

*This section is excerpted from a report on the acceptance tests prepared for Professor Z. Sekera.

The effect is not observable in the corresponding I signal since the gain there is a factor of 100 lower. (Note: The gain factors in data taken by G.E. are given as 2, 20, and 200. In my own reduction of the data I read these as 1, 10, and 100 to avoid the absurdity of dividing every piece of data by 2.)

The effect due to the target inhomogeneity will be discussed in the following remarks.

0% Polarization Test. - The laboratory set-up for the photo-polarimeter performance tests are shown in Fig. 11. The photo-polarimeter was mounted in a rotatable mount, not indicated in the figure. For lack of evidence to the contrary, we will assume that the axis of the mount is coincident with that of the photo-polarimeter so that, as the instrument is rotated, the area viewed by the $\frac{1}{2}$ barrel, for example, generates a doughnut-shaped area on the target. $0^O$ rotation of the photopolarimeter indicates that the $\frac{1}{2}$ barrel is at the topmost position in the rotatable mount. The B barrel is then viewing the $120^O$ position on the target, i.e., the area viewed by the $\frac{1}{2}$ barrel when the instrument is rotated through $120^O$, (this defines the direction of rotation) and the D barrel is viewing the $240^O$ position. Thus the instrument notated by "$\frac{1}{2}$ at $0^O$", "B at $120^O$", and "D at $240^O$" are equivalent statements.

The trim factors f and g are defined on pages 124-125 in S046FR and a method for determining these factors given on pages 126-127. (See Section 3.1.1 of the report body.) Ideally, these factors are unity and should be the same for all color channels. Unfortunately, the method given in S046FR is unsuitable when using the integrating sphere as a source. The data from the no-polarizer rotation tests are shown in Fig. 12 for the 5000 Å and 5800 Å channels. The trim screw adjustments were made for the 5800 Å channel with the instrument at $0^O$. This corresponds to the $0^O$ point for 5800 Å being closest to the center of the graph. (Distance from the center is the degree of polarization.) The circles about each data point indicate the error limit due to the fluctuations discussed in the previous section. It is clear that the deviation of the points is much greater than could be accounted for by these fluctuations. Note that except for the $240^O$ point in both cases the data points roughly describe an ellipse as the instrumet rotated. From page 127 of S046FR such an ellipse would be expected if the source were uniform, but with some small residual polari-zation. The center of the ellipse would be given by 1-f*, 1-g and the ellipticity would also be related to the trim factors. In that

---

*At the time this report was prepared, the $90^O$ misorientation of the B and D prisms had not been discovered.

case, however, the point would travel around the ellipse twice as the instrument is rotated through 360°, so residual polarization could be only a small contribution to the deviations. This is confirmed also by the fact that the ellipticity does not correspond to the ratio of g/f, i.e., the figures would be more like circles to correspond to the location of the centers.

As indicated in Fig. 12, it was found that it was impossible to trim the instrument well for all the color channels simultaneously. This has been explained by the difference in the transmission properties of the compensator calcite block in the ½ barrel compared to the Glan Thompson prisms in the B and D barrels (Table 1). Thus the 5000 Å data is considerably displaced from the origin when the instrument is trimmed for 5800 Å.

Such an effect should be expected since the ratios of the trim factors for the different color channels are related to the barrel transmissions by equations such as:

$$\frac{f(\lambda_1)}{f(\lambda1)} \quad \frac{T(\lambda_1,B)}{T(\lambda_1,1)} \cdot \frac{T(\lambda_2,B)}{T(\lambda_2,1)}$$

where $f(\lambda)$ is the trim factor f for color $\lambda$ and $T(\lambda,X)$ is the overall transmission of barrel X at color $\lambda$, etc.

With data like this, the best method of determining the trim factors is to rough in an ellipse to the data, and graphically determine the center. (This was done and the results used for reducing the data in the subsequent test.)

Let us consider that the discrepancies are due solely to the spatial inhomogeneity of the target. Assuming that the polarization is exactly zero and f and g are both unity, then it is readily seen that

$$\frac{q(\theta)}{i(\theta)} = \frac{I(\theta) - I(\theta + 120°)}{I(\theta)}$$

$$\frac{u(\theta)}{i(\theta)} = \frac{I(\theta) - I(\theta - 120°)}{I(\theta)}$$

134

(Note: Following S046FR q($\theta$) and u ($\theta$) designate the quantities as read out directly from the instrument when rotated by $\theta$. I($\theta$) designates the intensity of the target at position $\theta$ on the target, i.e., as measured by the $\frac{1}{2}$ barrel at $\theta$.)

Thus, deviation from zero by .008 (.8%) for P would correspond to the same order of inhomogeneity. This could easily account for the distribution of points observed and conceivably the readings of the $\frac{1}{2}$ barrel as the instrument is rotated might be taken into account in reducing the data. Unfortunately, the time between readings is too long and the long term source fluctuation leads to changes in the intensity of a comparable magnitude ($\pm$0.5%).

100% Polarization. - For the 100% polarization test, a sheet of HN-22 Polaroid film is taped to the front of the integrating sphere with its transmission axis horizontal, i.e., effectively parallel to the transmission axis of the B barrel.

Fig. 13 shows a plot of the raw data from this test for 5800 Å and 5000 Å, together with a circle for ideal 100% polarization. In this case, the gross deviations from the unit circle can be reduced by taking into account the source inhomogeneity. This works because the inhomogeneity is due not so much to the sphere properties as to the non-uniform transmission characteristics of the polaroid. On the basis of the data, this may vary as much as 6% around the doughnut. Fig. 14 with the data corrected according to the formulas

$$I(\theta) = i(\theta),$$

$$\frac{Q(\theta)}{I(\theta)} = 1 - \frac{i(\theta) - q(\theta)}{fi(\theta + 120)}$$

$$\frac{U(\theta)}{I(\theta)} = 1 - \frac{i(\theta) - u(\theta)}{gi(\theta - 120)}$$

shows considerable improvement. (The f and g values used are$_0$ those determined from the zero polarization data.) The 5800 Å data have an average value of P and 0.992 with RMS deviation 0.0027 while the 5000 Å data average is 0.985 with RMS deviation 0.005. The relative deviation between the two color channels is compatible with the relative fluctuations (compare the circles about the data points in Fig. 12). The absolute error is in turn compatible with the ellipse of the no-polarization data ( $\Delta P \sim \pm 0.007$ ) ), indicating that this is the best that can be done in terms of the data presently available.

One more comment must be added. It was impossible to obtain a ratio of less than $\sim 10^{-3}$ when measuring the extinction ratio of the B and D barrels using the polaroid sheet. Measuring the polaroid's extinction ratio by crossing two pieces of film in front of the $\frac{1}{2}$ barrel verified that this was due to the polaroid.

The preceding discussion clearly indicates that the tests performed with the integrating sphere are inadequate to demonstrate the ultimate capabilities of the instrument.
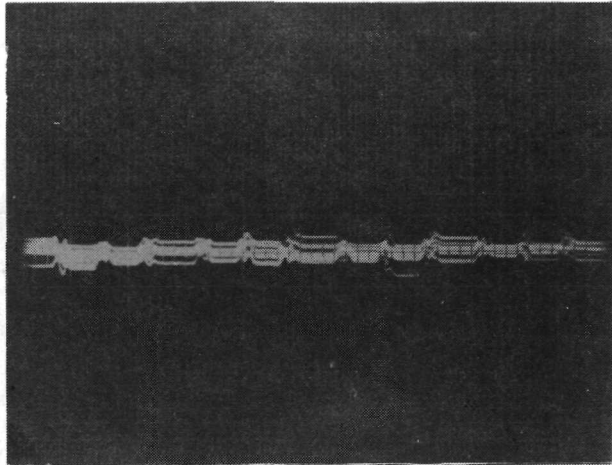
Fig. 9 -- Ten Consecutive Traces of the Processor Output with All Barrels Blocked Off. The time from one end to the other is one second, the duration of the instrument cycle (see Fig. 10). This illustrates the limiting noise of the system. The scale is 0.5 v/cm and the instrument gain is 200.
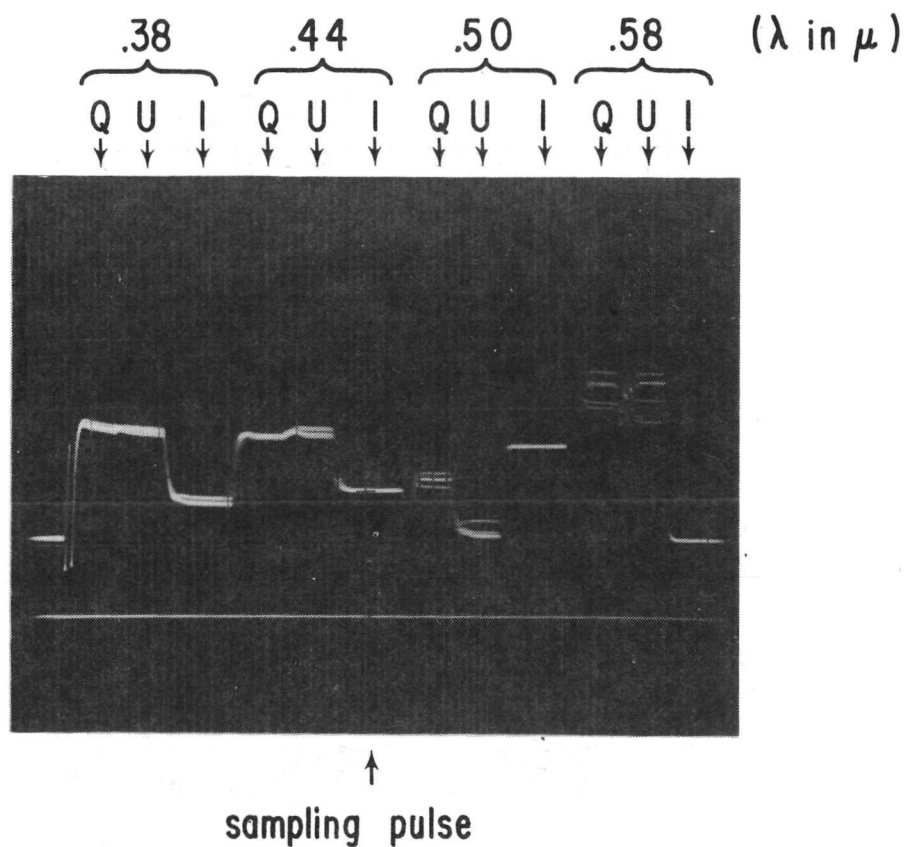
Fig. 10 -- Five Consecutive Traces of the Processor Output with All Barrels Open and the Instrument at 0° Looking into the Integrating Sphere (no polaroid). The information sequence is shown above the photo. The lower trace shows the sampling pulse of the test circuit sampling here I of the 4400 A channel. The scope scale is 2 v/cm and the instrument gain factors for the signals are (reading from left to right) 200, 200, 200, 200, 200, 20, 200, 200, 2, 200, 200, 2.

Fig. 11 -- Block Diagram of Laboratory Set-Up for Performance Tests of the UCLA PPM.

Fig. 12 -ᵧ Uncorrected Data From 0% Polarization Tests for 5800 Å and 5000 Å.

Fig. 13 - Uncorrected Data from 100% Polarization Tests for 5800 Å and 5000 Å.

Fig. 14 - Corrected Data From 100% Polarization Tests for 5800 Å and 5000 Å.

3.2 Power Supply Problems. - When the instrument was first delivered to UCLA by Dr. Frost a variable voltage power supply was used to test t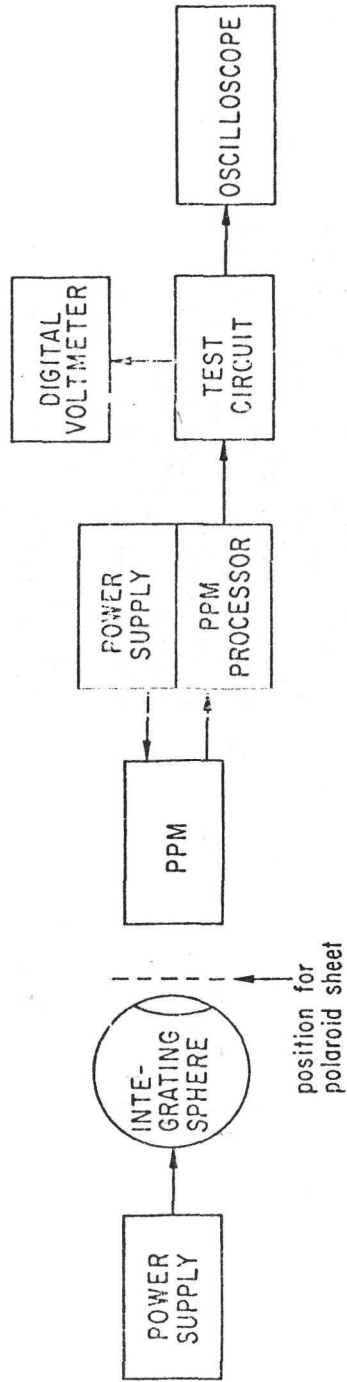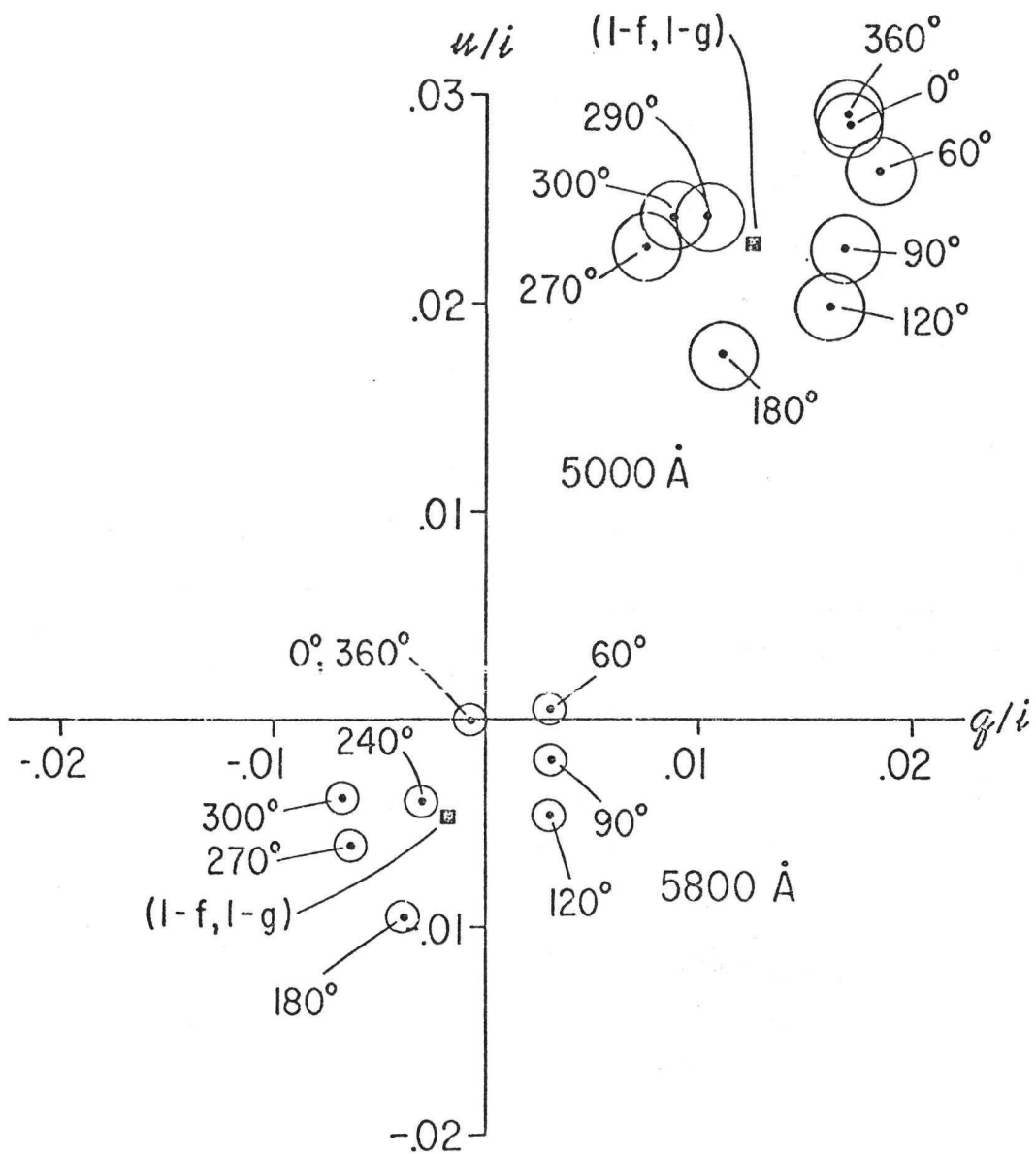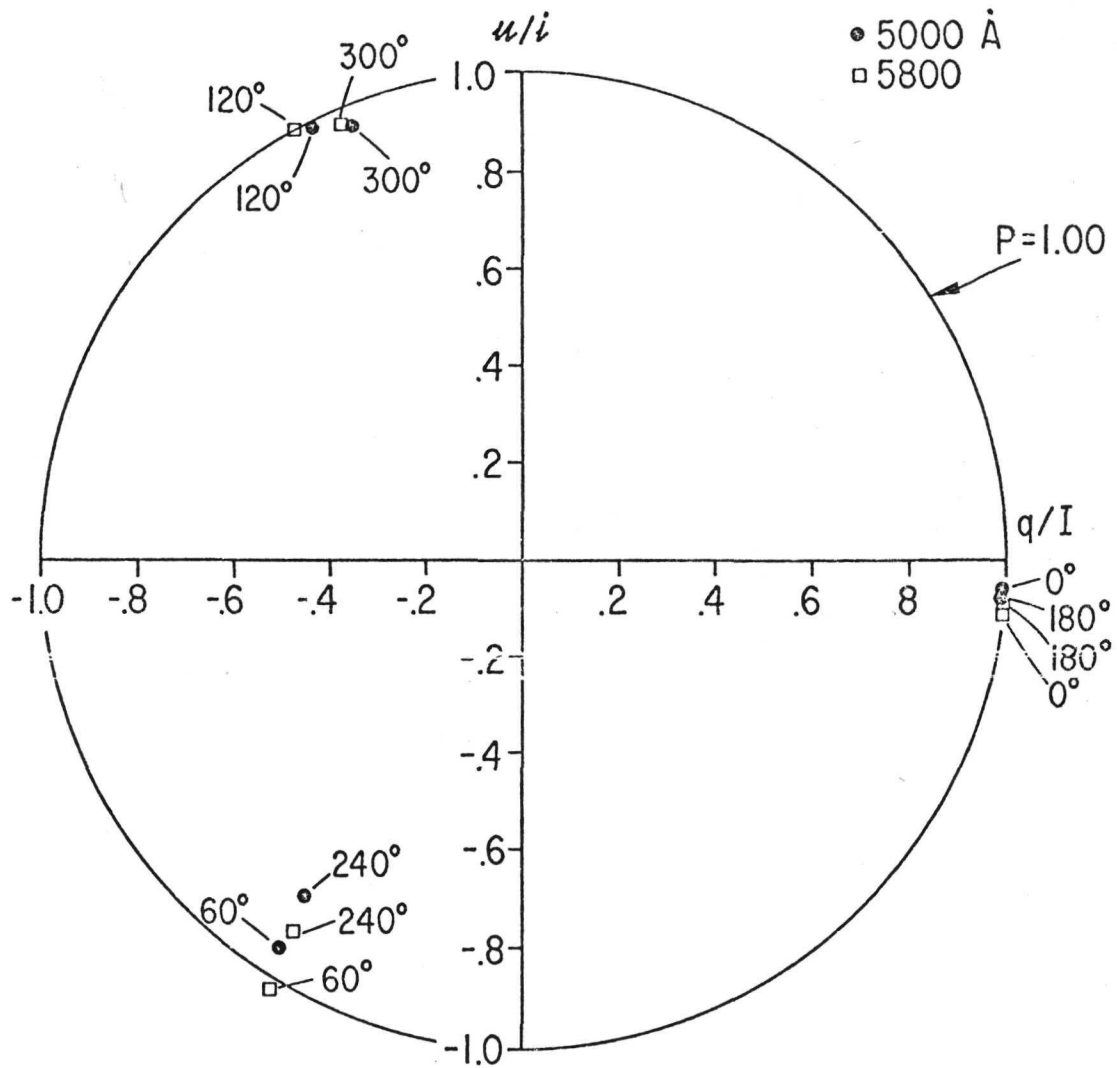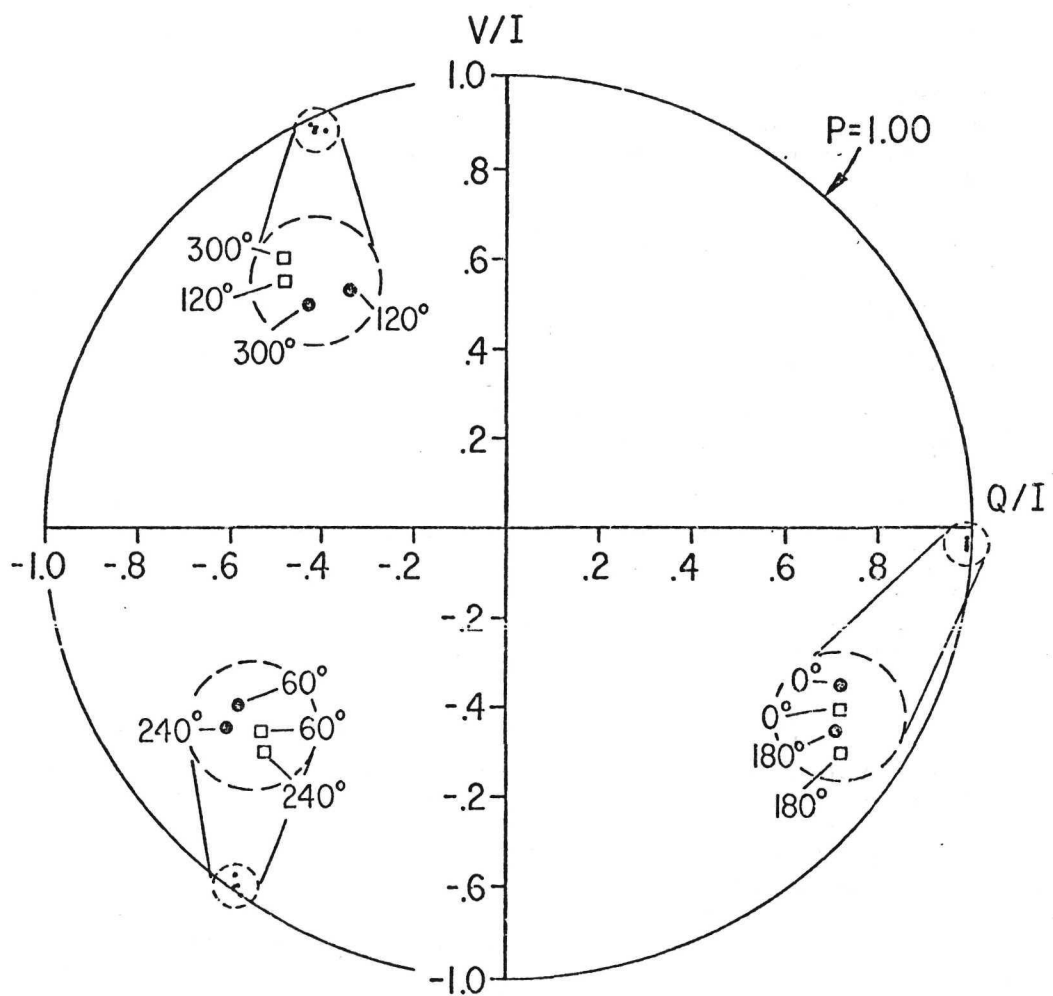he instrument to insure that it had survived its transit. Even though great care was taken to prevent an overvoltage, the instrument failed to function the next time. It was determined that every transistor in the power converter section of the primary electronics box was gone, due perhaps to an overvoltage spike from the variable voltage supply when it was turned off.

Construction of the proper external supply was rapidly completed and no further difficulties of this type were encountered. A power failure in the course of the flights was corrected by giving positive retention to the one circuit board in the power converter section which did not have it.

These comments are included not so much as a criticism of the instrument, but as a word of caution to its user.

3.3 Integrating Sphere Tests: Linearity, Gain Accuracy, "Polarization" of I.- In order to have a source usable for rudimentary laboratory tests at UCLA an 18" integrating sphere with a 6" circular target suspended in the center by wires was constructed with a quartz-iodine lamp as a source. A variable voltage regulated D.C. power supply was constructed for the lamp. No noise due to ripple was present.

Linearity of the I barrel for color channels 3 and 4 (5000 $\overset{O}{A}$ and 5800 $\overset{O}{A}$, respectively) was checked using a set of calibrated neutral density filters in conjunction with the sphere. Some discrepancies were noted, but by recalibrating the filter with a Cary Spectrophotometer Model 14 it was verified that these were due to errors in the calibration curves. These filters were also used to check the accuracy of the gain settings in the AGC. Within the accuracy of the filter calibration the gains are what they should be (10/1).

The rotatable mount used by GE was borrowed temporarily until our own could be constructed. It was noted that due to a displacement of the optical axis (the "center of gravity" of the three barrels) from the mechanical axis (the center of the mounting bolt circle) the three barrels did not view identical areas of the sphere target under the $\pm 120^{\circ}$ permutations discussed in Section 3. To remedy this, an eccentric collar was provided in UCLA's rotatable mount. The mount was also provided with locating holes every 15$^{\circ}$ and a spring loaded locating pin. The instrument could thereby be rotated quickly and accurately through integral multiples of 15$^{\circ}$ as desired (see Fig. 15). This collar was used primarily in the trim calibration factor determinations by observing zenity skylight from the roof of the Mathematical Sciences Building (MS) at UCLA. This is discussed in detail later on. The integrating sphere is inadequate for determining the calibration factors, but once

143

these factors are known the instrument can be used to evaluate the sphere. In this manner, the polarization of the target region viewed by I at $0^o$ was determined to be .05 $\pm$ .01. (The primary source of the error is due to spatial variations in the target intensity.)

There had been some question as to whether the presence of the compensator block and the fibre optics might engender a polarization sensitivity in the I barrel. With the instrument viewing the integrating sphere at $0^o$, a polaroid was rotated in front of I, care being taken to insure that the center of rotation was on the axis of the I barrel. An intensity variation equivalent to .055 $\pm$002 polarization was observed for color 3. Thus, for the I barrel at color 3 the difference in transmission for the ortho-gonal polarization components could <u>at most</u> be 1%. It is felt that the accuracy of this test could be improved if time did not prohibit further testing.

3.4  <u>Zero Levels and Noise</u>. - During the initial testing of the instrument on the roof of the MS building exceptionally large abnormalities were observed which were traced to pick-up of 60 cps signals being radiated by some other roof-top experiment. It was discovered that the detector cable shield was ungrounded (according to design) and the situation was remedied by putting the microdot cable through a grounded copper braid shield. This solved most of the noise problems previously experienced.

In subsequent tests of the instrument with all barrels blocked, it was found that while the RMS deviations were typic-ally 0.6 mv, the mean reading of a given parameter could be non-zero by as much as 10mv, the I's usually being highest. These zero levels (Z's) could change spontaneously. It was verified that the Z's could not be due to light leakage or scattered light but might possibly be due to static charges on the chopper wheel or filters. In most cases these Z's would lead to insignificant errors but they have been taken into account in data reduction as a matter of course. During data runs the barrels would be blocked before and after and the Z's averaged. This practice was followed both in ground and flight measurements, primarily as a check on the instrument behavior. It should be noted that the noise parameter given above is effectively the same as the 0.5 mv error limit specified for the electronics. This excellent behavior was also observed in the flight experiment data.

3.5  <u>Comparison with Another Polarimeter</u>. - In mid-October the photopolarimeter and a rotating prism instrument (Dr. N. C. R. Rao's) were run simultaneously for ten minutes while viewing the zenity from the roof of the MS building. The instruments were separated both vertically and horizontally by distances of about 15 feet. At no time during this period did results from these
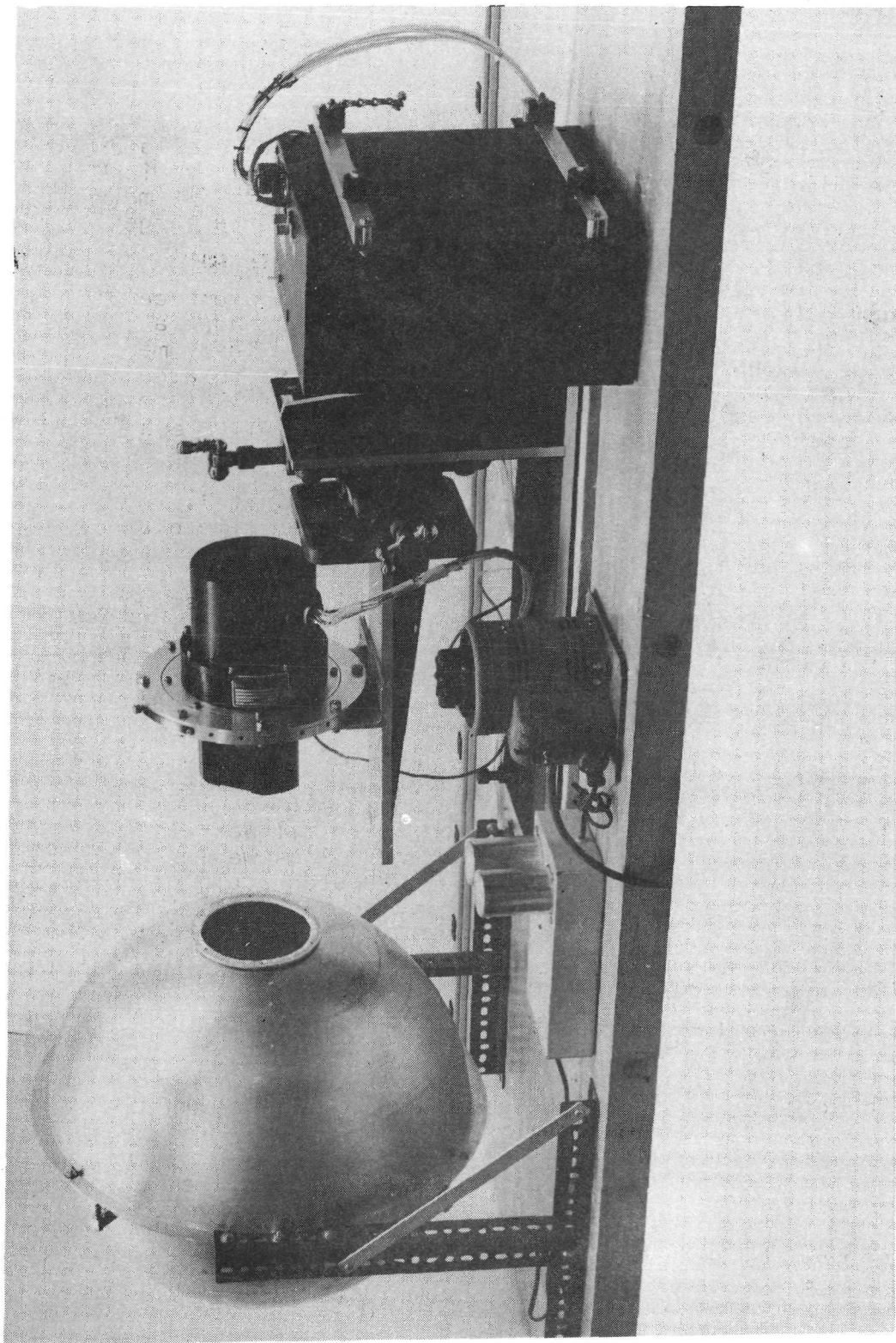
144

Fig. 15 -- Photo of Laboratory Set Up Showing the Photopolarimeter Mounted in a Rotatable Ring Viewing the 18" Integrating Sphere.

instruments differ by more than 3% of the polarization, the average difference being 1.8% for the 5000 Å channel which was the only common filter region for the two instruments.

3.6 <u>Residual Charge Effects</u>. - Some concern was expressed about the possibility of parameter mixing due to residual charge effects in the processing capacitor. Originally it was suggested that residual voltages from the usually high signal color 4 channel might be carried over into the usually low signal color 1 channel (The intensity difference is more exaggerated with laboratory light sources than with skylight radiations ) and a model processor was built to study such effects. It was real-ized that if such residual voltages might be carried over from one color channel to another, then the effect would even be larger within the parameters of one color channel where the time differ-ences were much shorter.

For example, if after the Q cycle a fraction $\epsilon Q$ remains on the processor capacitor, then the U reading will be $U + \epsilon Q$ and the I reading would be $I + \epsilon U + \epsilon^2 Q \approx I + \epsilon U$. Correspondingly, we would have

$$\eta_1' = \frac{Q}{I + \epsilon U} \approx \eta_1 - \epsilon \eta_1 \eta_2$$

$$\eta_2' = \frac{U + \epsilon Q}{I + \epsilon U} \approx \eta_2 + \epsilon \eta_1 - \epsilon \eta_2^2 \ ,$$

or, assuming we can ignore terms of "third order" ($\eta_1$ and $\eta_2$ are less than unity by definition)

$$\eta_1' = \eta$$

$$\eta_2' = \eta_2 + \epsilon \eta_1 .$$

146

This leads to an elliptical distortion indistinguishable from that due to prism misorientation (See Section 1.1.3 in the body of the report).

To search for such an effect in all color channels, a test was run viewing zenith skylight. When the B and D barrels are blocked the readings of the Q, U, and I outputs should be -1, -1, 1, respectively. The results of this test showed clearly that within the usual fluctuations, the readings were identical (except for sign, of course) indicating no intrachannel parameter mixing. Actually, the elliptical distortion from such an effect would be in the opposite direction from that observed (See section 2.3.1 in the body of the report).

3.7 Black Paint: A Major Problem. - In late October the detector housing and detector were removed in order to investigate the sudden appearance of abnormally high Z's. It had also been noted that the detector was loose in the housing and could easily be turned in the process of connecting the detector cable (This can be avoided by disconnecting the Microdot coupling and not the BNC-to-Microdot adaptor) and it was absolutely necessary to retighten it.

When removed it was discovered that the detector housing had been sprayed with black paint which was deteriorating and peeling. It was also noted that the edge of the housing had been grazed by the chopper wheel. The black paint was removed and a black oxide coating was plated on the brass housing.

Before replacing the detector, it was necessary to separate the optical and mechanical modules to clean the remains of the peeled paint from the chopper compartment. Instructions for this disassembly were relayed by phone by Mr. T. Wise and the use of a laminar flow bench facility in the Engineering Department was provided by Professor C. R. Visiwanathan of the Electrical Sciences Division.

When the modules were separated, it was observed that the headers of the fibre optic bundles were also coated with the same paint. Though the brass could be seen on the sharp edges, there was no flaking on large areas as there had been in the case of the detector housing. To remove these headers for cleaning and black oxide coating would have necessitated returning the instrument to GE for re-assembly and readjustment. The time delay would have forced cancellation of the flight program.

Analysis of the data from the flights indicated the presence of loose flakes in the chopper compartment, particularly on the filters. The detector was subsequently removed and such pieces of dirt were observed as shown in Fig. 15. This represents a major but correctable defect in the instrument prohibiting accurate analysis of the data from the flights. This effect has been

illustrated in the body of the report in Section 2.4.1.

In re-assembling the instrument, the cover of the mechanical module was rotated 45° to facilitate mounting in the instrument compartment of the scan platform.

3.8 <u>Additional Comments and Conclusions</u>. - Since proper determination of the calibration factors of the instrument is essemtial in data reduction and analysis, exhaustive discussion of this has been presented in the main report. (some arbitrariness has been exercised in deciding which particular items should be detailed in this appendix). To summarize, we will briefly reiterate major points concerning this as presented in both report and appendix:

1) An elliptical distortion equivalent to 4% mixing of Q and U was observed during calibration factor determination prior to flight.

2) The character of this distortion indicates strongly that it is due to slight misorientation of the polarizing prisms, but attempts to measure the orientation neither confirm nor deny this as a cause.

3) Parameter mixing in the electronics has been definitely ruled out as a cause of the distortion.

4) Analysis of the effect of the non-symmetric angular acceptance of the polarizing prisms shows that this cannot account for the elliptical distortion since such effects would introduce odd harmonic terms of the polarization angle in the $\eta$-plane (Q/I, -U/I).

5) Until the cause of this distortion is pinned down there is some indefiniteness in the absolute value of the polarization determined by the instrument.

6) This effect is, however, minimal in interpreting the flight data due to other problems, mainly the effects of the external windows and the loose dirt in the chopper compartment.

7) It is felt that this distortion can eventually be accounted for and will present no significant problem.

Going beyond this, we point out the major problems with the instrument which could be corrected:

1) The remaining black paint <u>must</u> be removed from the fibre optics bundle headers and residual dirt removed from the chopper compartment. Also, the edge of the detector housing should be trimmed down to eliminate grazing by the chopper.

148

Fig. 16 -- Flakes of Black Paint on One of the
Interference Filters. This photograph was taken
through the opening for the detector mount after
removing the detector from the instrument.

2)   It would be desirable to replace the polarizing prisms
with those with symmetric angular response. some additional
expense mighti be incurred but there should be no reason why a
more suitable cement cannot be found.   T. Wise's observation that
the optical path deviates from that expected indicates that these
prisms are not as well fabricated as they should be.

3)   Some arrangement is desired to cope with the saturation
problem (discussed in the body of the report).   One such possi-
bility is some real time indicator of saturation to enable the
operator to lower the preamp gain manually.   (The current optional
gain is too low and in the cases encountered would have dropped
the  signals in the unsaturated colors to undesirably low levels.)
Alternatively, it might be arranged to have different preamp gains
for the first two and last two color channels.   This might necessi-
tate another sync signal generated by the filter wheel to elec-
tronically switch gains.

1)   The 0.6 mv noise figure with barrels blocked as observed
in flight represents achievement of the $\frac{1}{2}$ millivolt error limit
matching the drift limit of the processor electronics.

2)   The instrument and its electronics out-performed our ex-
pectations.   Comparison of the flight data with similar data from
other polarimeters indicates the superiority of this instrument
with regard to low scatter.

3)   The rate of data acquisition is virtually instantaneous
compared to polarimeters typically used (though to be honest, there
is technically no reason why rotating prism polarimeters could not
be constructed with similar data acquisition rates).

4)   The instrument is sturdy and compact.

150

REFERENCES

1.  Chandrasekhar, S.  (1950), <u>Radiative Transfer</u>, Clarendon Press.
    Oxford.

2.  Chandrasekhar, S., and D. D. Elbert (1954), "The Illumination
    and Polarization of the Sunlit Sky on Rayleigh Scattering,"
    Transcations of the American Philosophical Society (new series)
    <u>44</u>, part 6.

3.  Sekera, Z., and G. Blanch (1952), "Tables Relating to Rayleigh
    Scattering of Light in the Atmosphere," Sci. Rpt. #3, Dept.
    of Meteorology, Contract #AF19(122)-239, University of Calif-
    ornia, Los Angeles.

4.  Sekera, Z., K. L. Coulson, and J. V. Dave (1960), <u>Tables
    Related to Radiation Emerging from a Planetary Atmosphere
    with Rayleigh Scattering</u>, University of California Press,
    Berkeley and Los Angeles.

5.  Sekera, Z.  (1956), "Recent Developments in the Study of
    the Polarization of Skylight," <u>in Advances in Geophysics</u>
    (Landsberg, H. E., ed.), Academic Press inc., New York, <u>3</u>,
    43.

6.  Sekera, Z. (1957), "Light Scattering in the Atmosphere and
    the Polarization of Skylight," <u>J. Opt. Soc. Amer.</u>, <u>47</u>, 484.

7.  Sekera, Z., and J. V. Dave (1959), "Effect of Ozone on the
    Total Sky and Global Radiation Received on a Horizontal
    Surface," <u>J. Meteorolog.</u>, <u>16</u>, 211.

8.  Bullrich, K. (1964), "Scattered Radiation in the Atmosphere
    and the Natural Aerosol," <u>in Advances in Geophysics</u>,
    (Landsberg, H.E., ed.), Academic Press, Inc., New York, 10,
    101.

9.  Kerker, M. (1969), <u>The Scattering of Light</u>, Academic Press,
    Inc., New York and London

10. Sekera, Z.  (1967), "Determination of Atmospheric Parameters
    from Measurements of Polarization of Upward Radiation by
    Satellite or Space Probe," <u>Icarus</u>, <u>6</u>, 348.

11. Deirmendjian, D. (1969), <u>Electromagnetic Scattering on
    Spherical Polydispersions</u>, American Elsevier Pub. Col, Inc.,
    New York.

12. Takashima, T. (1971), "Dependence of the Polarization Features
    of the Diffust Radiation Field of the Earth's Atmosphere on

151

the Location of a Concentrated Aerosol Layer," Ph.D. Dissertation, Dept. of Meteorology, University of California, Los Angeles.

13. Romanova, L. M. (1963), "Solution of Radiation Transfer Equations with a Distinctly Nonspherical Scattering Indicatrix," Optika i specktroskopiya XIII, Nos. 3 & 6, 1962; XIV, No. 2, 1963.

14. Weinman, J. A. (1968), "Axially Symmetric Transfer of Light Through a Cloud of Unisotropically scattering Particles," Icarus, 9, 67.

15. Saxon, D. S., Z. Sekera, and D. Deirmendjian (1960), "Approximation of Light Scattering by Large Dielectric Spheres," Sci. Rpt. #3, Dept. of Meteorology, Contract No. AF19(604)-2429, University of California, Los Angeles.

16. Deirmendjian, D. (1957), "Theory of the Solar Aureole," Ann. de Geophys., 13, 286.

17. Penndorf, R. (1957), "New Tables of Total Mie Scattering Coefficients for Spherical Particles of Real Refractive Indexes," J. Opt. Soc. Amer., 47, 11.

18. Saxon, D.S. (1955), "Lectures on the Scattering of Light," Sci. Rpt. #9, Contract No. AF19(122)-239, Dept. of Meteorology, University of California, Los Angeles.

19. Potter, J. F. (1970), "Delta Function Approximations in Radiative Transfer Theory," J. Atmos. Sci. 27, 943.

20. Coulson, K. L. (1959), "Characteristics of the Radiation Emerging from the top of a Rayleigh Atmosphere," Planet. Space Sci., 1, 265.

21. Chen, H.S., and C. R. N. Rao (1968), "Polarization of Light on Reflection by Some Natural Surfaces," Brit. J. Appl. Phys. (J. Phys. D.) 1, 1191.

22. Coulson, K. L. "Characteristics of Solar Radiation Reflection from Desert Soil," Sci. Rpt. #2 AFCRL Contract No. AF19-(604)-1303, Dept. of Meteorology, University of California, Los Angeles.

23. Coulson, K. L. (1968), "Effects of Surface Reflection on the Angular and Spectral Distribution of Skylight," J. Atm. Sci. 25, 759.

24. de Bary, E. (1963), private communication.

25.    Pang, K. (1970), "Determination of Some Optical Properties
       of the Earth's Atmosphere by Inversion of Scattered Radia-
       tion Measurements," Ph.D. Dissertation, Dept. of Meteorology,
       University of California, Los Angeles, unpublished.

26.    Stowe, L. L., Jr. (1971), "The Effects of Particulate
       Matter on the Radiance of Terrestrial Infrared Radiation,"
       Ph.D. Dissertation, Dept. of Meteorology, University of
       California, Los Angeles.

27.    Rozenberg, G. V. (1960), "Light Scattering in the Earth's
       Atmosphere," Usp. Fiz. Nauk, 71, 173:   English translation:
       Sov. Phys. Usp. 3, 346.

28.    Hariharan, T. A. (1969), "An Airborne Polarimeter for
       Atmospheric Radiatiation Studies," J. Sci. Instr. (J. Phys.
       D.) Ser. 2, 2, 10.

                        (1971), "Atmospheric Turbidity from Polarization,"
       Pure and Appl. Geophys. (Milan) 86, 198.

29.    Blifford, I. H., Jr. (1970), "Tropospheric Aerosols," J.
       Geophys. Res. 75, 3099.

                        and L. D. Ringer (1969), "The Size and
       Number Distribution of Aerosols in the Continental Atmos-
       phere," J. Atmos. Sci. 26, 716.

30.    Rao, C. R. N., H. S. Chen, and T. Takashima (1971), "Labora-
       tory Determination of the Characteristic Reflection Matrices
       of Natural Surfaces," J. Phys. D. (Appl. Phys.) 4, 1057.

31.    Experiment S046 (1968), Final Report:  "Visible Radiation
       Polarization Measurements," Phase C.  Prepared by the Space
       Sciences Laboratory, General Electric Co., King of Prussia,
       Pa.  (referred to as S046FR)

*"The aeronautical and space activities of the United States shall be conducted so as to contribute . . . to the expansion of human knowledge of phenomena in the atmosphere and space. The Administration shall provide for the widest practicable and appropriate dissemination of information concerning its activities and the results thereof."*

—NATIONAL AERONAUTICS AND SPACE ACT OF 1958

# NASA SCIENTIFIC AND TECHNICAL PUBLICATIONS

**TECHNICAL REPORTS:** Scientific and technical information considered important, complete, and a lasting contribution to existing knowledge.

**TECHNICAL NOTES:** Information less broad in scope but nevertheless of importance as a contribution to existing knowledge.

**TECHNICAL MEMORANDUMS:** Information receiving limited distribution because of preliminary data, security classification, or other reasons. Also includes conference proceedings with either limited or unlimited distribution.

**CONTRACTOR REPORTS:** Scientific and technical information generated under a NASA contract or grant and considered an important contribution to existing knowledge.

**TECHNICAL TRANSLATIONS:** Information published in a foreign language considered to merit NASA distribution in English.

**SPECIAL PUBLICATIONS:** Information derived from or of value to NASA activities. Publications include final reports of major projects, monographs, data compilations, handbooks, sourcebooks, and special bibliographies.

**TECHNOLOGY UTILIZATION PUBLICATIONS:** Information on technology used by NASA that may be of particular interest in commercial and other non-aerospace applications. Publications include Tech Briefs, Technology Utilization Reports and Technology Surveys.

*Details on the availability of these publications may be obtained from:*

**SCIENTIFIC AND TECHNICAL INFORMATION OFFICE**

**NATIONAL AERONAUTICS AND SPACE ADMINISTRATION**

**Washington, D.C. 20546**